

NASA

DECLASSIFIED-AUTHORITY-MEMO.U.
2313. TAINÉ TO SHAUKLAS
DATED JUNE 15, 1967Declassified by authority of NASA
Classification Change Notices No. 113
Dated ** 6/23/67TECHNICAL MEMORANDUM
X - 51SPAN LOADINGS AND AERODYNAMIC CHARACTERISTICS FOR A SERIES
OF TIP AND TRAILING-EDGE CONTROLS ON A 60° DELTA WING
AT MACH NUMBERS OF 1.61 AND 2.01

By K. R. Czarnecki and Douglas R. Lord

Langley Research Center
Langley Field, Va.

FACILITY FORM 602

67-31968

(ACCESSION NUMBER)

118
(PAGES)TMX-51
(NASA CR OR TMX OR AD NUMBER)

(THRU)

/ (CODE)

01 (CATEGORY)

This report is the property of the National Aeronautics and Space Administration. It is loaned to you for your information and use only. It is not to be distributed outside your organization. If you are an authorized person is p

NATIONAL AERONAUTICS AND SPACE ADMINISTRATION
WASHINGTON
September 1959

DECLASSIFIED

CONTENTS

Declassified by authority of NASA
Classification Change Notices No. 113
Dated ** 6/28/67

	Page	Figure
SUMMARY	1	
INTRODUCTION	2	
SYMBOLS	2	
APPARATUS	4	
Wind Tunnel	4	
Model and Model Mounting	5	1 to 4
TESTS	5	3
PRECISION OF DATA	6	
PRESENTATION OF RESULTS	6	
RESULTS AND DISCUSSION	8	
Span Loadings	8	5 to 42
Wing	8	
Trailing-edge controls	8	
Tip controls	10	
Configuration Span-Loading Comparisons	11	
Effect of Mach number	11	43 to 46
Effect of hinge-line location	11	47 to 48
Effect of offsetting tip control	12	49 to 50
Effect of fences	12	51 to 54
Effect of trailing-edge thickness	12	55 to 56
Wing and Control Characteristics	13	57 to 69
Effect of control deflection	13	
Effect of angle of attack	13	
Experimental Comparisons of Wing Characteristics	14	
Effect of offsetting tip control	14	70
Effect of fences	14	71
Effect of trailing-edge thickness	14	72
Correlation of Control Effectiveness Parameters	14	73
CONCLUSIONS	15	
REFERENCES	17	
TABLES	19	
FIGURES	28	

CONTENTS

DECLASSIFIED

NATIONAL AERONAUTICS AND SPACE ADMINISTRATION

TECHNICAL MEMORANDUM X-51

SPAN LOADINGS AND AERODYNAMIC CHARACTERISTICS FOR A SERIES
OF TIP AND TRAILING-EDGE CONTROLS ON A 60° DELTA WING
AT MACH NUMBERS OF 1.61 AND 2.01*

By K. R. Czarnecki and Douglas R. Lord

SUMMARY

An investigation has been made at Mach numbers of 1.61 and 2.01 and at a Reynolds number of 4.2×10^6 to determine the spanwise loadings and control effectiveness for a series of 20 controls on a 60° delta wing. Thirteen of the controls were of the balanced-tip type and seven of the controls were of the more conventional trailing-edge type. Tests were made at wing angles of attack from 0° to 15° for control deflections from -30° to 30°.

The experimental spanwise normal-force and pitching-moment loadings due to angle of attack were in good or fair agreement with linear theory at a Mach number of 1.61 but fell below the theoretical predictions at a Mach number of 2.01. The wing and control spanwise loadings due to control deflection were considerably smaller than those predicted theoretically at both Mach numbers. In most cases, increasing the Mach number caused larger decreases in the span loadings than predicted theoretically. Both the experimental carryover of load from control to wing and losses in load from the central part of the control region to the parting line were less than predicted. The most important differences between the span loadings for the trailing-edge and tip-type controls lie in the fact that tip controls have no regions of two-dimensional flow and are strongly dominated by the crossflows at the parting lines.

The wing and the control effectiveness characteristics were fairly linear and were in considerably better agreement with the linear theory predictions at a Mach number of 1.61 than at a Mach number of 2.01. The hinge-moment coefficient curves tended to be somewhat less linear than the control-effectiveness curves and the closely balanced controls became overbalanced at high angle of attack with negative control deflections. Correlations of the experimental and theoretical control-effectiveness parameters with control area and control-area moments were obtained.

*Title, Unclassified.

0371029 0300

INTRODUCTION

As part of a general program of research on controls, an investigation has been made in the Langley 4- by 4-foot supersonic pressure tunnel to determine the important parameters in the design of controls for use on a 60° delta wing at supersonic speeds. The results have been obtained from two series of tests by means of wing and control-surface pressure distributions and direct measurements of the hinge moments. The first series was conducted at a Mach number of 1.61 and included primarily tip controls, some fence configurations, and a trailing-edge control with and without a spoiler mounted on the wing just ahead of the control. The second series included tests of several trailing-edge controls, two additional tip controls, and several tab and fence configurations, each at a Mach number of 1.61, and four of the tip controls at a Mach number of 2.01. All the pressure-distribution and control hinge-moment results and some of the span-loading effectiveness results for the two series of tests have been presented in references 1 to 10.

Although preliminary span-loading analyses for some of the configurations have been presented in references 3 and 7, the purpose of the present report is to complete the span-loading analysis for all the configurations tested. The second objective of this paper is to present the wing aerodynamic characteristics as integrated from the pressure distributions for those configurations that have not been previously reported in references 5 and 6. Comparison of the experimental results with theoretical predictions and analysis of the effects of configuration changes are also included. Tests were made for a wing angle-of-attack range from 0° to 15° and for a control-deflection range from -30° to 30° at Mach numbers of 1.61 and 2.01. All configurations were tested at a Reynolds number of 4.2×10^6 , based on the wing mean aerodynamic chord of 12.10 inches.

This report concludes the analysis of the delta-wing results.

SYMBOLS

c_m	section pitching-moment coefficient (taken about $\frac{2}{3} c_r$)
$c_{m,f}$	section pitching-moment coefficient due to control load
c_n	section normal-force coefficient
$c_{n,f}$	section normal-force coefficient due to control load
C_L	semispan-wing lift coefficient, L/qS

~~CONFIDENTIAL~~L
2
5
8

C_b	semispan-wing root bending-moment coefficient, $B/2Sbq$
C_m	semispan-wing pitching-moment coefficient, $M'/qS\bar{c}$
C_m'	semispan-wing pitching-moment coefficient, $M''/qS\bar{c}$
C_h	control hinge-moment coefficient: for trailing-edge controls, $\frac{H}{q2Q}$; for tip controls, $\frac{H}{qS_c\bar{c}_c}$
$b/2$	wing semispan
B	semispan-wing root bending moment
c	wing local chord
c_{av}	wing average chord
c_r	wing root chord
\bar{c}	wing mean aerodynamic chord
\bar{c}_c	control mean aerodynamic chord
H	control hinge moment about hinge line
L	semispan-wing lift
M	stream Mach number
M_A	moment of S_c about y-axis (line through wing apex perpendicular to the wing root chord)
$M_{A(wing)}$	moment of S about y-axis
M_B	moment of S_c about wing root
$M_{B(wing)}$	moment of S about wing root
M'	semispan-wing pitching moment about 50-percent station of wing mean aerodynamic chord
M''	semispan-wing pitching moment about y-axis

03170201030

4

- q stream dynamic pressure
- Q area moment of control surface behind hinge line about hinge line
- R Reynolds number based on wing mean aerodynamic chord
- S semispan-wing plan-form area
- S_c control plan-form area
- x distance from wing apex in chordwise direction
- y distance from wing apex in spanwise direction
- α wing angle of attack
- δ control deflection relative to wing (positive when control trailing edge is deflected down)
- Δ prefix indicating change due to α or δ

$$C_{L,\delta} = \frac{\partial C_L}{\partial \delta}$$

$$C_{b,\delta} = \frac{\partial C_b}{\partial \delta}$$

$$C'_{m,\delta} = \frac{\partial C'_m}{\partial \delta}$$

All slopes were obtained at α = 0° and δ = 0°.

APPARATUS

Wind Tunnel

This investigation was conducted in the Langley 4- by 4-foot supersonic pressure tunnel, which is a rectangular, closed-throat, single-return wind tunnel with provisions for the control of the pressure, temperature, and humidity of the enclosed air. Flexible-nozzle walls were adjusted to give the desired test-section Mach numbers of 1.61 and 2.01. During the tests, the dewpoint was kept below -20° F so that the effects of water condensation in the supersonic nozzle were negligible.



Model and Model Mounting

L
2
5
8

The model used in this investigation consisted of a semispan delta wing having 11 interchangeable controls and various associated control adapters (or replacement sections) that were required to fit the controls to the basic wing component. The control configurations are presented in figure 1 grouped according to whether they were tip controls (fig. 1(a)), trailing-edge controls (fig. 1(b)), or tip controls with modifications such as fences or tabs (fig. 1(c)). A detailed description of the various control configurations can be found in the references listed in table 1. Table 1 presents a listing of all control configurations investigated and the various references where particular types of information, such as control description, effectiveness, hinge moments, span loadings, and so forth may be found. The location of the pressure orifices can be determined from tables 2 and 3 and the sketches in figure 2.

The basic wing had a leading edge swept back 60° , a root chord of 18.14 inches, and a semispan of 10.48 inches. The wing had a NACA 63-series streamwise section extending 30 percent of the root chord back from the leading edge, a constant-thickness center section with a thickness-chord ratio of 3 percent based on the root chord, and a sharp trailing edge. The trailing-edge bevel began at 86.7 percent of the root chord. Near the wing tip, the nose section joined directly to the tapered trailing edge without a flat midsection. Configurations J1 and J2 had thickened trailing edges as shown in the sketches of figure 1(b).

The basic wing and controls were constructed of steel. (For the details of construction, see ref. 1.) The spoiler and the fences were constructed of 1/16-inch stock brass.

The semispan wing was mounted horizontally in the tunnel from a turntable in a steel boundary-layer bypass plate which was located vertically in the test section about 10 inches from the side wall, as shown in figures 3 and 4.

TESTS

The model angle of attack was changed by rotating the turntable in the bypass plate on which the wing was mounted. (See fig. 3.) The angle of attack was measured by a vernier on the outside of the tunnel, inasmuch as the angular deflection of the wing under load was negligible. Control deflection was changed by a gear mechanism mounted on the pressure box which rotated the control hinge-moment strain-gage balance, the torque tube, and the control as a unit. The control deflections were set approximately with the aid of an electrical control-position indicator mounted on the torque tube close to the wing root and measured under load during testing with a cathetometer mounted outside the tunnel.

[REDACTED]

03:17:28:1030

The pressure distributions were recorded by photographing the multiple-tube manometer boards to which the pressure leads from the model orifices were connected.

Tests were made over an angle-of-attack range from 0° to 15° at increments of either 3° or 6° . The control-deflection range was from -30° to 30° at increments of 5° or 10° . Most of the tests were made at a tunnel stagnation pressure of 15 pounds per square inch absolute at $M = 1.61$ and 17.5 pounds per square inch absolute at $M = 2.01$ corresponding to a Reynolds number, based on the wing mean aerodynamic chord of 12.10 inches, of 4.2×10^6 . Although no attempt was made to fix transition on the model, the surface roughness was probably great enough to cause a turbulent boundary layer.

L
2
5
8

PRECISION OF DATA

The mean Mach numbers in the region occupied by the model are estimated from calibrations to be 1.61 and 2.01, local variations being smaller than ± 0.02 . There is no evidence of any significant flow angularities. The accuracy of the section loading coefficients, which were obtained by mechanically integrating the pressure distributions, is not known but may be relatively low for stations near the parting lines on the tip controls owing to the large fluctuations in local pressures in these regions (see ref. 10) and the relatively small number of orifices available to establish the pressure distributions. The overall accuracies of the wing coefficients, which were obtained by mechanically integrating the original working plots of the span loadings and not the normalized ones presented in this paper, are also not known. However, if the pressure-distribution fairings are assumed to be correct, the repeatability of the wing coefficients and the estimated accuracies of other pertinent quantities are:

α , deg	± 0.05
δ , deg	± 0.1
C_L	± 0.01
C_b	± 0.0025
C_m	± 0.0025
C_h	± 0.01

PRESENTATION OF RESULTS

The final results of this investigation are presented in five sections. The first section includes the span loadings for most of the

configurations investigated. These results are presented in figures 5 to 42. Included in these figures are the span loadings predicted by linearized theory. No results are included for configuration J4 (the spoiler-trailing-edge-flap configuration), in which the number of orifices was somewhat inadequate to obtain reliable span loadings. Results are not presented herein for configuration E1 for which the span loadings were not computed because the boom tab did not produce the desired balancing characteristics and for configurations B, C, and J3 for which there were insufficient orifices or orifice stations to establish with accuracy the section pressure distributions from which the span loadings must be determined. In the second section, comparisons of the span loading are presented to demonstrate the theoretical and experimental effects of Mach number and configuration changes on the span-loading characteristics. These comparisons are made in figures 43 to 56.

In the third section the integrated wing aerodynamic characteristics are presented in figures 57 to 69 for configurations F1, F2, F3, H, I, J1, and J2 at $M = 1.61$ and configurations A, E, F, and G at $M = 2.01$; these configurations have not been previously reported. A comparison of some of the wing aerodynamic characteristics is made in the fourth section (figs. 70 to 72) to indicate the effects of configuration changes that have not been covered in previous reports. These items are the effects of offsetting a tip control, the effect of fences on a closely balanced control (configuration F), and the effect of trailing-edge thickness. Finally, a correlation (fig. 73) is made of the theoretical and experimental control effectiveness parameters for those configurations investigated at $M = 2.01$ and this correlation is compared with a similar correlation for many of the controls obtained at $M = 1.61$.

In order to facilitate the presentation of the spanwise normal-force and moment loading results for the complete range of the tests, the normal-force loading parameters due to control deflection or angle of attack, normalized by the proper angle, are plotted across the wing span in figures 5 to 23. Similarly, the pitching-moment loading parameters are presented in figures 24 to 42. In each figure, the results for a given configuration and Mach number are presented in four parts for the trailing-edge configurations: (a) the load over the complete wing chord due to control deflection; (b) the load over the control chord due to control deflection; (c) the load over the complete wing chord due to angle of attack; and (d) the load over the control chord due to angle of attack. For the tip control configurations discussed in this paper, the loadings can be presented in two parts: (a) the load over the complete wing chord or control chord due to control deflection; and (b) the load over the complete wing chord or control chord due to angle of attack. When the effects due to control deflection are being considered, the data are presented for all the available control deflections at the three basic angles of attack (0° , 6° , and 12°). When the effects due to angle of attack are being considered, the data are presented for most of the

03712281030

available angles of attack at three selected control deflections (-20° , 0° , and 20°).

RESULTS AND DISCUSSION

Span Loadings

Throughout this section on the spanwise loadings, the linear-theory predictions are used as a basis for discussion.

Wing.- The span-loading characteristics of the wing are illustrated by the plots of spanwise normal-force loading due to α for $\delta = 0^\circ$ in figures 5 to 23 and the plots of spanwise pitching-moment loading due to α for $\delta = 0^\circ$ in figures 24 to 42. In general, the experimental normal-force results exhibit spanwise trends that are in very good agreement with the predictions of linear theory except for a tendency for the experimental loadings to fall somewhat below the theoretical values outboard of about 55 percent of the semispan. (See, for example, figs. 5(c), 7(b), 10(b), and 15(b).) This trend, particularly the sharp drop-off in span loading across the parting line for some of the tip controls, is believed to be exaggerated in most cases by the way the rather sparse experimental pressures were faired in the separated flow regions near the wing leading edge at these outboard stations for integration purposes. This indication became apparent only after the greatest portion of the data had been faired and integrated and it was possible to compare configurations with one another and to compare a few of the configurations at reversed angles of attack. If the apparently low section loading coefficients were corrected, the experimental results would then be in good or fair agreement with theory across the complete wing span for the angle-of-attack range of 12° or 15° of this investigation. The experimental results for the various configurations are also in reasonably good agreement with one another.

The trends discussed for the normal-force loadings also apply to the spanwise pitching-moment loading distributions. If the apparent errors in fairing the chordwise pressure distributions are taken into consideration, the pitching-moment distributions are in excellent agreement with theory across the span and with one another for the various configurations. (See, for example, figs. 24(c), 25(b), 33(b), 35(c), and 42(b).)

Trailing-edge controls.- In general, the normal-force loadings due to control deflection for the trailing-edge control configurations (configurations A, I, J, J1, and J2; the (a) and (b) parts of figures 5 and 16 to 20) exhibit the same type of loading characteristics as found for trailing-edge control configurations on an essentially unswept wing

11

as reported in reference 11. The linear theory overestimates the normal-force loadings on the wing or control due to δ by a considerable amount. Examination at the same spanwise stations of the differences between the wing (part (a) of the figures) and control span loadings (part (b) of the figures) at identical conditions indicates that, for the highest control deflections, particularly positive δ values at positive angle of attack, there is a substantial carryover of the load to the wing ahead of the control hinge line due to shock detachment and boundary-layer separation at the hinge line as found in the previous tests. Also, as reported previously in reference 11, the wing normal-force loading plots show that the integrated carryover from the control to the wing station adjacent to the parting lines of the partial-span controls (figs. 5(a), 16(a), and 20(a)) is considerably less than that predicted by theory and in many cases is negligible. On the control, the normal-force loadings do not indicate the relatively sharp drop-offs in loadings predicted theoretically for the stations close to the parting line. (See figs. 5(b), 16(b), and 20(b).) The crossflows in the region of the parting lines, discussed in detail in references 10 and 11 and not accounted for by the theory, apparently explain the lack of carryover load to the wing and the conservation of the loading on the control near the parting line.

The points to be noted from observation of the wing or control pitching-moment loadings due to control deflection (the (a) and (b) parts of figs. 24 and 35 to 39) are practically identical with those previously emphasized under the normal-force loading discussion and will not therefore be discussed in detail. These are: overestimation by the linear theory of the loading on the midspan or two-dimensional portions of the controls, lack of appreciable carryover effect near the parting lines, and failure of the loadings on the control to decrease as much as predicted near the parting lines. The effects of hinge-line separation or shock detachment, previously discussed in conjunction with the normal-force loadings, appear as a trend toward a decrease in moment loadings at the highest values of δ due to the forward movement of the center of pressure of the loading. This effect is reflected in the decreased hinge-moment and pitching-moment coefficient slopes at high control deflections. (See, for example, ref. 5.)

The normal-force loadings on the wing or control due to angle of attack for the trailing-edge controls (parts (c) and (d) of figs. 5 and 16 to 20) are generally similar at the three control deflections shown and exhibit little variation with angle of attack. The experimental results generally are in good agreement with theory and, if compared with the results for a wing with leading-edge sweep of 23° in reference 11, show the effects of wing leading-edge sweep on the control loadings. This effect, which is exemplified by the increase in control loading toward the wing or control tip, was practically nonexistent for the wing with a leading-edge sweep of 23° . Examination of the results

031710001030

also shows that the effect of control deflection on the wing normal-force loadings due to angle of attack is usually very small.

The conclusions derived from the inspection of the wing or control pitching-moment loadings due to α (parts (c) and (d) of figs. 24 and 35 to 39) are identical to those just discussed for the normal-force loadings.

Tip controls.- For the tip-type controls the normal-force loadings due to control deflection (configurations D, E, F, G, and H; part (a) of figs. 6, 7, 10, 14, 15, 21, 22, and 23) do not exhibit any extent of two-dimensional or constant-span loading characteristics as did some of the trailing-edge controls. This result is to be expected. The experimental results also show a considerable increase in scatter. The lack of two-dimensional flow characteristics is, of course, ascribed to the long parting lines and smaller aspect ratios for the tip controls. The increased scatter in the data is ascribed to the fact that the parting-line effects dominate the loadings over a large part of the area influenced by the control, and, as was shown in the analysis of the chordwise pressures in reference 10, the loading is very erratic in this region and difficult to integrate accurately with the relatively small number of pressure orifices available. An increase in the scatter may also be expected from the fundamental character of the loadings in this region in that the rather abrupt pressure rises and flow expansions on the wing and control tend to shift their positions rapidly with changes in α or δ . As in the case of the trailing-edge controls, linearized theory considerably overestimates the loadings for the tip controls in the regions away from the parting lines.

A comparison of the parting-line effects for the tip controls (for example, figs. 6(a), 7(a), 14(a), and 21(a)) with those for the trailing-edge controls (for example, figs. 5(a), 16(a), 17(a), and 20(a)) indicate that the effects are basically very similar. The carryover of the loading to the wing at the station close to the parting line is nonexistent or negligible; the dropoff in loading for the control station close to the parting line that is predicted theoretically is not realized. In fact, for the tip controls the parting-line effect may be somewhat more severe in that there are indications of actual reversed loadings for the wing station next to the parting line for some combinations of angle of attack and control deflection (for example, figs. 6(a) and 7(a); $\alpha = 6^\circ$ and 12° ; $\delta = -30^\circ$).

The characteristics just described for the normal-force loadings also apply directly to the pitching-moment loadings due to control deflection for the tip controls (part (a) of figs. 25, 26, 29, 34, 40, 41, and 42).

L
2
5
8

The normal-force loadings due to α for the tip controls (part (b) of figs. 6, 7, 10, 15, 21, 22, and 23) are, of course, identical to the loadings for the basic wing at $\delta = 0^\circ$. If allowance is made for the probability that the integrated experimental loadings may be somewhat low in the wing-tip region, the experimental loadings can be considered to be in fair agreement with linear theory. No large effects on the wing normal-force loading due to α appear to be discernible for the cases where the control was deflected. The same conclusions apply to the control and wing pitching-moment loadings due to angle of attack. (See figs. 25(b), 26(b), 29(b), 40(b), 41(b), and 42(b).)

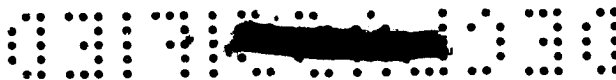
Configuration Span-Loading Comparisons

Effect of Mach number.— The effects of Mach number on the wing and control normal-force and pitching-moment loadings are presented in figures 43 and 44 for a trailing-edge-control configuration and in figures 45 and 46 for a tip-control configuration for a few representative combinations of angle of attack and control deflection. In general, increasing the Mach number decreased the wing and control normal-force loadings due to both δ and α . The decrease was generally larger than that predicted by linear theory. For the normal-force loadings due to angle of attack and for the normal-force loading due to δ for the tip-control configurations, the explanation of the discrepancy appears to lie in the fact that for the higher Mach number ($M = 2.01$) the Mach line theoretically lies along the wing (and tip-control) leading edge. The linear theory is at its weakest for this condition. (See, for example, ref. 12.) The explanation of the discrepancy in loading due to δ between theory and experiment for the outboard trailing-edge control probably lies in the fact that the outside edge of the control also lies along the leading edge of the wing.

An increase in Mach number also caused a decrease in pitching-moment loading due to α that was on the average greater than might have been expected on the basis of linear theory. This effect did not extend to the inboard stations where the agreement between theory and experiment appears to be equally good at both Mach numbers but was limited to the wing tip region where both the tip and trailing-edge controls were located. These changes in moment are due to the reduction in leading-edge separation as the Mach number is increased. At the inboard stations this condition causes a negative increment in moment which improves the agreement between theory and experiment whereas at the outboard stations this condition causes a positive increment in moment which leads to an increase in the disagreement between theory and experiment.

Effect of hinge-line location.— The effect of changing the hinge-line location of the tip-control configurations on the normal-force and pitching-moment loadings due to α and δ is shown in figures 47 and 48.

CONFIDENTIAL



Again the comparison is limited to a few typical combinations of α and δ . On the basis of linearized theory there should be no effect on the span loadings due to changes in hinge line. The experimental results confirm this expectation although there is a fair amount of random scatter in the data.

Effect of offsetting tip control.- The effect of offsetting a half-delta tip control with respect to the wing is illustrated in figure 49 for the normal-force loadings and in figure 50 for the pitching-moment loadings. The linear-theory curves included in the figures are for the control without the offset (configuration F). A comparison of the configuration with and without the offset shows no conclusive effects on the span-loading characteristics.

Effect of fences.- The effect of fences at the parting lines of two of the tip controls is shown in figures 51 to 54. Configurations E2 and F1 are similar, the fences extending from 0.3 inch ahead of the leading edge to 0.3 inch downstream of the trailing edge. Configurations E3 and F3 are also similar, the fences of each extending from 0.3 inch ahead of the leading edge to about the hinge line. Configuration F2 had a fence extending from the hinge line to 0.3 inch downstream of the trailing edge. The theoretical curves for the configurations without fences were obtained by the usual linear-theory methods. The theoretical curves, represented by the short dashes, were obtained by using the linear theory and the assumption that the fence was sufficiently large to intercept the wing or control-pressure fields and act as a perfect reflection plane. This assumption may be reasonable for the control-deflection case but is not for the wing flow field due to angle of attack. For this reason the theoretical curve or the loading due to α for the fence case were computed only for the region of the wing outside the fences.

An examination of the comparisons indicate that there is a substantial amount of scatter in the experimental data and that it is difficult to derive any conclusions as to the effect of fences on the span loadings. If all the data for each configuration are considered (figs. 7 to 13 for the normal-force loadings and figs. 26 to 32 for the pitching-moment loadings), it may be concluded that the full-chord fence may be fairly effective in preventing any carryover of any load on the wing due to control deflection. The full-chord fence also appears to decrease the loading due to α on the control somewhat in comparison with the configuration with no fence. The changes in experimental loadings, however, are considerably smaller than those predicted theoretically. It may be concluded that the fences are probably too small to intercept completely the wing or control flow fields and act as an infinitely large reflection plane as assumed in the theory.

Effect of trailing-edge thickness.- The effect of increasing the trailing-edge thickness from 0 to a value equal to that at the hinge



line is shown in figure 55 for the normal-force loadings and in figure 56 for the pitching-moment loadings. Apparently, the changes are small and probably within the experimental accuracy.

Wing and Control Characteristics

Effect of control deflection.- The data for configurations not reported previously are presented in figures 57 to 67 (configurations F1, F2, F3, H, I, J1, and J2 at $M = 1.61$ and configurations A, E, F, and G at $M = 2.01$) in the form of variations of wing lift, bending-moment, pitching-moment, and control hinge-moment coefficients with control deflection. In general, the variations of lift and bending-moment coefficients with control deflection are fairly linear. There is a tendency, however, for the lift and bending-moment effectiveness to increase at large positive control deflections at high angles of attack for the trailing-edge configurations (for example, figs. 61, 62, and 64) and to decrease for the tip-control configurations (for example, figs. 58, 59, and 65). The reverse is true for the large negative control deflections. (Compare figs. 61, 62, and 64 with figs. 57, 58, and 67.) These trends are the results of flow separation at the hinge line for the trailing-edge controls (see refs. 11 and 13) and leading-edge separation for the tip controls. (See ref. 10.) The pitching-moment curves are also generally fairly linear in the control-deflection range from -20° to 20° . At control deflections exceeding these values there is a tendency for the curves to become nonlinear for some of the configurations. The hinge-moment coefficient curves, on the other hand, tended toward nonlinearity except for the trailing-edge configurations I, J1, and J2. (See figs. 61, 62, and 63.) For these configurations the curves were linear over the δ range from -20° to 20° with a tendency for the hinge moments to decrease in slope at still higher control deflections. It should be noted that all configurations in the F category are closely balanced as is configuration H. Some of these configurations tend to overbalance at negative control deflections at the higher angles of attack. (See figs. 58, 60, and 66.) Control configuration G (fig. 67) is overbalanced at all times.

Effect of angle of attack.- The experimental and theoretical variations of the basic-wing ($\delta = 0^\circ$) lift, bending-moment, and pitching-moment coefficients with angle of attack are presented for the two test Mach numbers in figures 68 and 69. These curves are averages for all the configurations discussed in this report. The experimental results used to determine the average curves were in fair agreement with one another and in good agreement with the data presented for other configurations in reference 6.

The experimental curves of figures 68 and 69 are fairly linear, the slopes gradually increasing as α is increased. The variations at other



control deflection could not be defined too well because of lack of sufficient data. At $M = 1.61$ the experimental lift and bending-moment results are in reasonably good agreement with linear theory at the lower angles of attack. (See fig. 68.) At $M = 2.01$ (fig. 69) the experimental results fall considerably below the theoretical curves for the reason that the linear theory is at its weakest when the Mach line theoretically lies along the leading edge as previously discussed. The linear-theory prediction of pitching-moment coefficient due to α appears to be poor but in reality is very good since the choice of the pitch center at the wing centroid magnifies the discrepancy. The moment increment is equivalent to a center-of-pressure shift of about 3 and 5 percent of the mean aerodynamic chord at the Mach numbers of 1.61 and 2.01, respectively.

Experimental Comparisons of Wing Characteristics

Effect of offsetting tip control.- A comparison of variations of wing lift, bending-moment, and pitching-moment coefficients with control deflection for tip configuration F with configuration F offset to make configuration H is shown in figure 70. In general, configuration H appears to have more linear characteristics and somewhat lower lift, bending-moment, and pitching-moment effectiveness than configuration F. In view of the scatter in span-loading data indicated for these configurations in figures 49 and 50, the aforementioned trend is probably questionable.

Effect of fences.- The variation of the control-effectiveness parameters with control deflection for configuration F with and without fences mounted at the wing-control parting line is shown in figure 71. There appears to be somewhat more effect of the fences on the control effectiveness of configuration F than was indicated in reference 6 for configuration E. This indication may be fortuitous because of the relatively poor accuracies experienced for the fence configurations in the span loadings which were integrated to obtain the wing coefficients. It appears, however, that the use of a full-chord fence may result in more linear effectiveness characteristics than for the same control without any fence.

Effect of trailing-edge thickness.- In figure 72 are presented the effects of increasing the trailing-edge thickness on configuration J. As in the case of the span-loading distributions the effects, if any, are within the experimental accuracy of the investigation.

Correlation of Control Effectiveness Parameters

Correlations of the experimental and theoretical wing lift, bending-moment, and pitching-moment coefficient slopes due to control deflection



as functions of ratios of area to wing area, area moment about the root chord, and area moment about the wing apex, respectively, are presented in figure 73 for the four control configurations investigated at $M = 2.01$ along with the correlation obtained previously for many of the control configurations at $M = 1.61$ in reference 6. Both the theoretical and experimental points correlate on approximately straight lines, the slopes of the experimental correlations being about 50 percent of the corresponding theoretical correlations at $M = 2.01$. This value is considerably lower than the 77 percent of theoretical correlation found for these same control configurations at $M = 1.61$ or the 70-percent figure for trailing-edge control configurations on a trapezoidal wing at $M = 2.01$. (See ref. 10.) Since three out of the four controls investigated at $M = 2.01$ were of the tip type and since the trailing-edge configuration A also has a side edge lying along the wing leading edge, this discrepancy is again ascribed to the fact that the controls have leading edges that lie along the theoretical Mach line.

CONCLUSIONS

The results of an experimental and theoretical investigation of a series of trailing-edge and tip controls on a 60° delta wing at Mach numbers of 1.61 and 2.01 are presented. From the investigation, which covered a range of angles of attack from 0° to 15° and control deflection from -30° to 30° , the following conclusions may be obtained:

For the span loadings:

1. The experimental spanwise wing and control normal-force and pitching-moment loadings due to angle of attack were in good or fair agreement with linear theory at a Mach number of 1.61 but fell below the theoretical predictions at a Mach number of 2.01.
2. The experimental spanwise wing and control normal-force and pitching-moment loadings due to control deflection were considerably smaller than those predicted theoretically at both test Mach numbers.
3. In most cases, whether for the normal-force or pitching-moment loadings or whether for the wing or control deflection, the effect of increasing the Mach number from 1.61 to 2.01 was to cause a larger decrease in the experimental loadings than that predicted theoretically.
4. The carryovers of loading from the control to the wing adjacent to a parting line were much less than linear theory estimated and in many cases were negligible and even reversed.

CONFIDENTIAL

5. The experimental losses in loading from the central region of the tip controls to the parting lines were less than those predicted by linear theory.

6. Basically, the most important differences between the span loadings for the trailing-edge and tip controls lie in the fact that the tip controls have no regions of two-dimensional flow and are strongly dominated by the rapidly changing crossflow effects at the parting lines.

7. Changing the hinge-line location, offsetting a tip control, installing various types of fences, and changing the trailing-edge thickness had only small effects, if any, on the span loadings that were generally within the experimental accuracy.

For the wing and control characteristics:

1. The integrated wing lift, bending-moment, and pitching-moment characteristics were generally linear with a tendency toward non-linearity at high angles of attack and/or control deflection.

2. The control hinge-moment characteristics tended to be somewhat less linear, the closely balanced controls becoming overbalanced at high angles of attack and negative control deflection.


3. Linear theory overestimated the effects of angle of attack on the wing lift and bending moments and underestimated the wing pitching moments at both Mach numbers.

For the correlations:

1. Correlations were obtained both theoretically and experimentally that showed the wing lift, root bending moment, and pitching-moment effectiveness to be functions primarily of control area, control-area moment about the wing root, and control-area moment about the pitch center, respectively.

2. The experimental correlations of the control effectiveness parameters at a Mach number of 2.01 were about 50 percent of the theoretical predictions in comparison with the value of 77 percent found in previous correlations for the same controls at a Mach number of 1.61.

Langley Research Center,
National Aeronautics and Space Administration,
Langley Field, Va., April 23, 1959.



REFERENCES

1. Czarnecki, K. R., and Lord, Douglas R.: Hinge-Moment Characteristics for Several Tip Controls on a 60° Sweptback Delta Wing at Mach Number 1.61. NACA RM L52K28, 1953.
2. Czarnecki, K. R., and Lord, Douglas R.: Preliminary Investigation of the Effect of Fences and Balancing Tabs on the Hinge-Moment Characteristics of a Tip Control on a 60° Delta Wing at Mach Number 1.61. NACA RM L53D14, 1953.
3. Czarnecki, K. R., and Lord, Douglas R.: Load Distributions Associated With Controls at Supersonic Speeds. NACA RM L53D15a, 1953.
4. Lord, Douglas R., and Czarnecki, K. R.: Recent Information on Flap and Tip Controls. NACA RM L53I17a, 1953.
5. Lord, Douglas R., and Czarnecki, K. R.: Aerodynamic Characteristics of a Full-Span Trailing-Edge Control on a 60° Delta Wing With and Without a Spoiler at a Mach Number of 1.61. NACA RM L53L17, 1954.
6. Lord, Douglas R., and Czarnecki, K. R.: Aerodynamic Characteristics of Several Tip Controls on a 60° Delta Wing at a Mach Number of 1.61. NACA RM L54E25, 1954.
7. Czarnecki, K. R., and Lord, Douglas R.: Simplified Procedures for Estimating Flap-Control Loads at Supersonic Speeds. NACA RM L55E12, 1955.
8. Lord, Douglas R., and Czarnecki, K. R.: Tabulated Pressure Data for a Series of Controls on a 60° Delta Wing at Mach Numbers of 1.61 and 2.01. NACA RM L55L05, 1956.
9. Lord, Douglas R., and Czarnecki, K. R.: Hinge-Moment Characteristics for a Series of Controls and Balancing Devices on a 60° Delta Wing at Mach Numbers of 1.61 and 2.01. NACA RM L57B01, 1957.
10. Lord, Douglas R., and Czarnecki, K. R.: Analysis of Pressure Distributions for a Series of Tip and Trailing-Edge Controls on a 60° Delta Wing at Mach Numbers of 1.61 and 2.01. NACA RM L58C07, 1958.
11. Lord, Douglas R., and Czarnecki, K. R.: Pressure Distributions and Aerodynamic Loadings for Several Flap-Type Trailing-Edge Controls on a Trapezoidal Wing at Mach Numbers of 1.61 and 2.01. NACA RM L55J03, 1956.

03:17:00:00:00:00:00:00

12. Ulmann, Edward F., and Bertram, Mitchel H.: Aerodynamic Characteristics of Low-Aspect-Ratio Wings at High Supersonic Mach Numbers. NACA RM L53I23, 1953.
13. Lord, Douglas R., and Czarnecki, K. R.: Aerodynamic Characteristics of Several Flap-Type Trailing-Edge Controls on a Trapezoidal Wing at Mach Numbers of 1.61 and 2.01. NACA RM L54D19, 1954.

L
2
5
8

[REDACTED]

TABLE 1.- BIBLIOGRAPHY OF DELTA-WING CONTROL TESTS

[Numbers refer to references in this text]

Configuration	Modifications	Tabulated pressures	Pressure analysis	Chordwise loadings	Spanwise loadings	Effectiveness	Hinge moments
A	-----	8	10	*	*	4, 6, *	1, 4, 9
B	-----	8	10	---	---	4, 6	1, 4
C	-----	8	10	*	---	4, 6	1, 4
D	-----	8	10	---	*	4, 6	1, 4
E	-----	8	10	3	3, 7, *	4, 6, *	1, 2, 4, 9
E	Large attached tab	---	---	---	---	---	2
E	Small attached tab	---	---	---	---	---	2
E	Inset tab	---	---	---	---	---	9
E	Detached tab	---	---	---	---	---	9
E1	Boom tab	8	10	---	---	---	9
E2	Full fence	8	10	---	*	6	2, 4, 9
E3	Forward fence	8	10	---	*	6	2, 9
F	-----	8	10	*	*	4, 6, *	1, 4, 9
F1	Full fence	8	10	---	*	*	9
F2	Rearward fence	8	10	---	*	*	9
F3	Forward fence	8	10	---	*	*	9
G	-----	8	10	---	*	4, 6, *	1, 4, 9
H	-----	8	10	---	*	4, *	9
I	-----	8	10	---	*	*	9
J	-----	8	5, 10	3, *	3, 7, *	5, *	5, 9
J	Inboard tab	---	---	---	---	---	9
J	Outboard tab	---	---	---	---	---	9
J1	1/2 thick trailing edge	8	---	---	*	*	9
J2	Thick trailing edge	8	---	---	---	---	9
J3	Paddle balance	8	10	---	---	---	9
J4	Spoiler	8	3, 5	---	---	5	5
K	-----	---	---	---	---	---	9

* Signifies present report.

TABLE 2.- SPANWISE LOCATION OF ORIFICE STATIONS

[Chordwise extent of stations shown in figure 2 and table 3]

Configuration	Values of $2y/b$ at station -								
	1	2	3	4	5	6	7	8	9
A	0.048	0.210	0.372	0.537	0.592	0.745	0.860	(a)	---
B	.048	.210	.372	.537	(a)	.602	(a)	0.734	(a)
C	.048	.210	.372	.537	.601	.640	.683	.758	(a)
D	.055	.242	.430	.619	.688	.776	.876	.958	---
E, E1, E2, E3, F F1, F2, F3, G, H	.048	.210	.372	.537	.597	.733	.869	.967	---
I	.048	.210	.372	.537	.592	.745	(a)	-----	---
J, J1, J2, J3, J4	.048	.210	.372	.537	.592	.745	(a)	-----	---

^aSee figure 2.

(b) Configuration B

[illegible]

١٠٣٣

[illegible]

(d) Configuration D

[illegible]

TABLE 3.- CHORDWISE LOCATION OF ORIFICES - Continued

(e) Configurations E, E1, E2, E3, F, F1, F2, F3, G, H

Orifice	Values of x/c_r at station -								
	1	2	3	4	5	6	7	8	9
1	0.048	0.210	0.372	0.535	0.597	0.730	0.864	0.987	
2	.075	.238	.400	.562	.625	.758	.892		
3	.219	.381	.538	.700	.674	.808	.941		
4	.334	.502	.659	.846	.746	.879	.986		
5	.445	.612	.747	.901	.840	.973			
6	.588	.756	.846	.950	.939	^a .990			
7	.742	.846	.901	.984	.988				
8	.846	.901	.950						
9	.901	.950	.984						
10	.950	.984							
11	.984								
12									
13									

^aConfiguration E1 at $M = 1.61$ and E at $M = 2.01$ only.

03711201930

TABLE 3.- CHORDWISE LOCATION OF ORIFICES - Continued

(f) Configuration I

Orifice	Values of x/c_r at station -								
	1	2	3	4	5	6	7	8	9
1	0.048	0.210	0.372	0.535	0.597	0.753	0.890		
2	.075	.238	.400	.562	.624	.778	.985		
3	.219	.381	.538	.700	.719	.853			
4	.334	.502	.659	.860	.839	.945			
5	.445	.612	.747	.852	.919	.995			
6	.588	.756	.860	.896	.972				
7	.742	.860	.852	.935					
8	.860	.852	.896	.984					
9	.852	.896	.935						
10	.896	.935	.984						
11	.935	.984							
12	.984								
13									

L
2
5
8

DECLASSIFIED

27

TABLE 3.- CHORDWISE LOCATION OF ORIFICES - Concluded

(g) Configurations J, J1, J2, J3, J4

Orifice	Values of x/c_r at station -								
	1	2	3	4	5	6	7	8	9
1	0.048	0.210	0.372	0.535	0.592	0.745	0.852		
2	.075	.238	.400	.562	.619	.772	.872		
3	.219	.381	.538	.700	.713	.816	.910		
4	.334	.502	.659	.860	.779	.860	.948		
5	.445	.612	.747	.852	.860	.872	.986		
6	.588	.756	.860	.872		.905			
7	.742	.860		.905		.949			
8	.860	.852		.949		.982			
9	.872	.872		.982					
10	.905	.905		^a 1.000					
11	.949	.949							
12	.982	.982							
13		^a 1.000							

^aOn blunt bases of configurations J1 and J2 only.

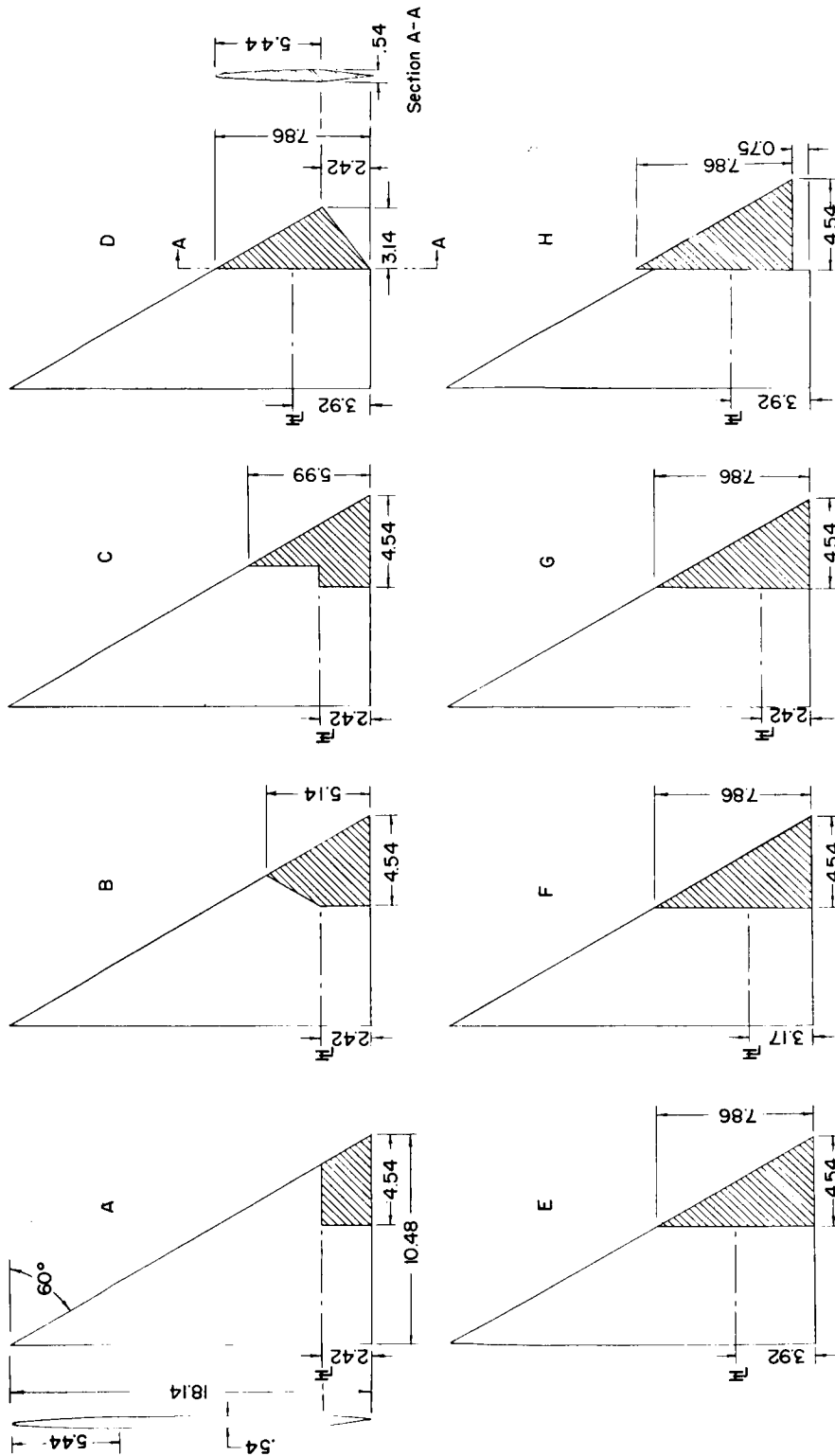
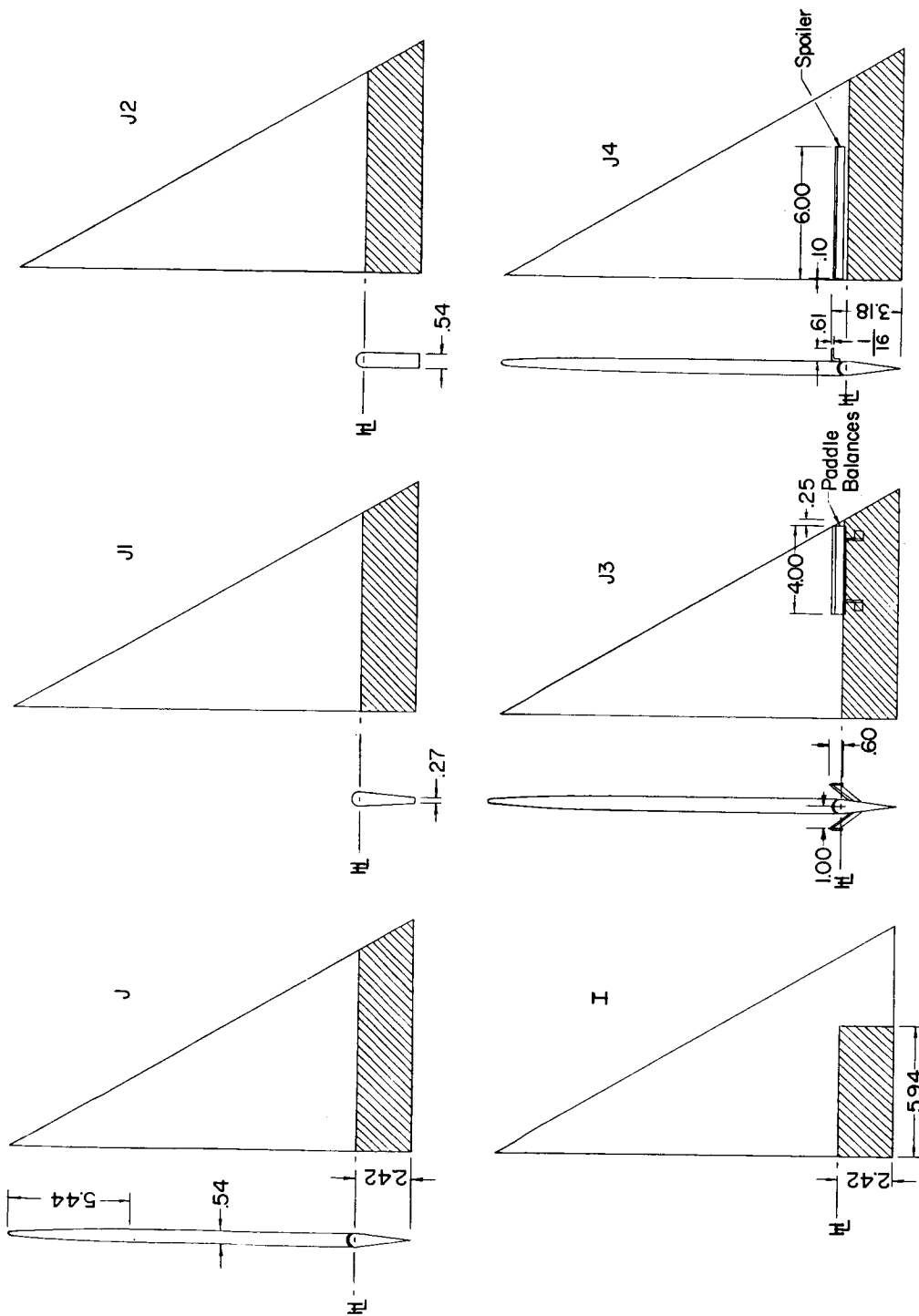
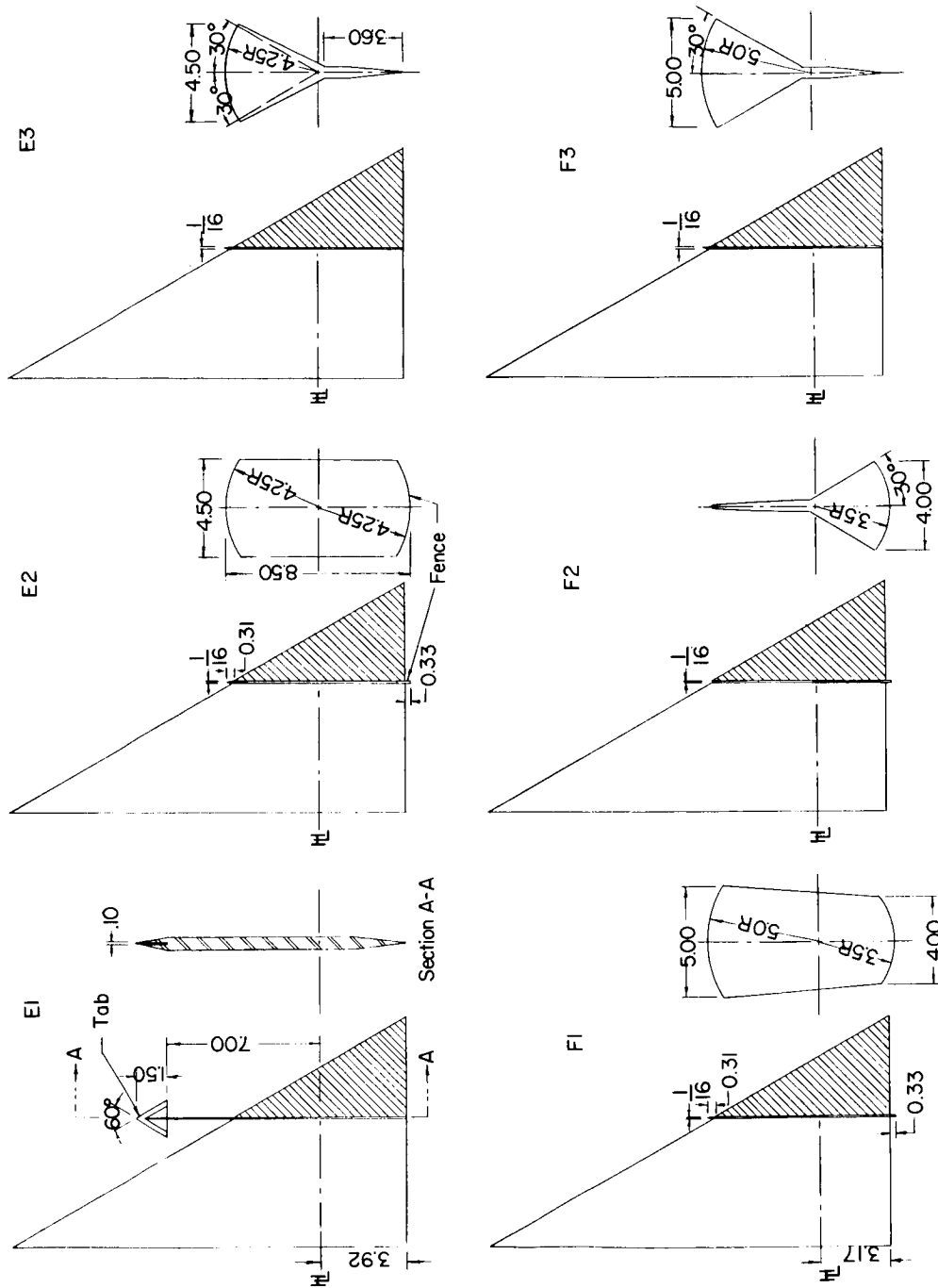


Figure 1.- Dimensional sketches of test configurations. All dimensions are in inches.



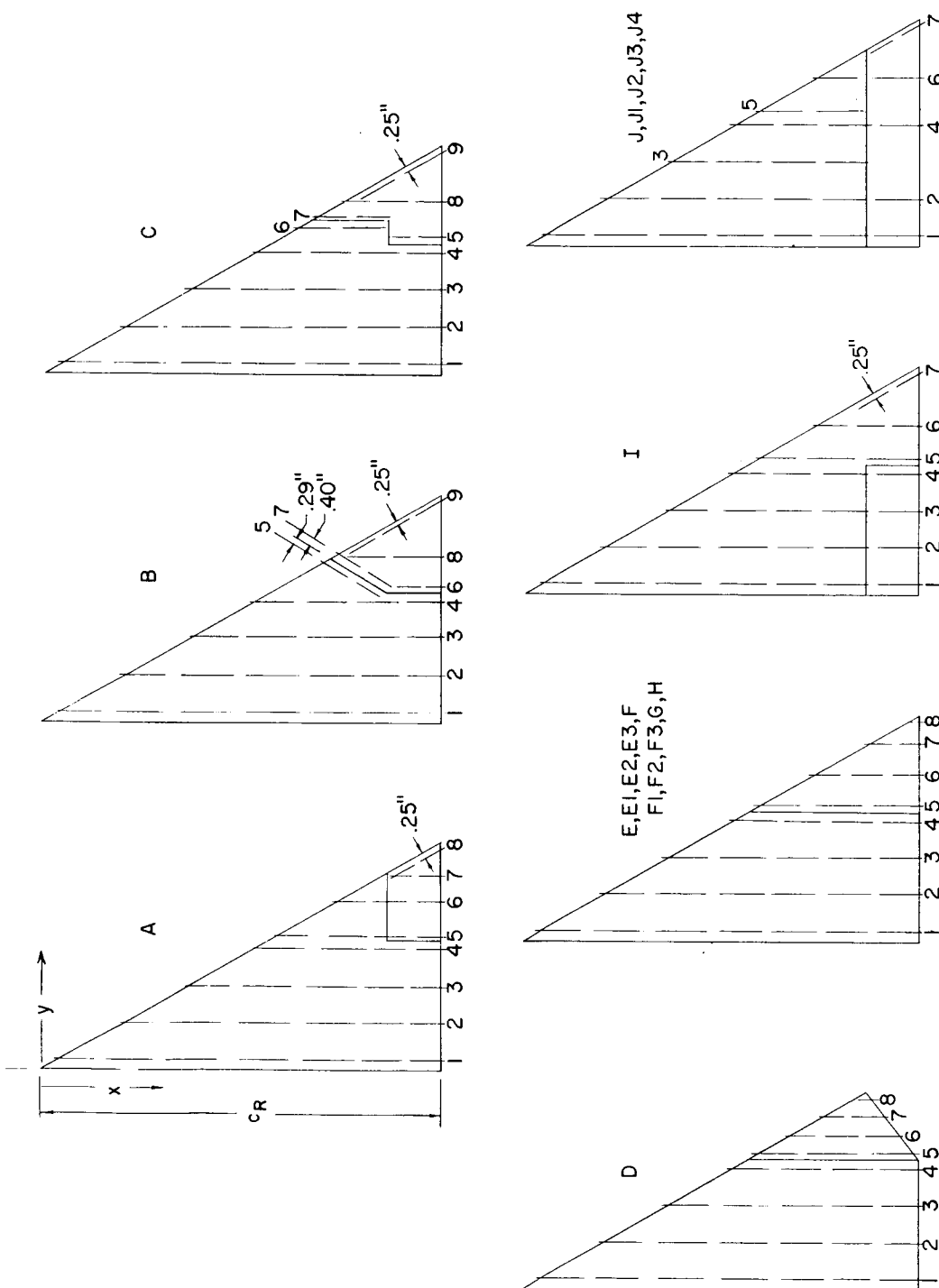
(b) Trailing-edge-control configurations. (Configuration A could be included here also.)

Figure 1.- Continued.

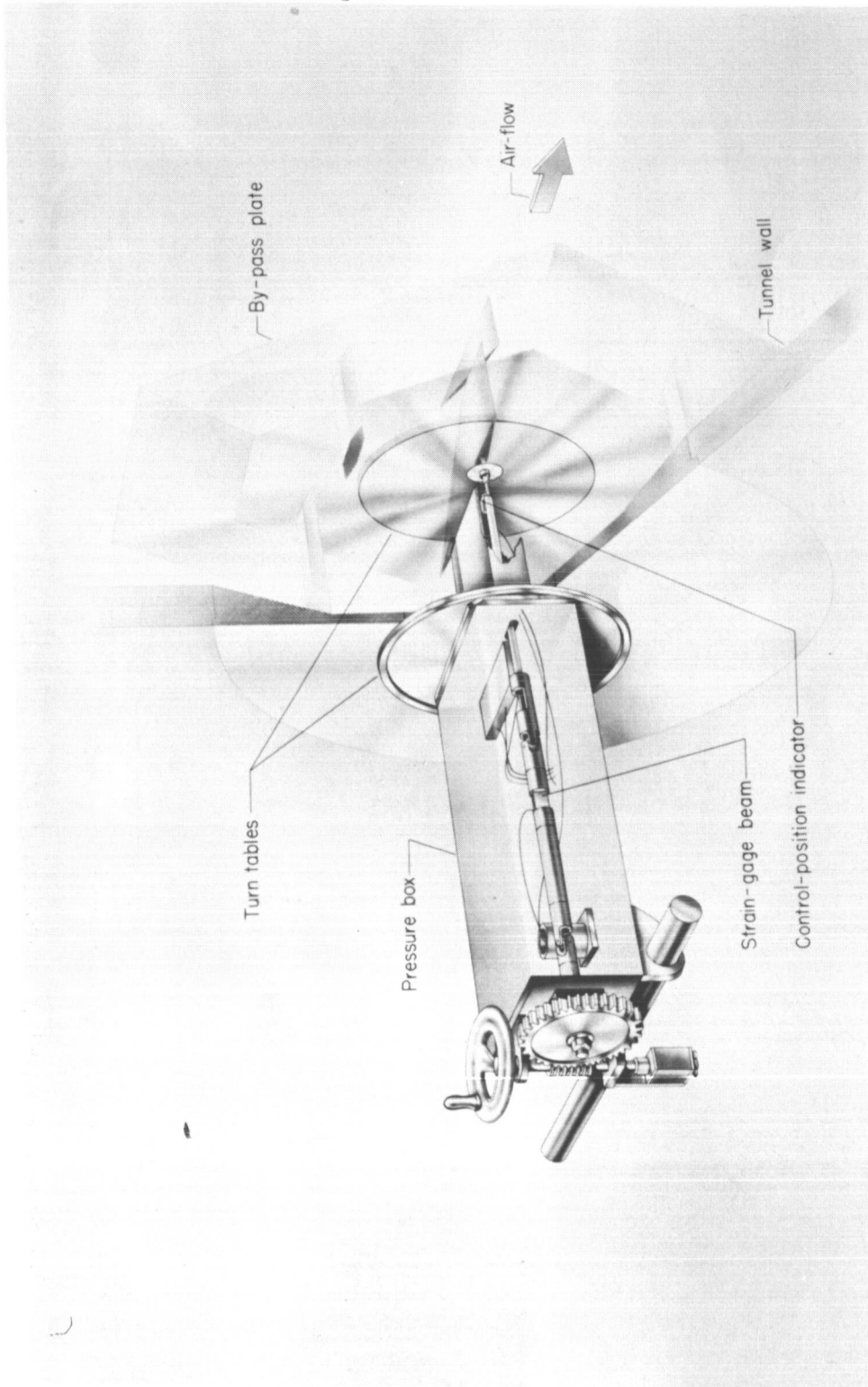


(c) Tab and fence configurations.

Figure 1.- Concluded.

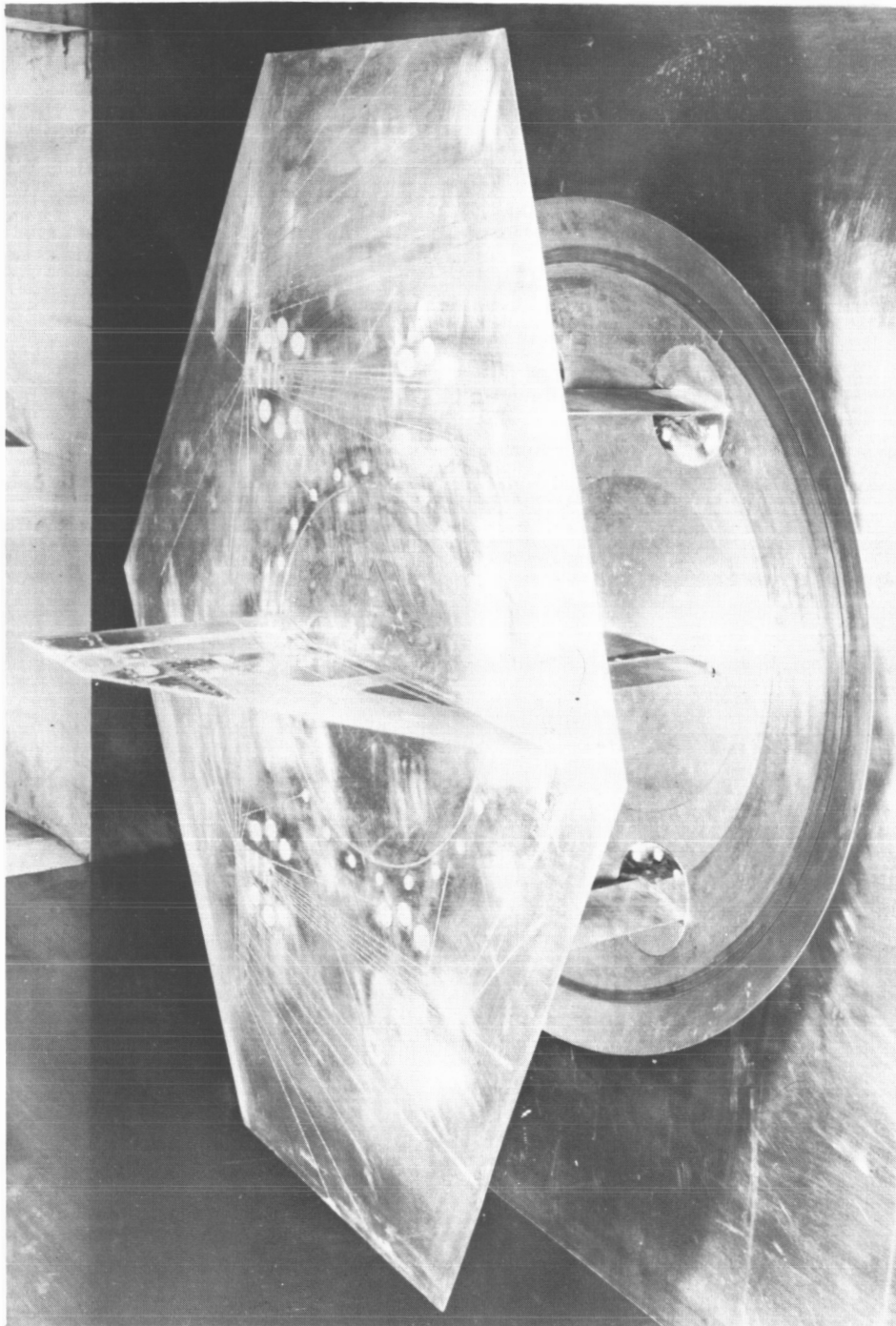


CONFIDENTIAL

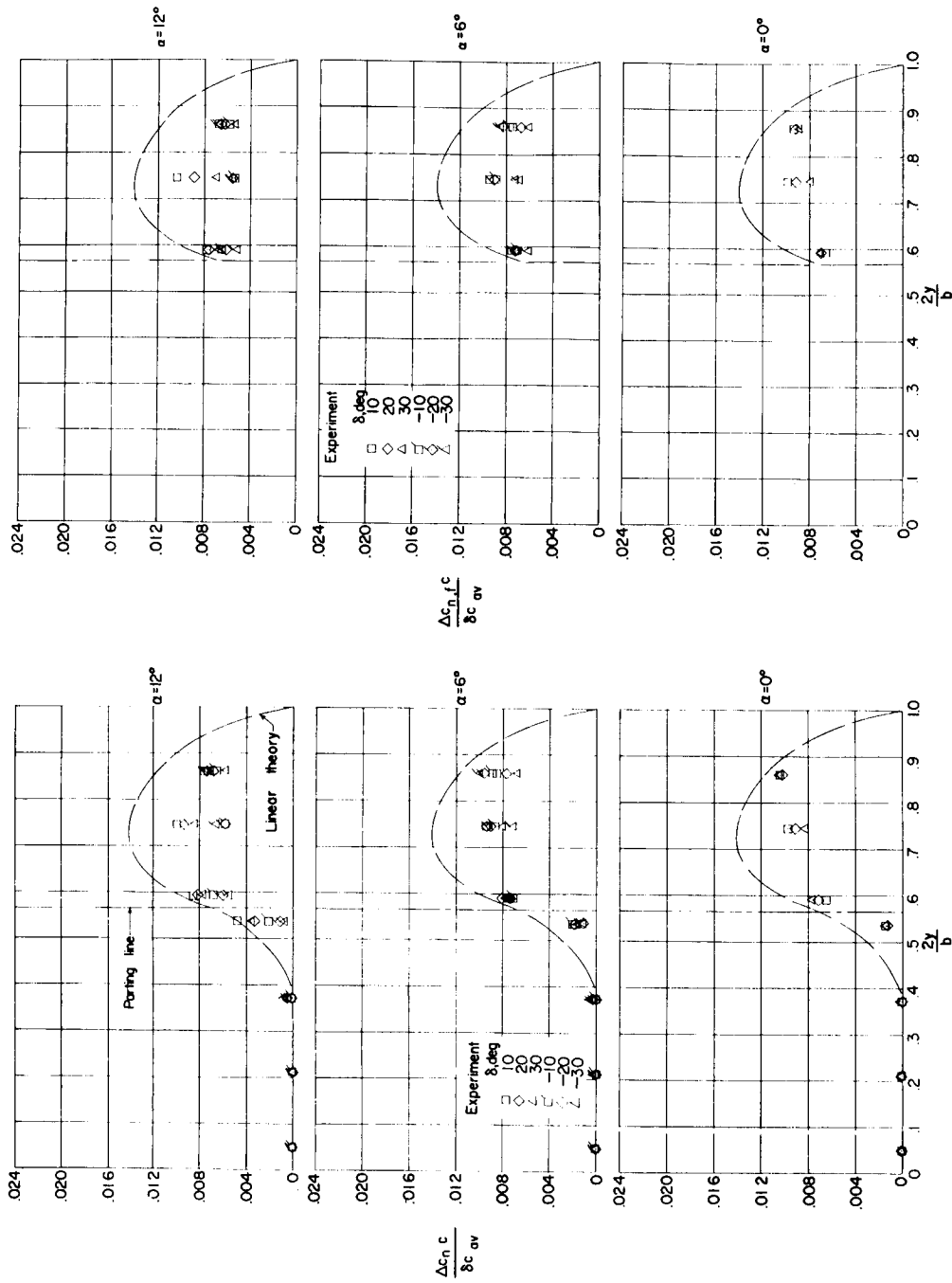


I-77038
Figure 3.- Sketch of test setup showing one of the tip-control installations.

CONFIDENTIAL

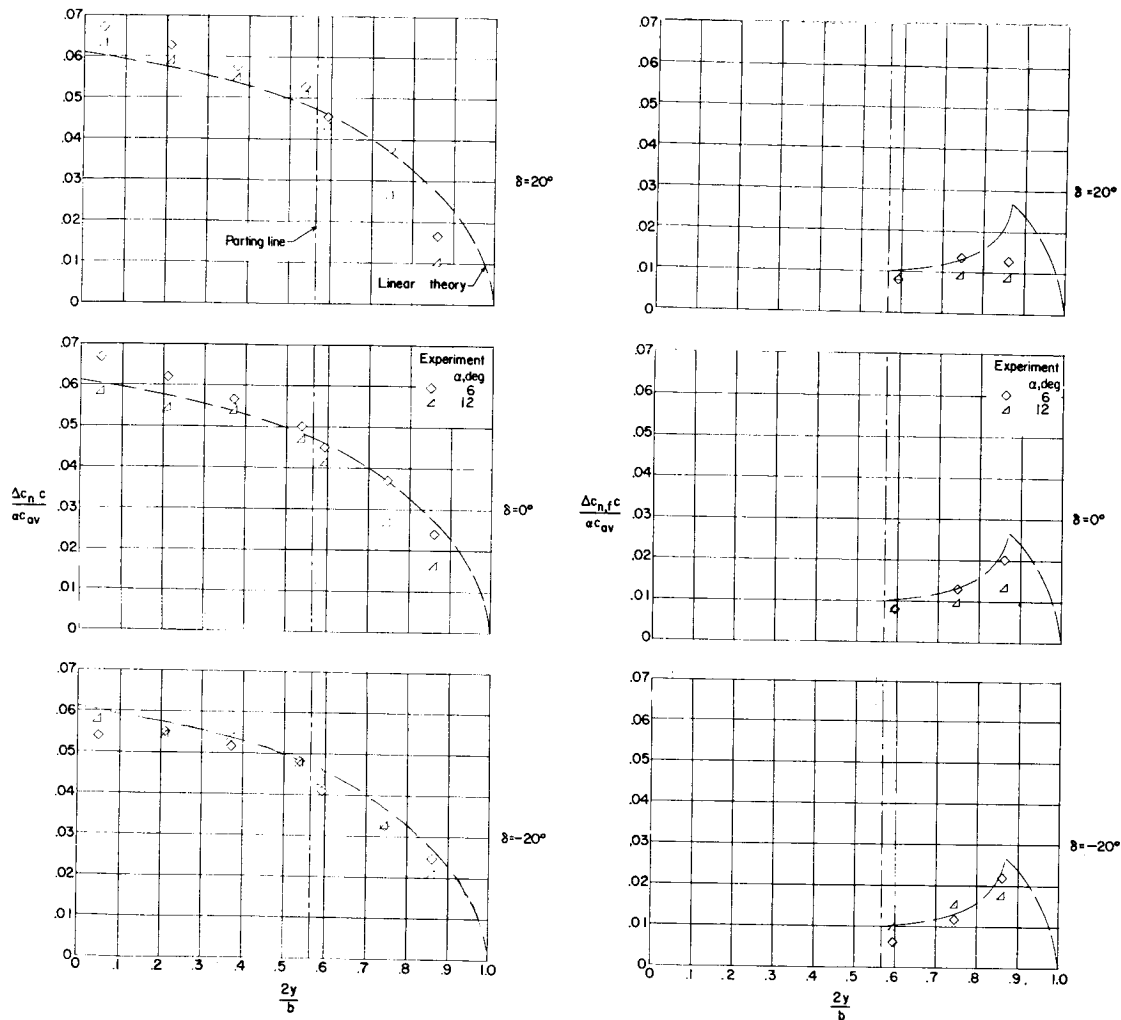


L-75294.1
Figure 4.- Photograph of configuration J mounted on the boundary-layer
bypass plate.



(a) Wing normal-force loading due to δ . (b) Control normal-force loading due to δ .

Figure 5.- Spanwise normal-force loading distributions for configuration A. $M = 1.61$.

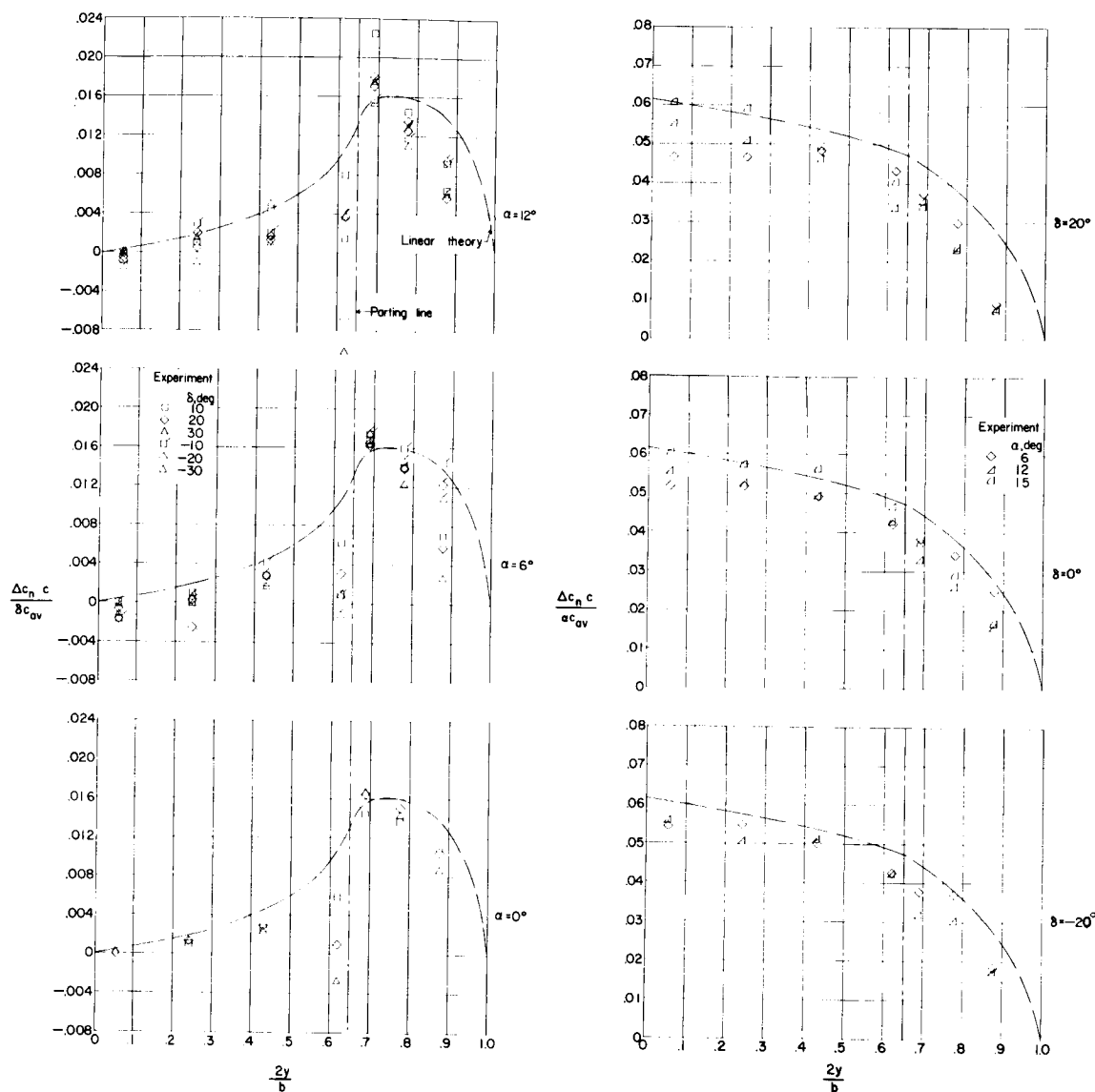


(c) Wing normal-force loading due to α .

(d) Control normal-force loading due to α .

Figure 5.- Concluded.

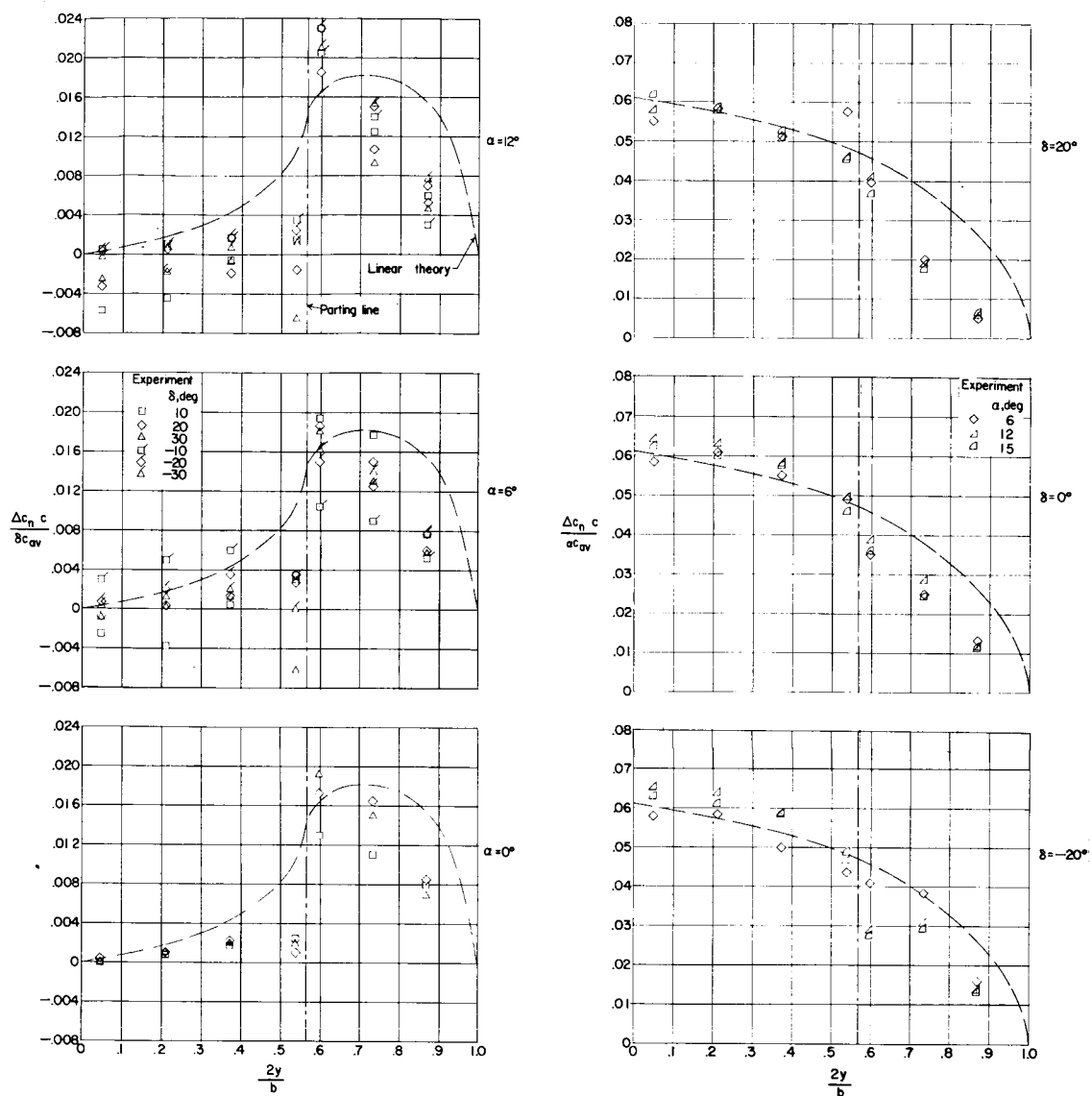
037102000000



(a) Wing normal-force loading due to δ .

(b) Wing normal-force loading due to α .

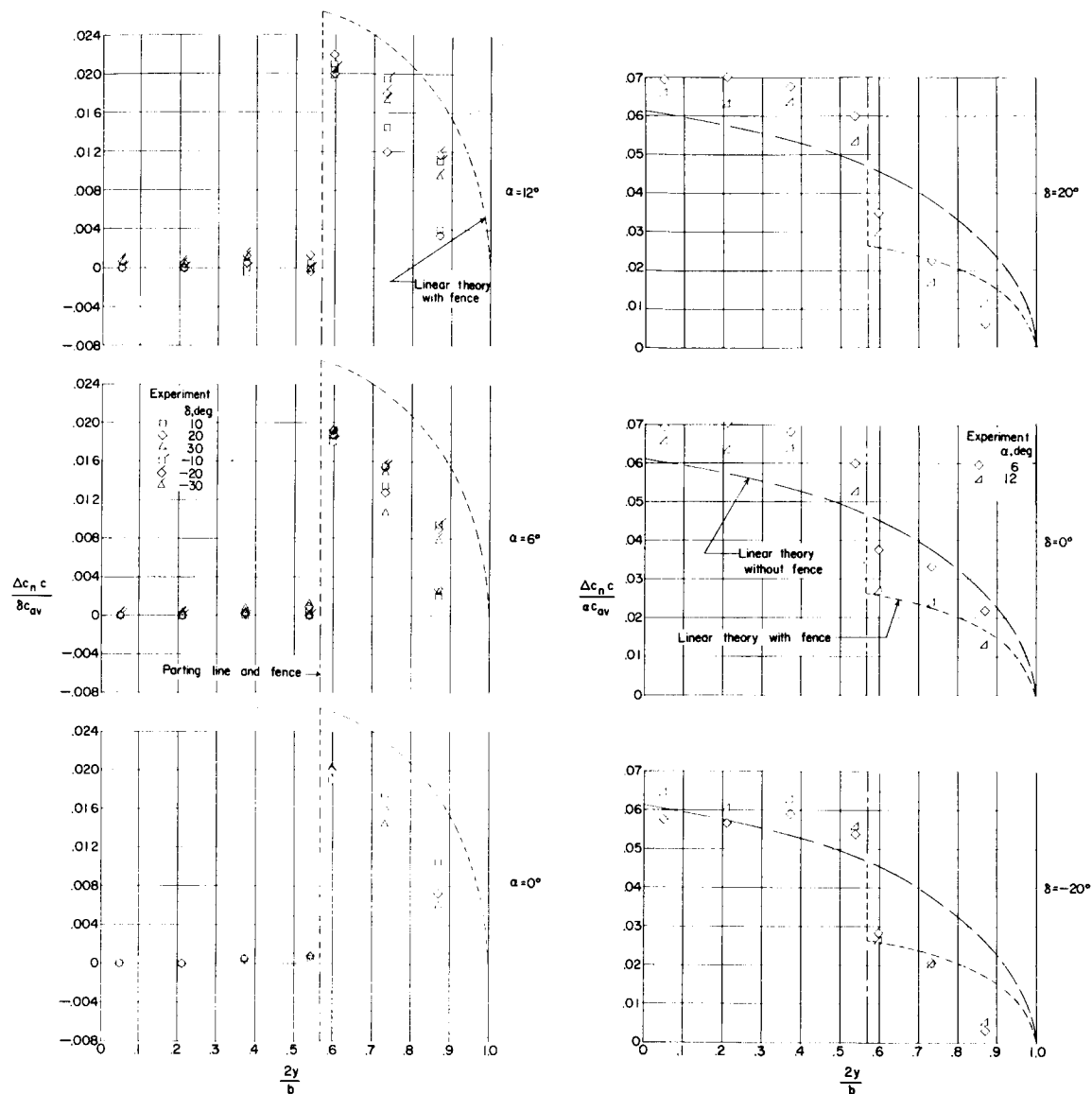
Figure 6.- Spanwise normal-force loading distributions for configuration D. $M = 1.61$.



(a) Wing normal-force loading due to δ .

(b) Wing normal-force loading due to α .

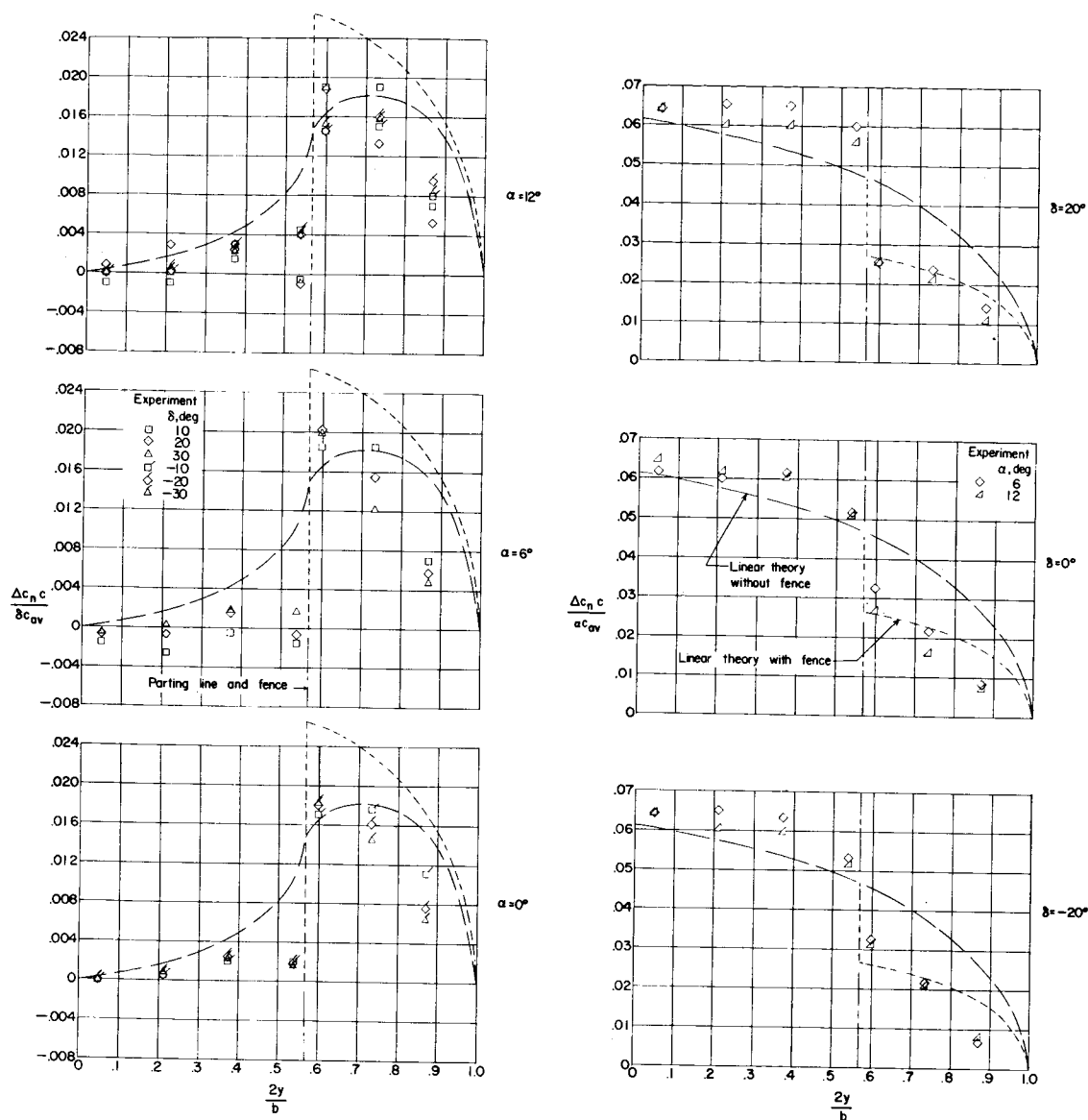
Figure 7.- Spanwise normal-force loading distributions for configuration E. $M = 1.61$.



(a) Wing normal-force loading due to δ .

(b) Wing normal-force loading due to α .

Figure 8.- Spanwise normal-force loading distributions for configuration E2. $M = 1.61$.

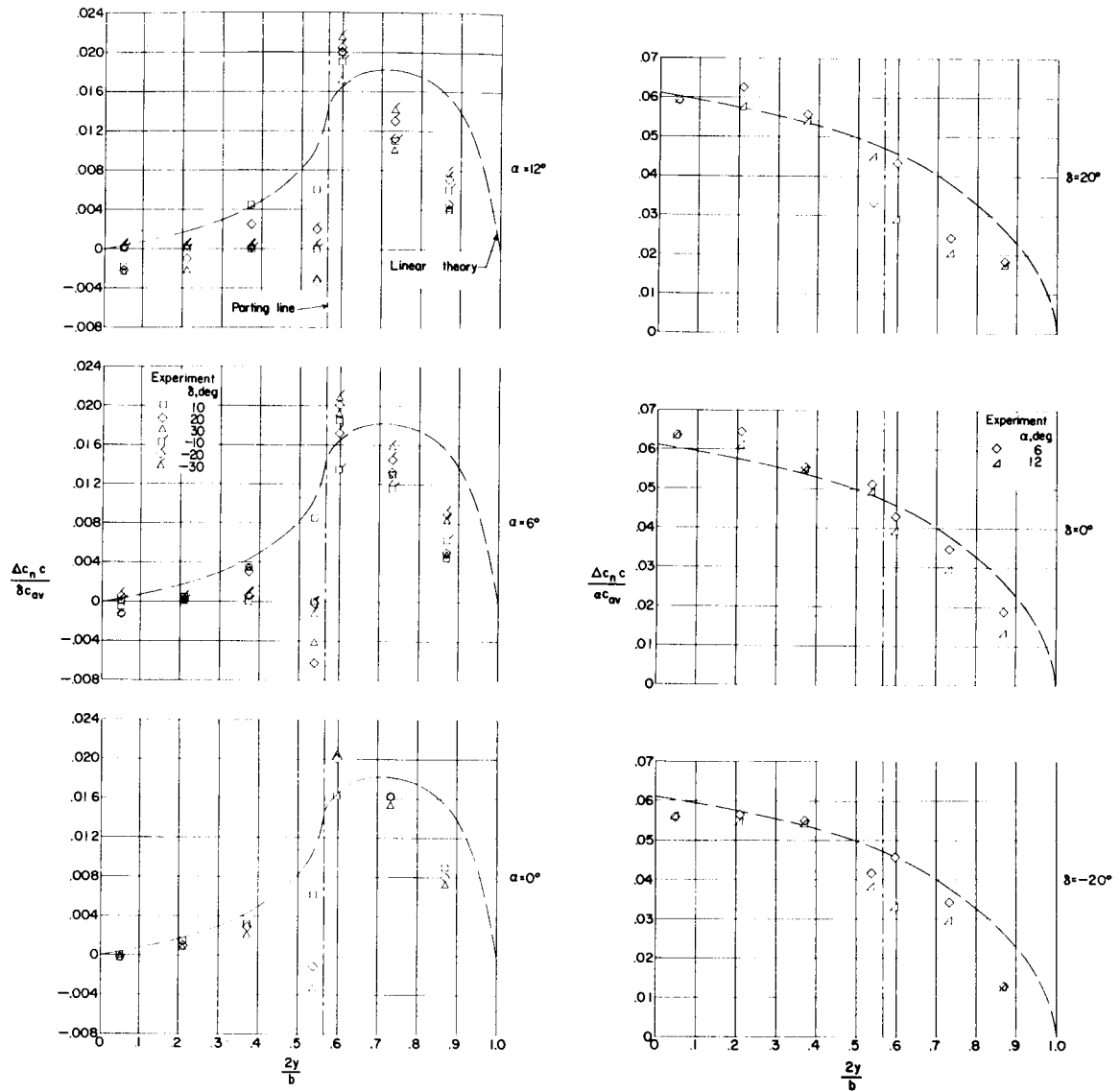


(a) Wing normal-force loading due to δ .

(b) Wing normal-force loading due to α .

Figure 9.- Spanwise normal-force loading distributions for configuration E3. $M = 1.61$.

CONFIDENTIAL



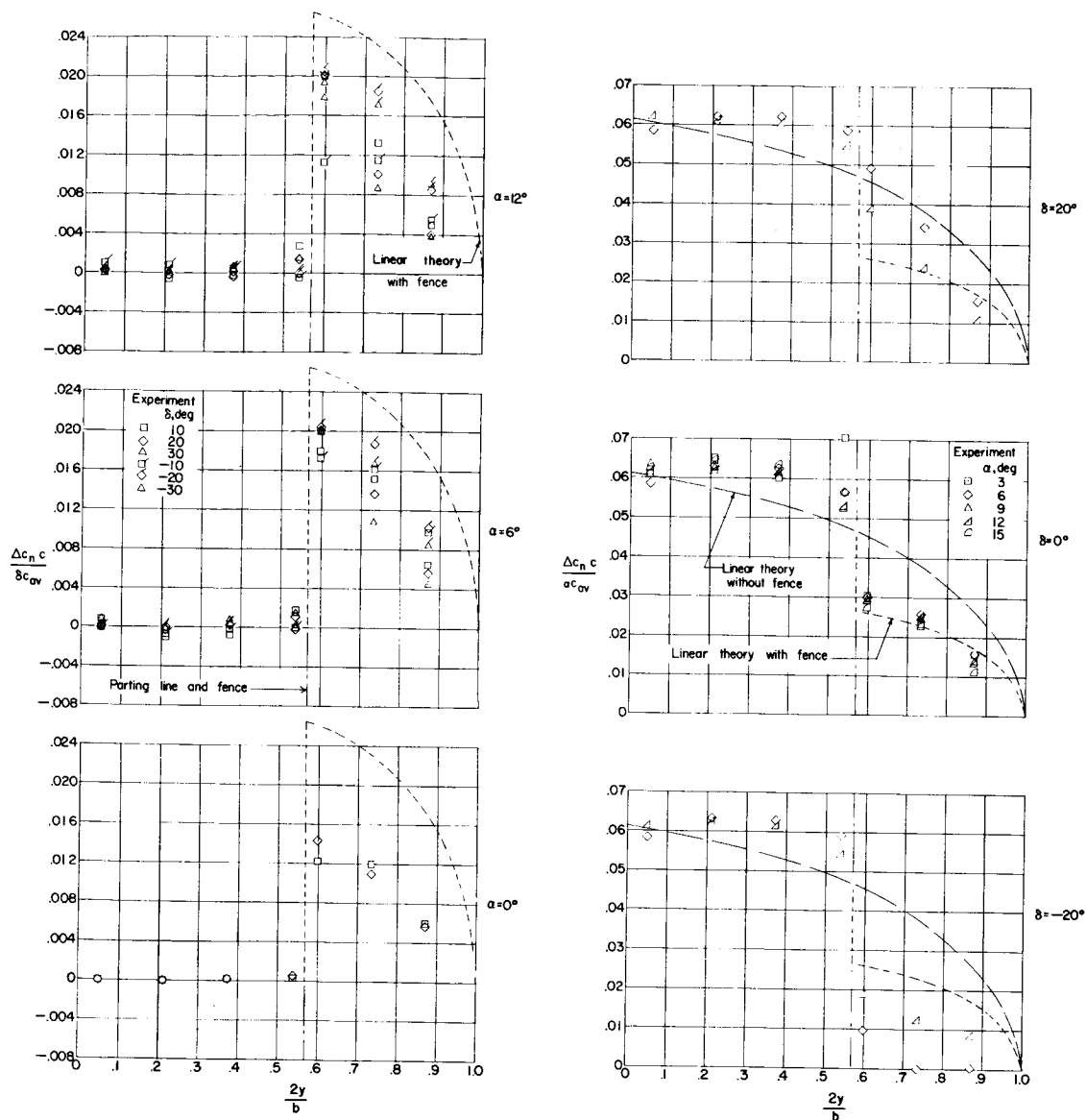
(a) Wing normal-force loading due to δ .

(b) Wing normal-force loading due to α .

Figure 10.- Spanwise normal-force loading distributions for configuration F. $M = 1.61$.

CONFIDENTIAL

L-258

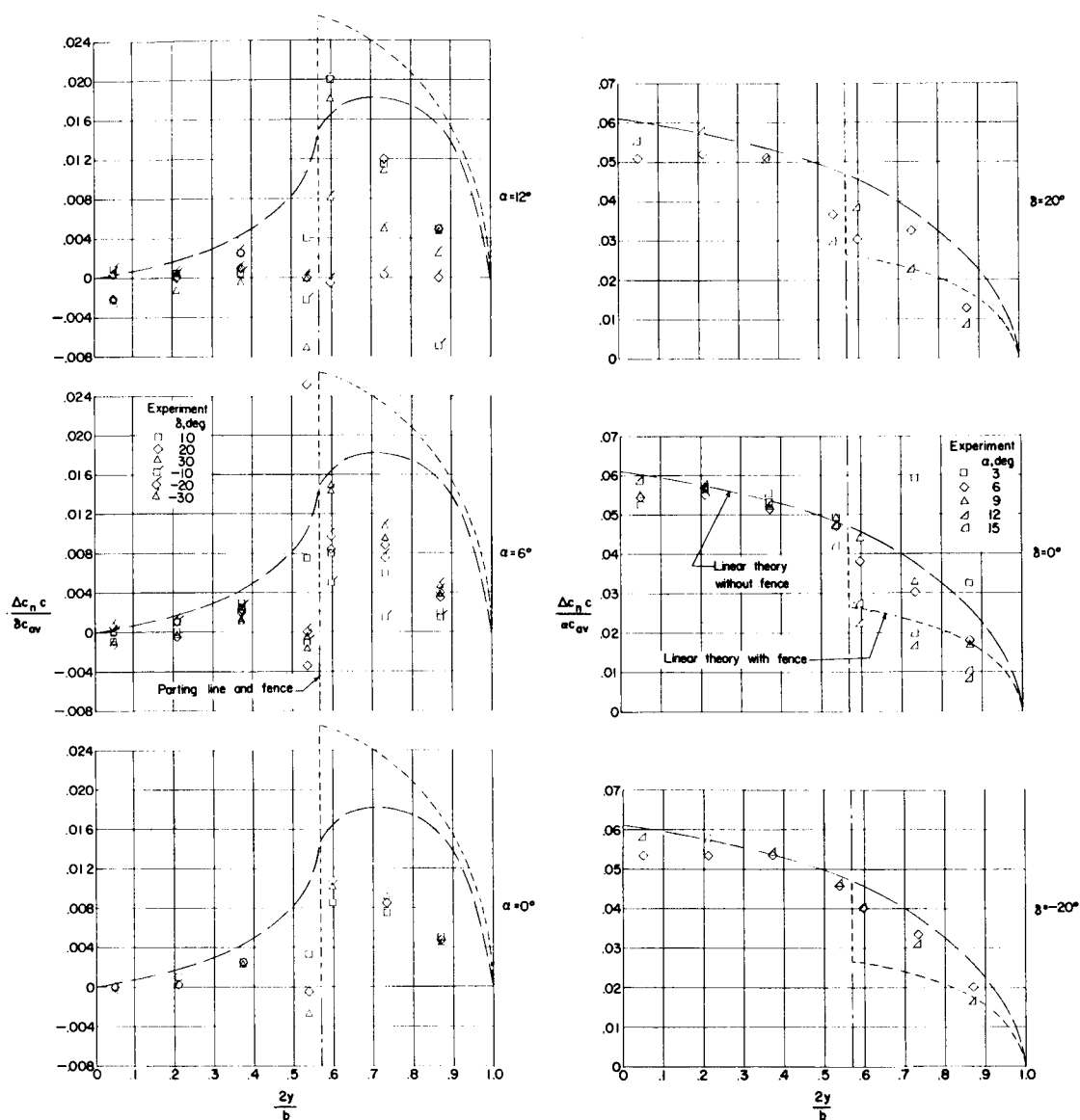


(a) Wing normal-force loading due to δ .

(b) Wing normal-force loading due to α .

Figure 11.- Spanwise normal-force loading distributions for configuration F1. $M = 1.61$.

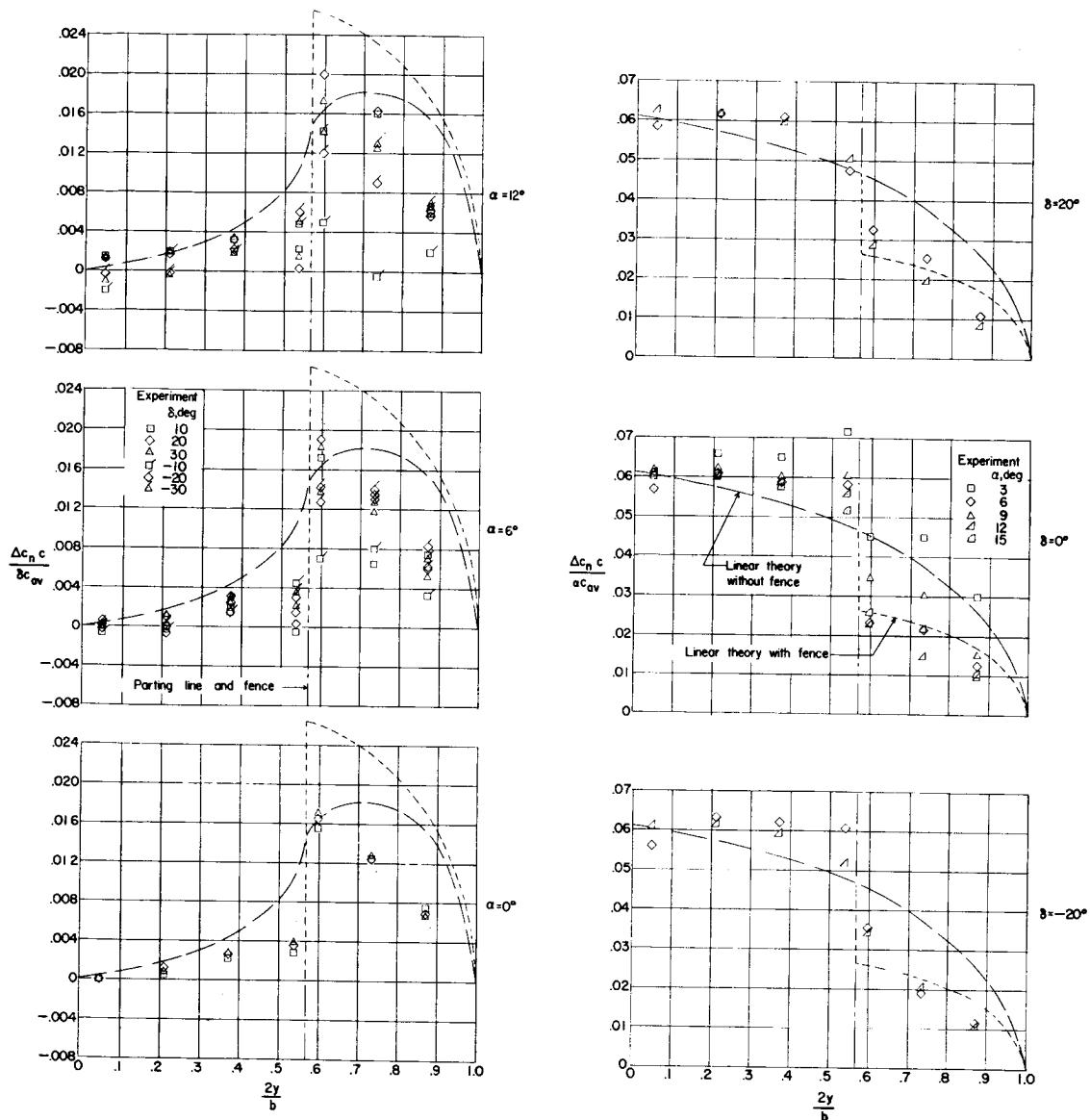
CONFIDENTIAL



(a) Wing normal-force loading due to δ .

(b) Wing normal-force loading due to α .

Figure 12.- Spanwise normal-force loading distributions for configuration F2. $M = 1.61$.

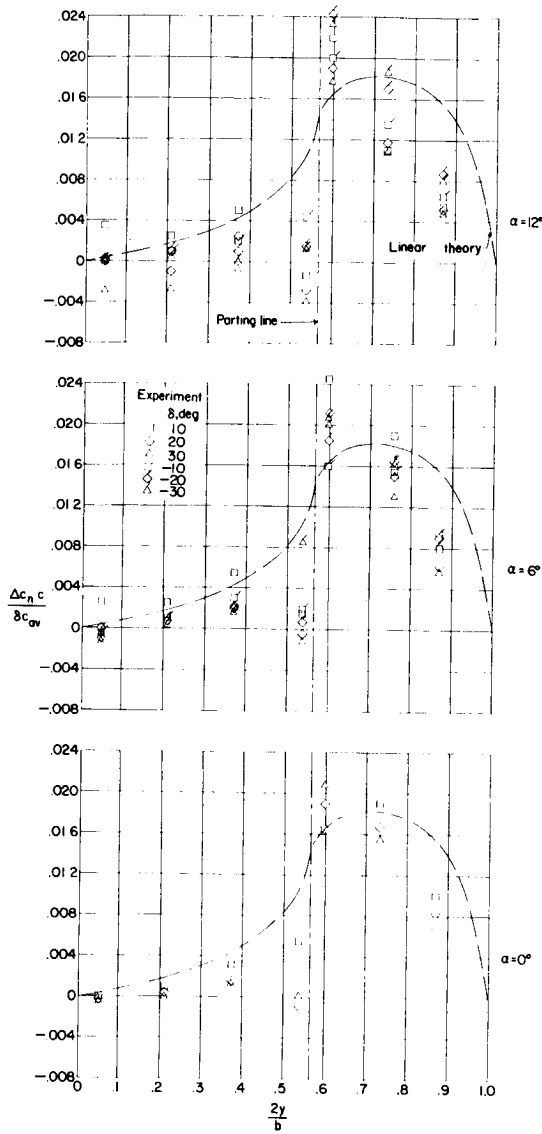


(a) Wing normal-force loading due to δ .

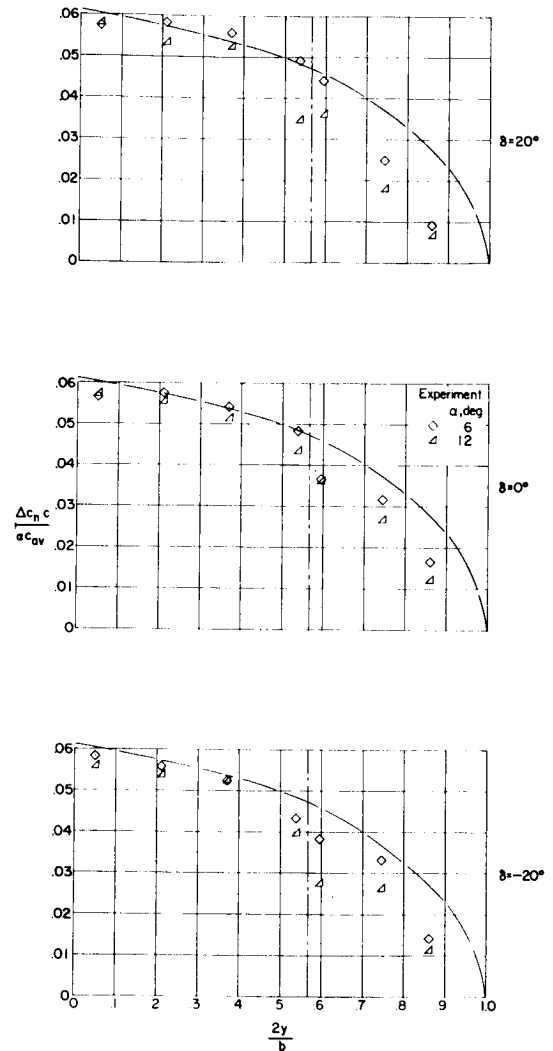
(b) Wing normal-force loading due to α .

Figure 13.- Spanwise normal-force loading distributions for configuration F3. $M = 1.61$.

0371226123

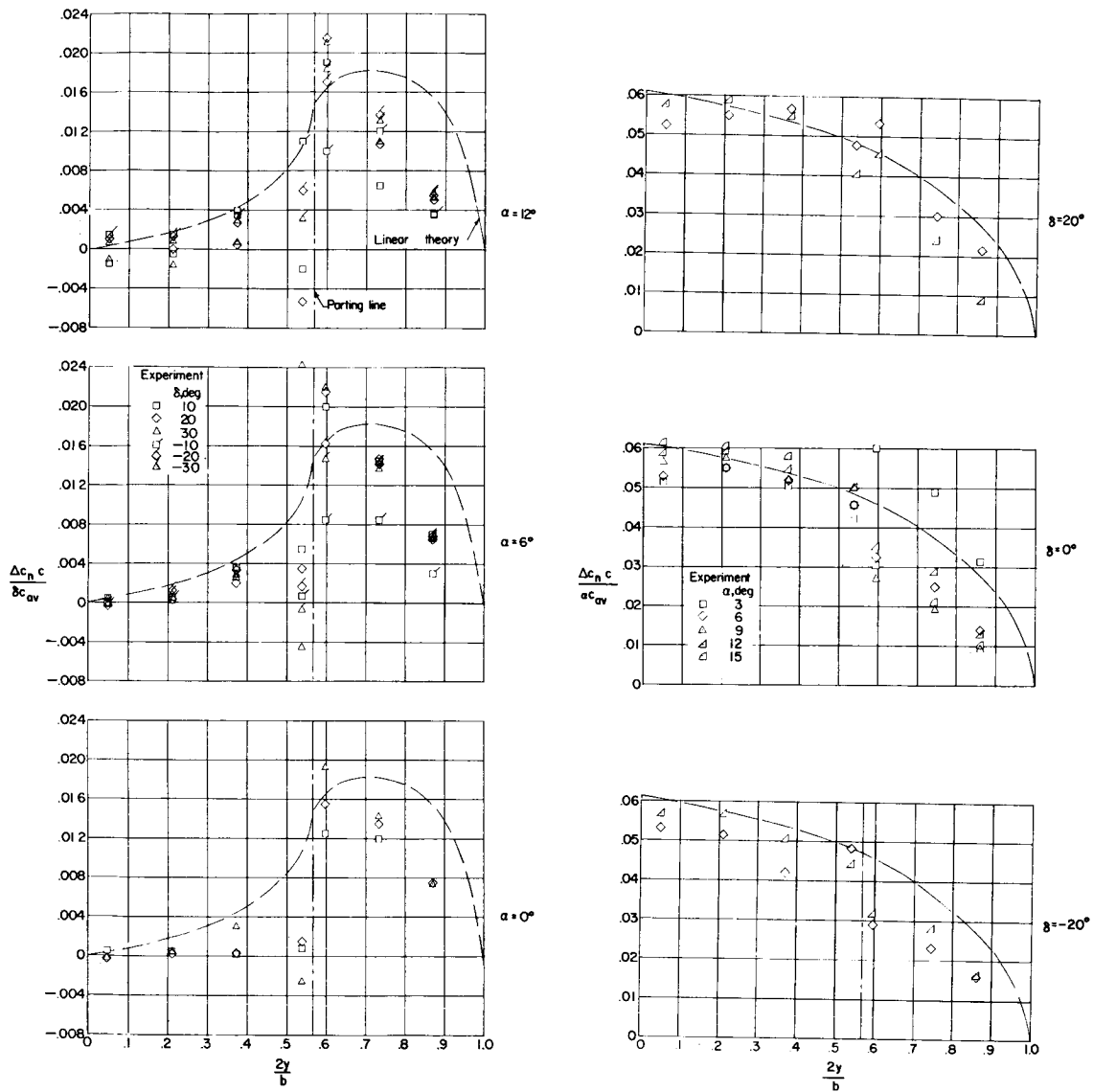


(a) Wing normal-force loading due to δ .



(b) Wing normal-force loading due to α .

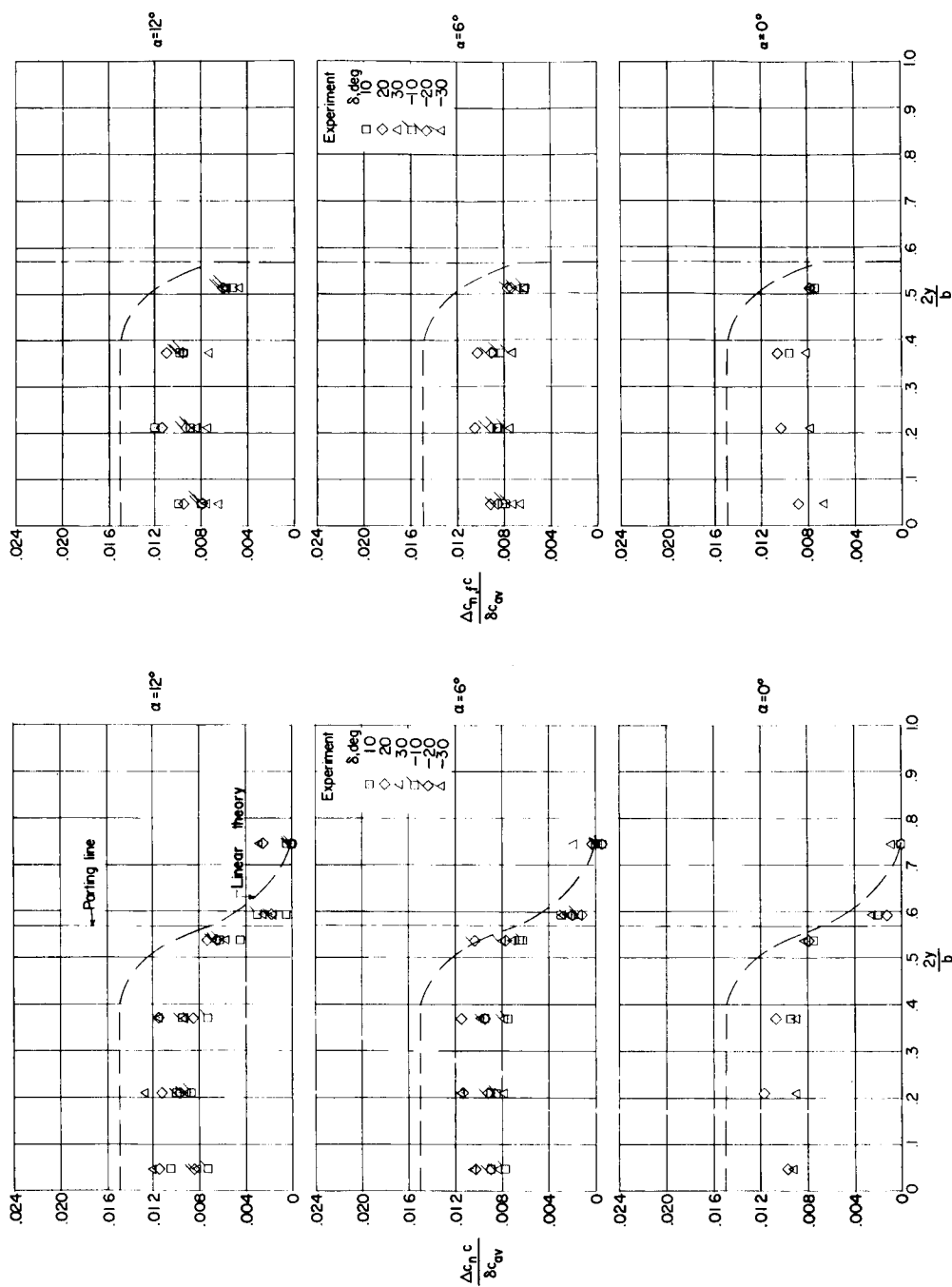
Figure 14.- Spanwise normal-force loading distributions for configuration G. $M = 1.61$.



(a) Wing normal-force loading due to δ .

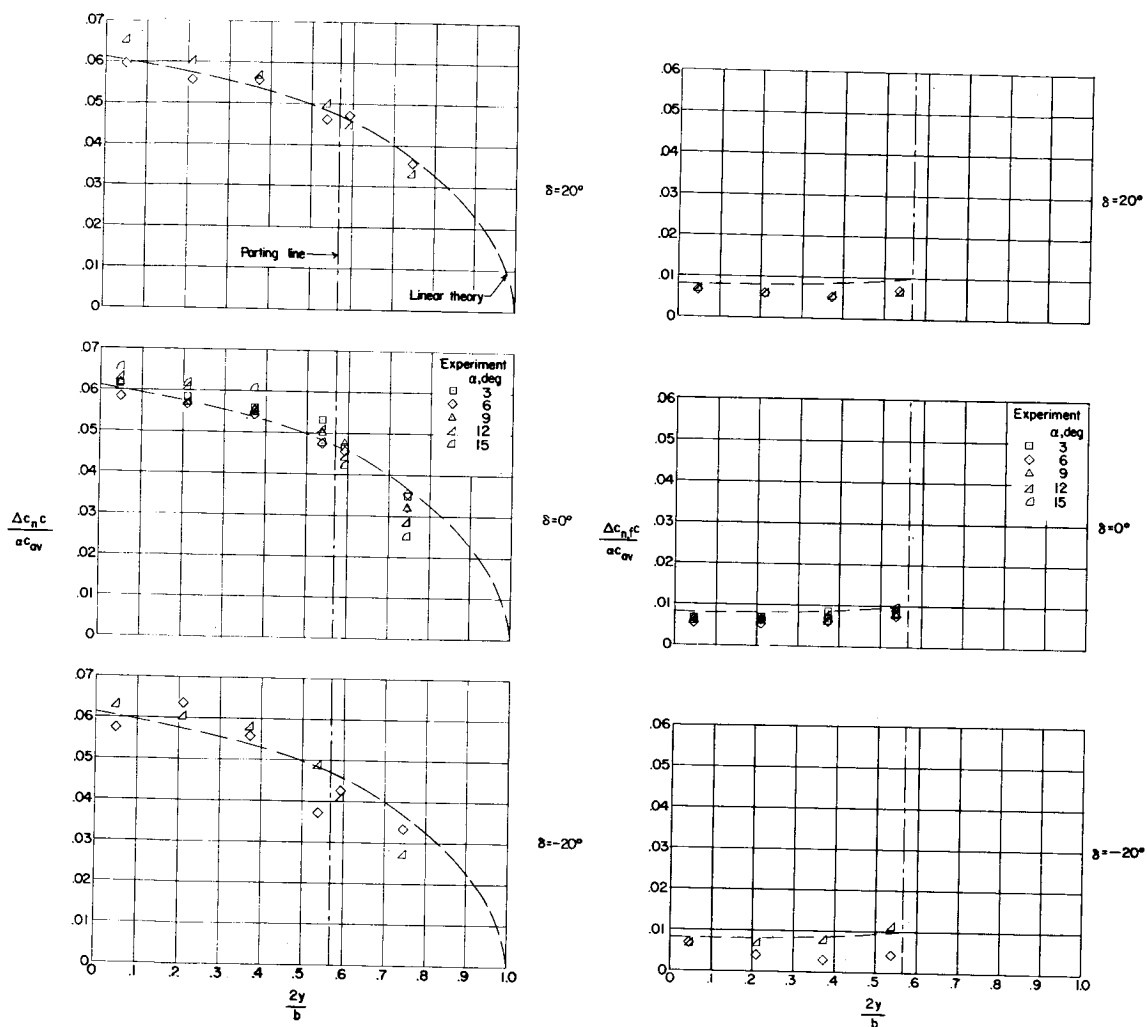
(b) Wing normal-force loading due to α .

Figure 15.- Spanwise normal-force loading distributions for configuration H. $M = 1.61$.



(a) Wing normal-force loading due to δ . (b) Control normal-force loading due to δ .
 Figure 16.- Spanwise normal-force loading distributions for configuration I. $M = 1.61$.

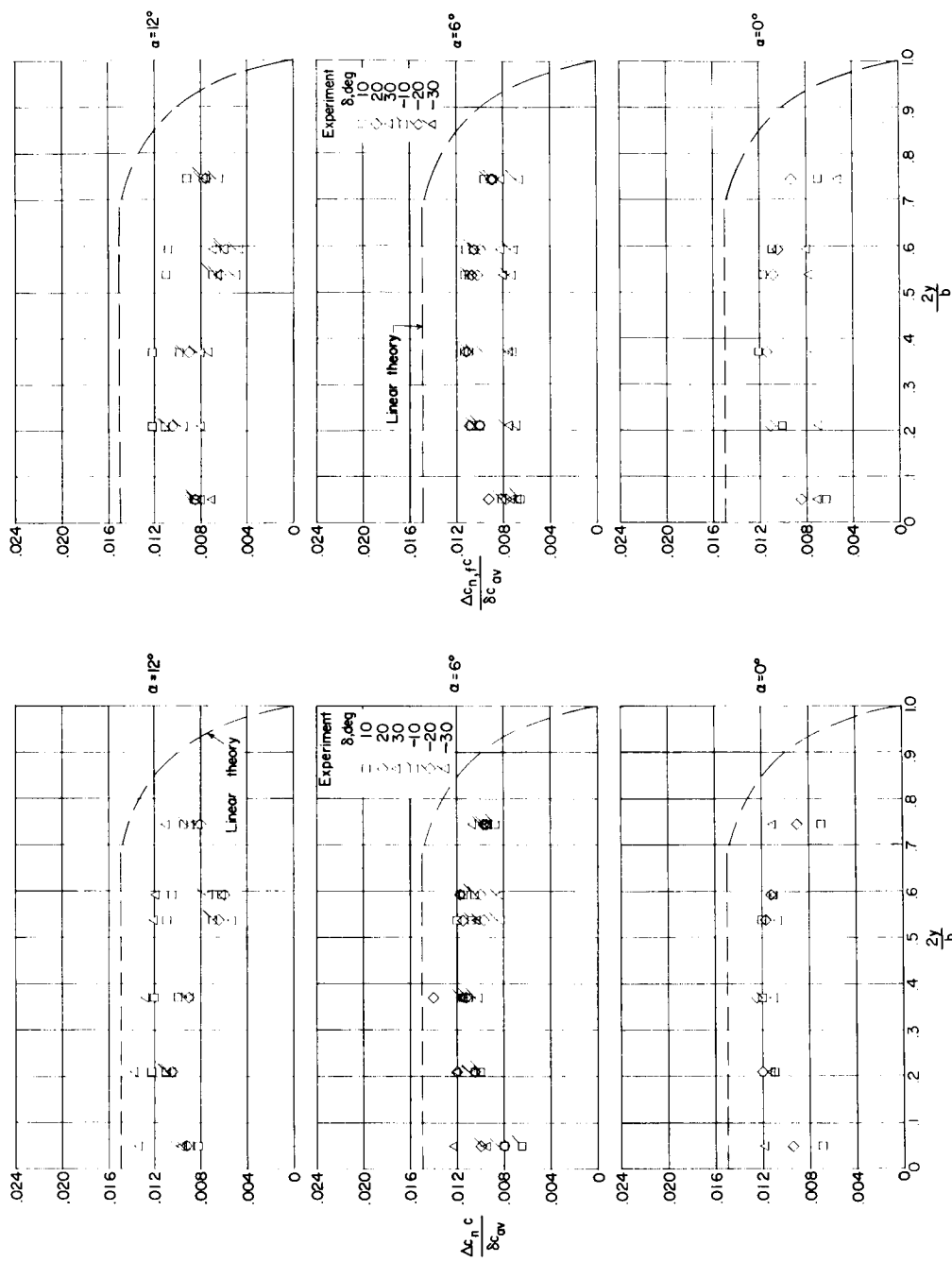
CONFIDENTIAL



(c) Wing normal-force loading
due to α .

(d) Control normal-force loading
due to α .

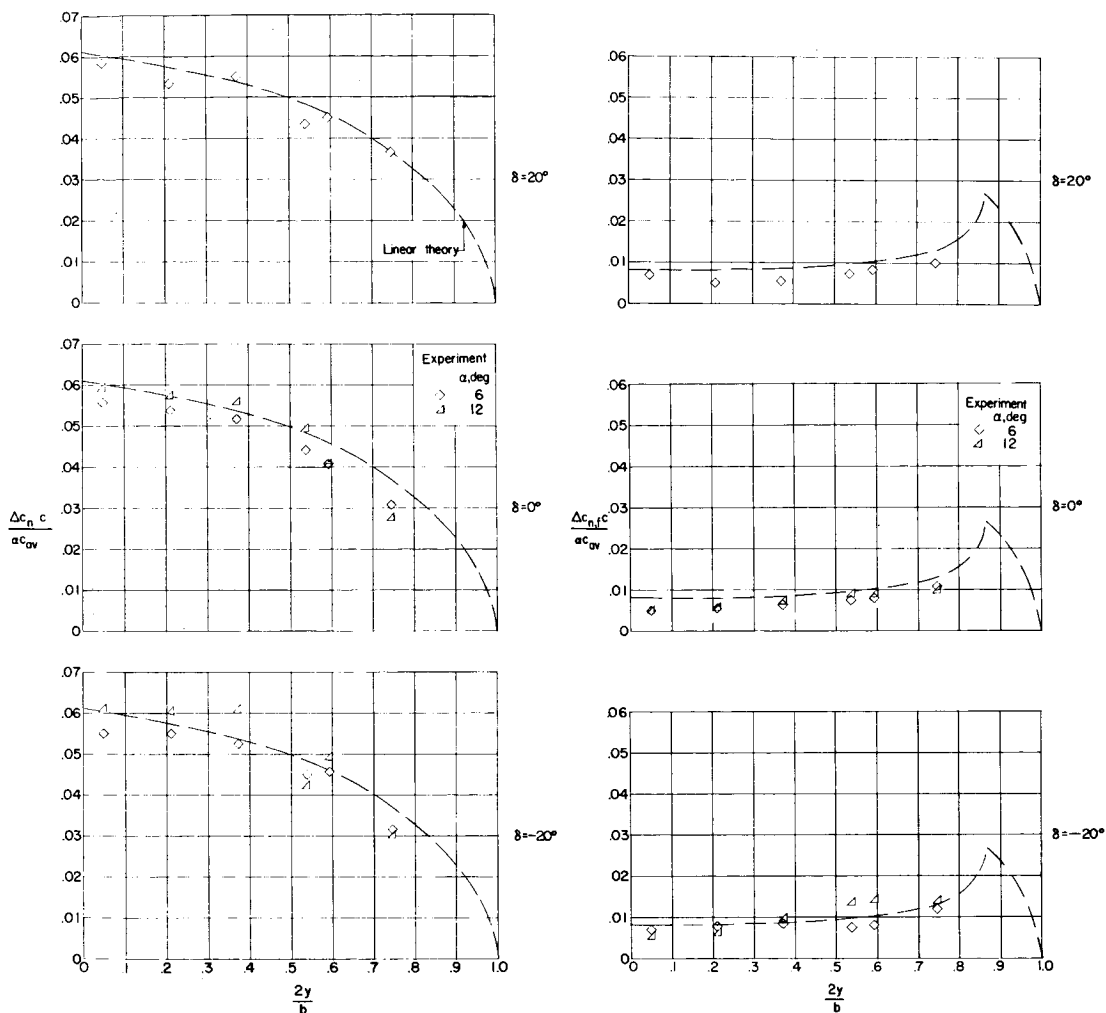
Figure 16.- Concluded.



(a) Wing normal-force loading due to δ . (b) Control normal-force loading due to δ .

Figure 17.- Spanwise normal-force loading distributions for configuration J. $M = 1.61$.

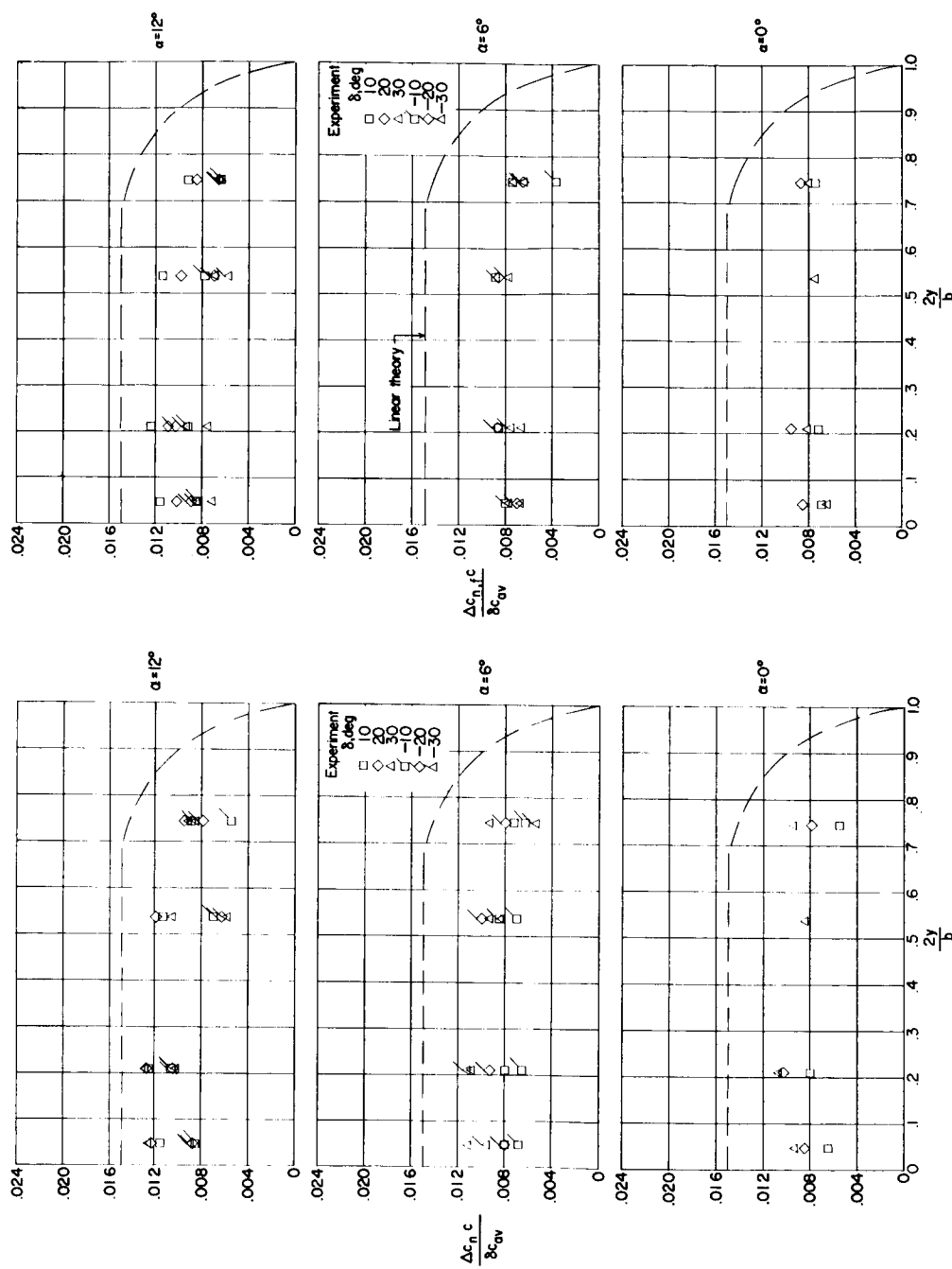
L-258



(c) Wing normal-force loading due to α .

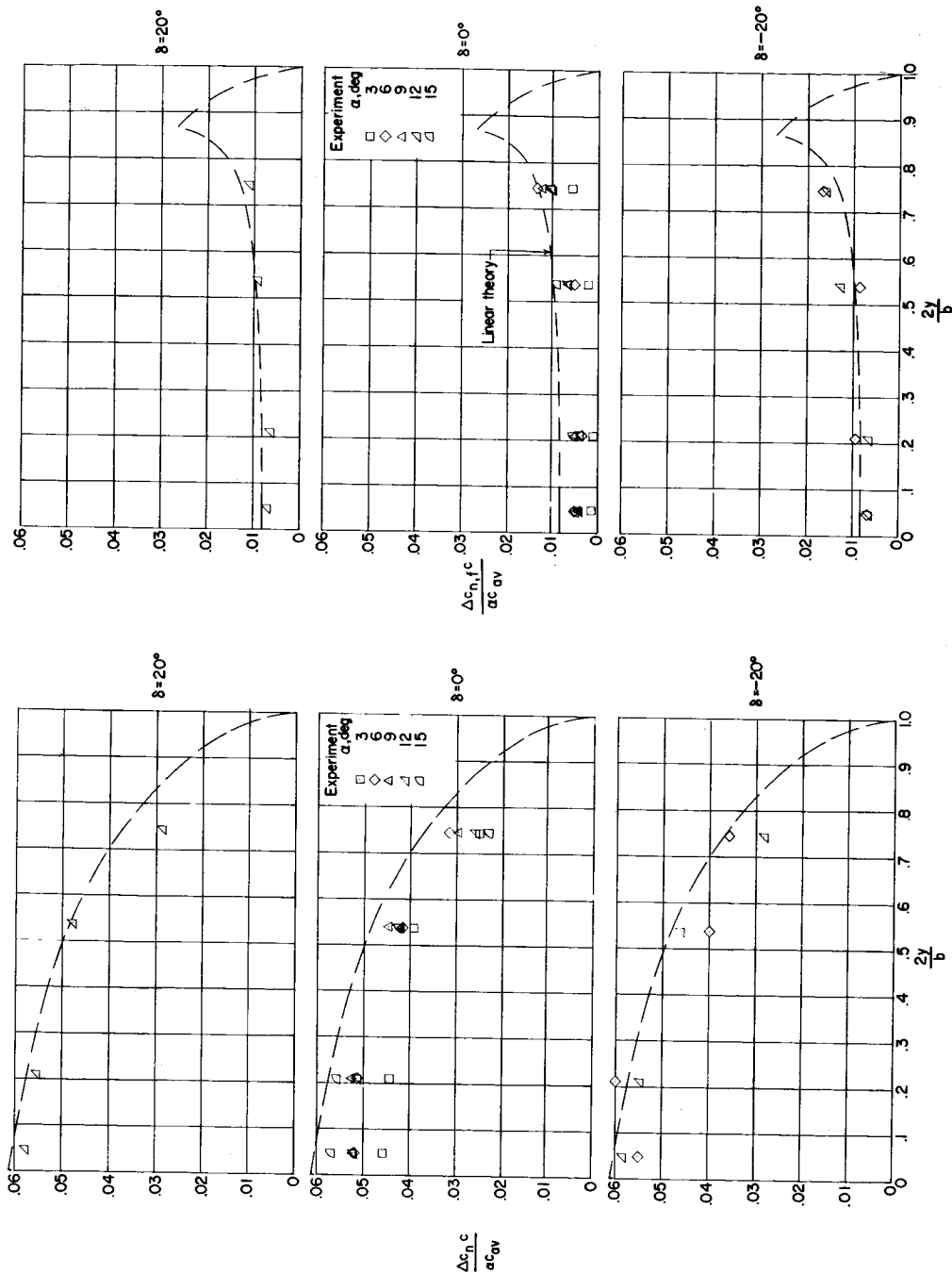
(d) Control normal-force loading due to α .

Figure 17.- Concluded.



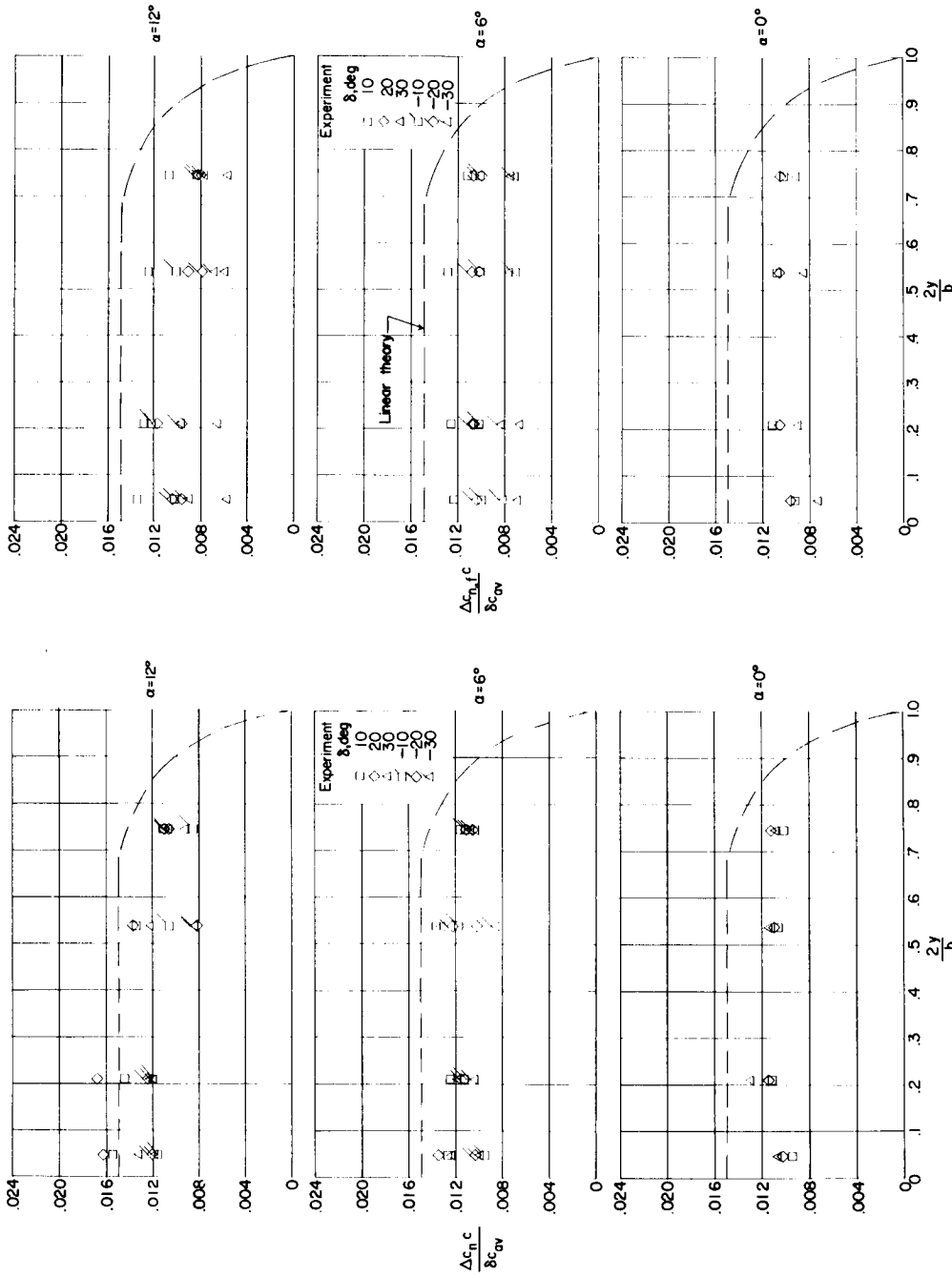
(a) Wing normal-force loading due to δ . (b) Control normal-force loading due to δ .

Figure 18.- Spanwise normal-force loading distributions for configuration J1. $M = 1.61$.



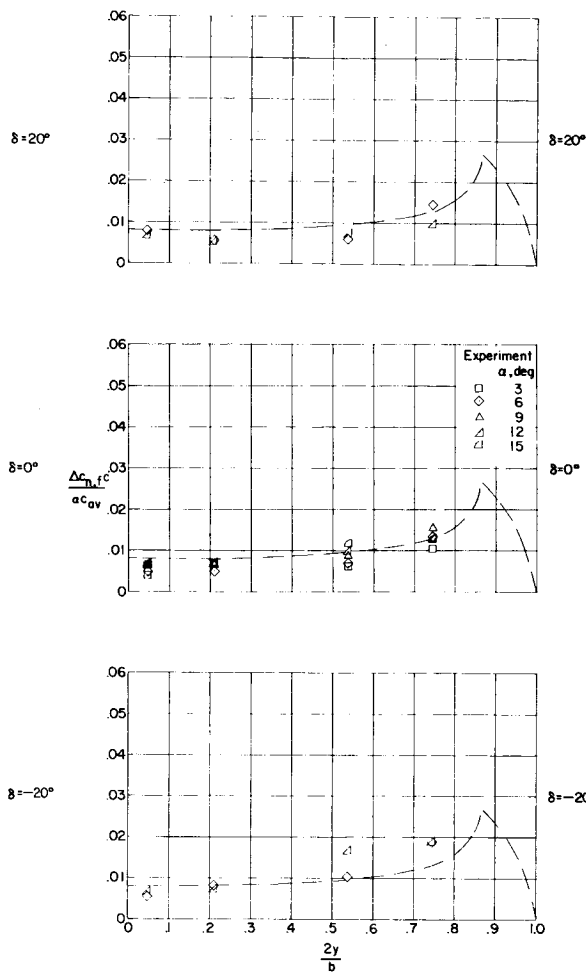
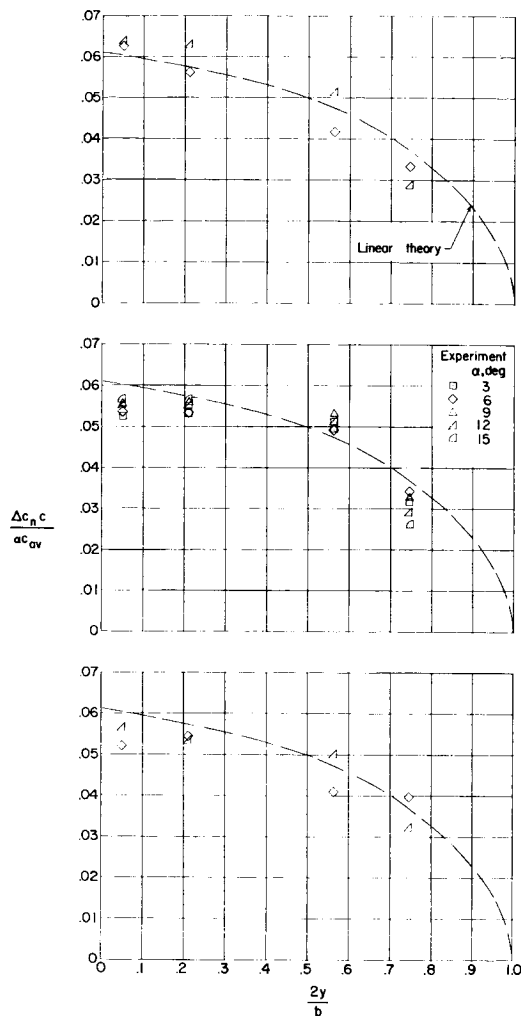
(c) Wing normal-force loading due to α . (d) Control normal-force loading due to α .

Figure 18.- Concluded.



(a) Wing normal-force loading due to δ . (b) Control normal-force loading due to δ .

Figure 19.- Spanwise normal-force loading distributions for configuration J2. $M = 1.61$.

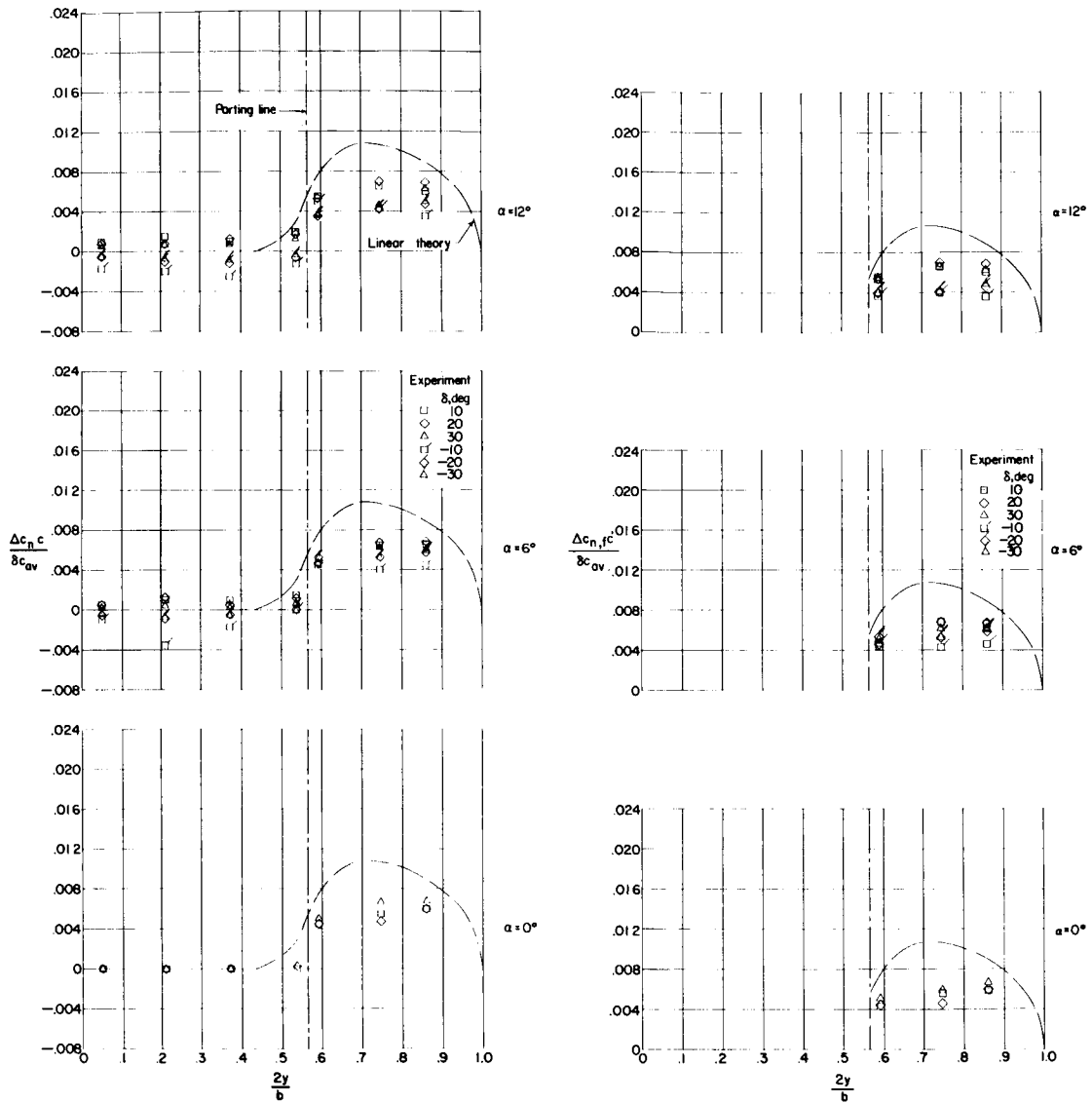


(c) Wing normal-force loading due to α .

(d) Control normal-force loading due to α .

Figure 19.- Concluded.

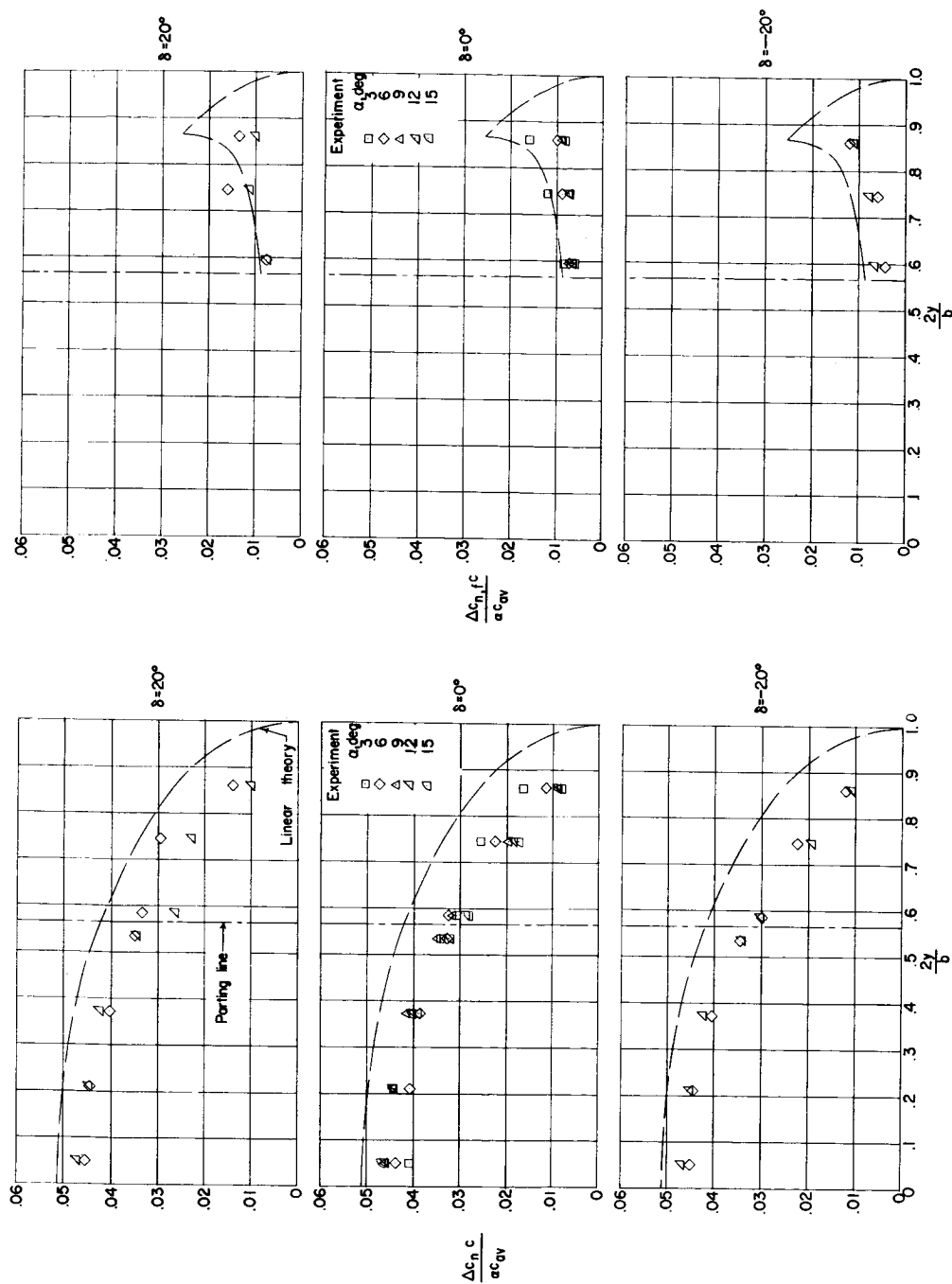
03710 [REDACTED] 30



(a) Wing normal-force loading
due to δ .

(b) Control normal-force loading
due to δ .

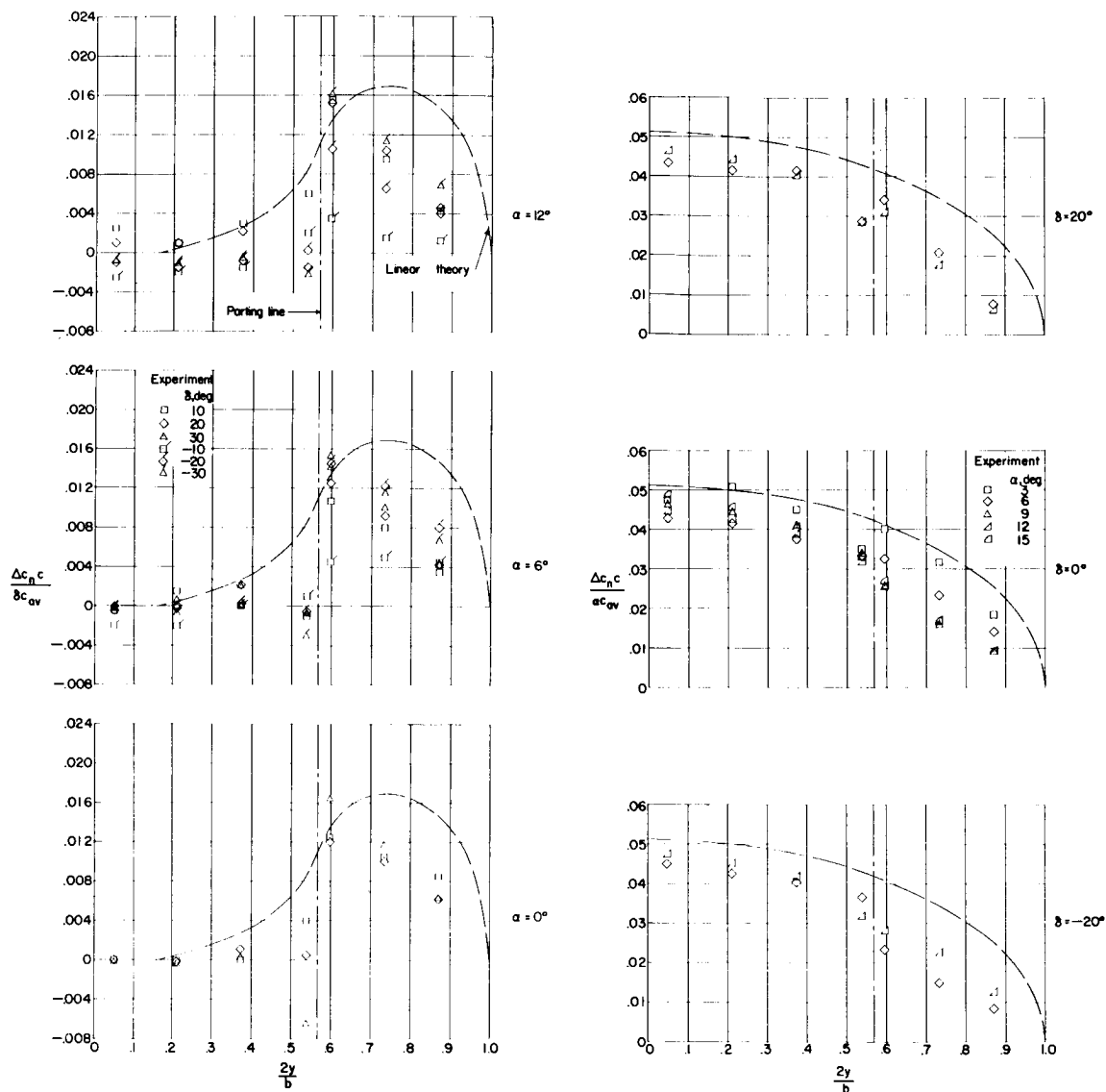
Figure 20.- Spanwise normal-force loading distributions for configuration A. $M = 2.01$.



(c) Wing normal-force loading due to α . (d) Control normal-force loading due to α .

Figure 20.- Concluded.

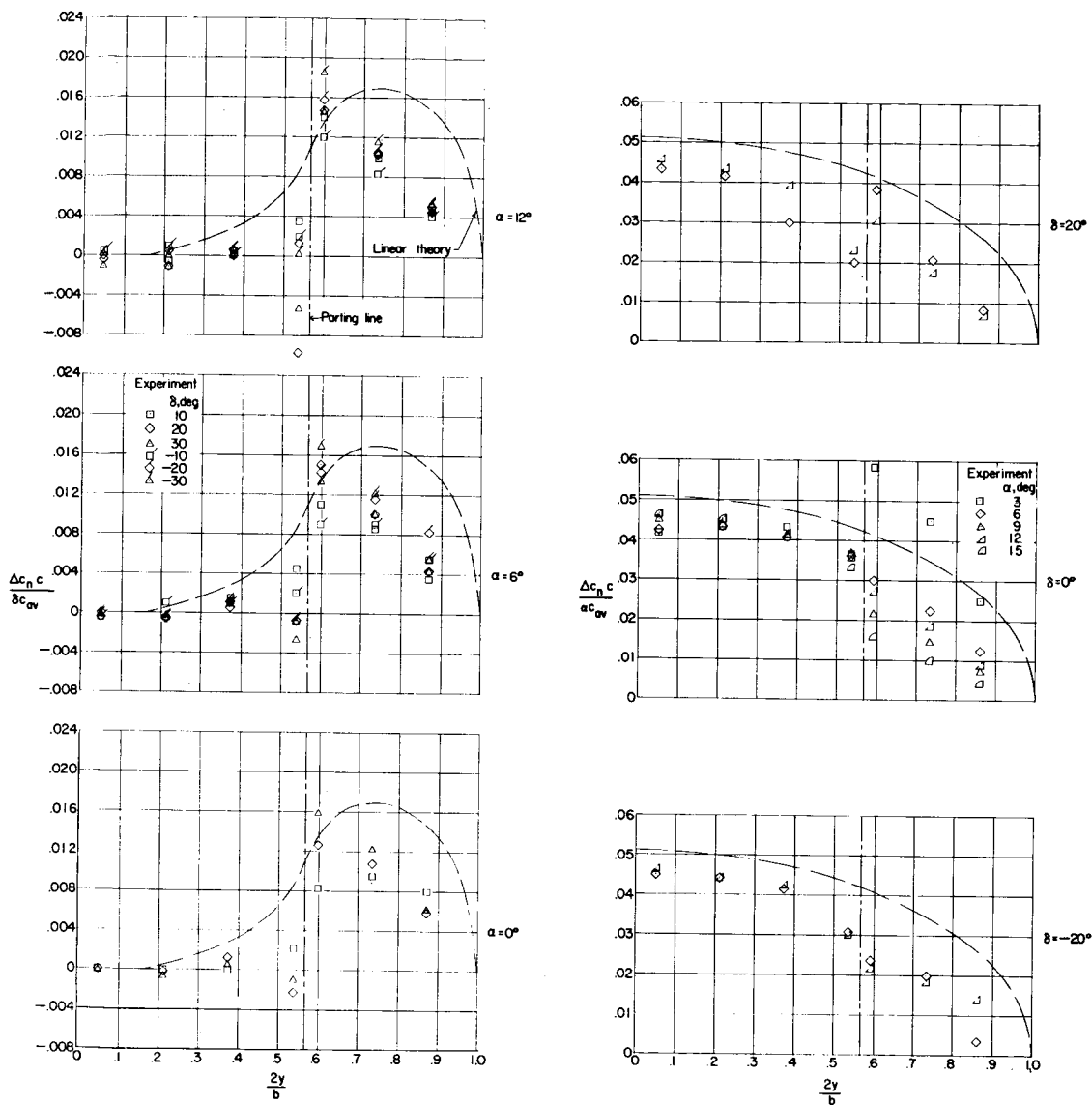
03710 [REDACTED] 30



(a) Wing normal-force loading due to δ .

(b) Wing normal-force loading due to α .

Figure 21.- Spanwise normal-force loading distributions for configuration E. $M = 2.01$.

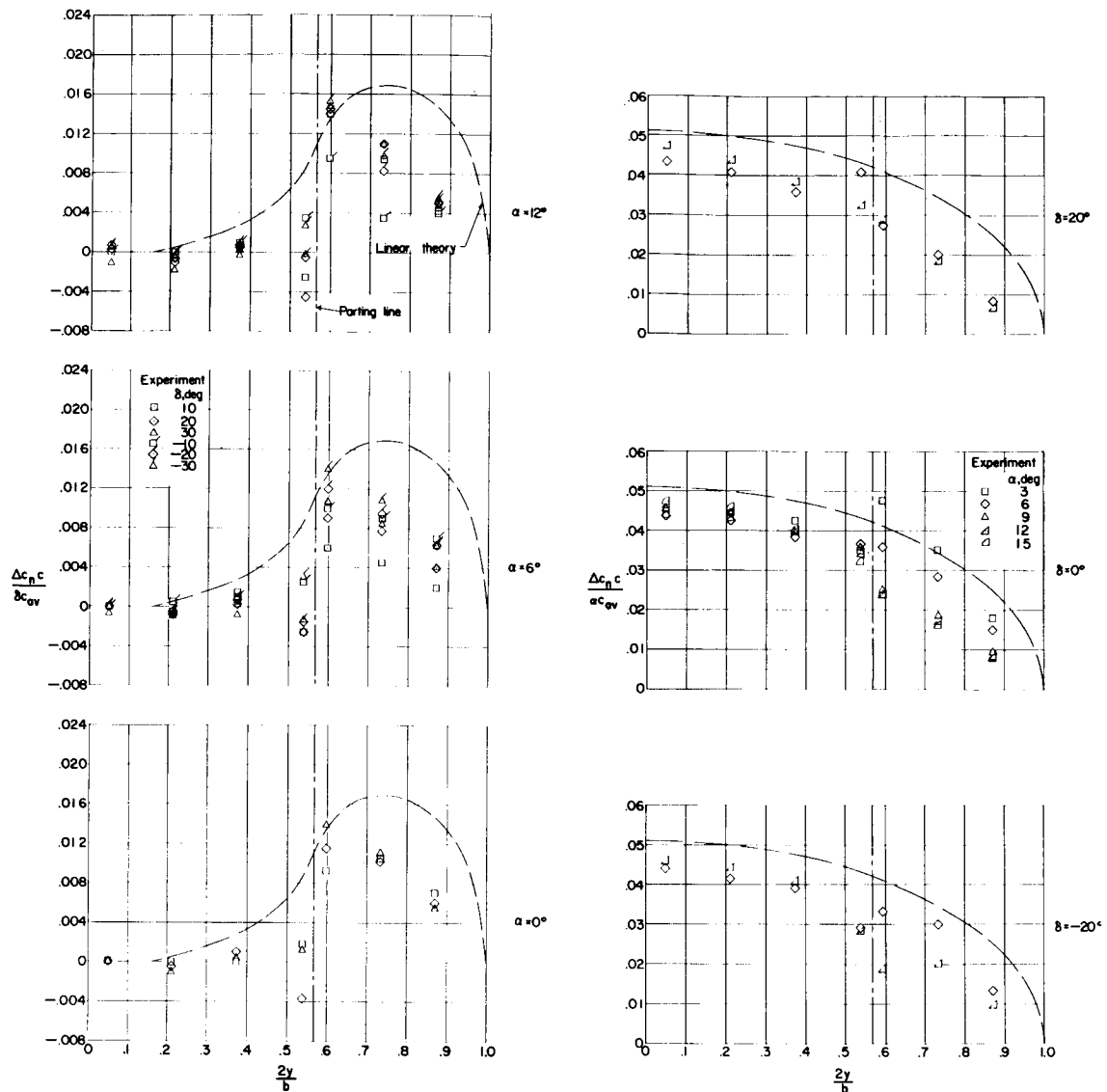


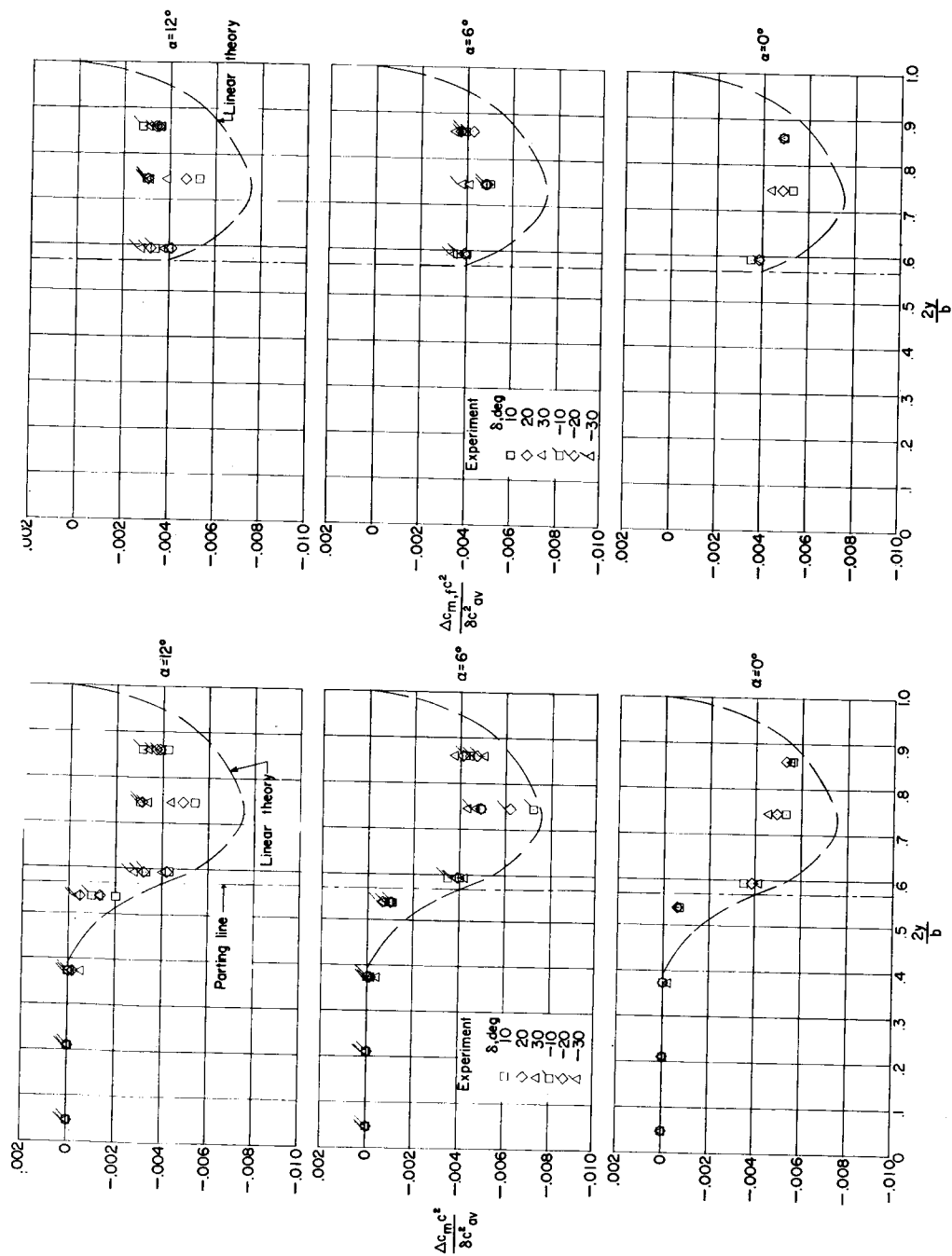
(a) Wing normal-force loading due to δ .

(b) Wing normal-force loading due to α .

Figure 22.- Spanwise normal-force loading distributions for configuration F. $M = 2.01$.

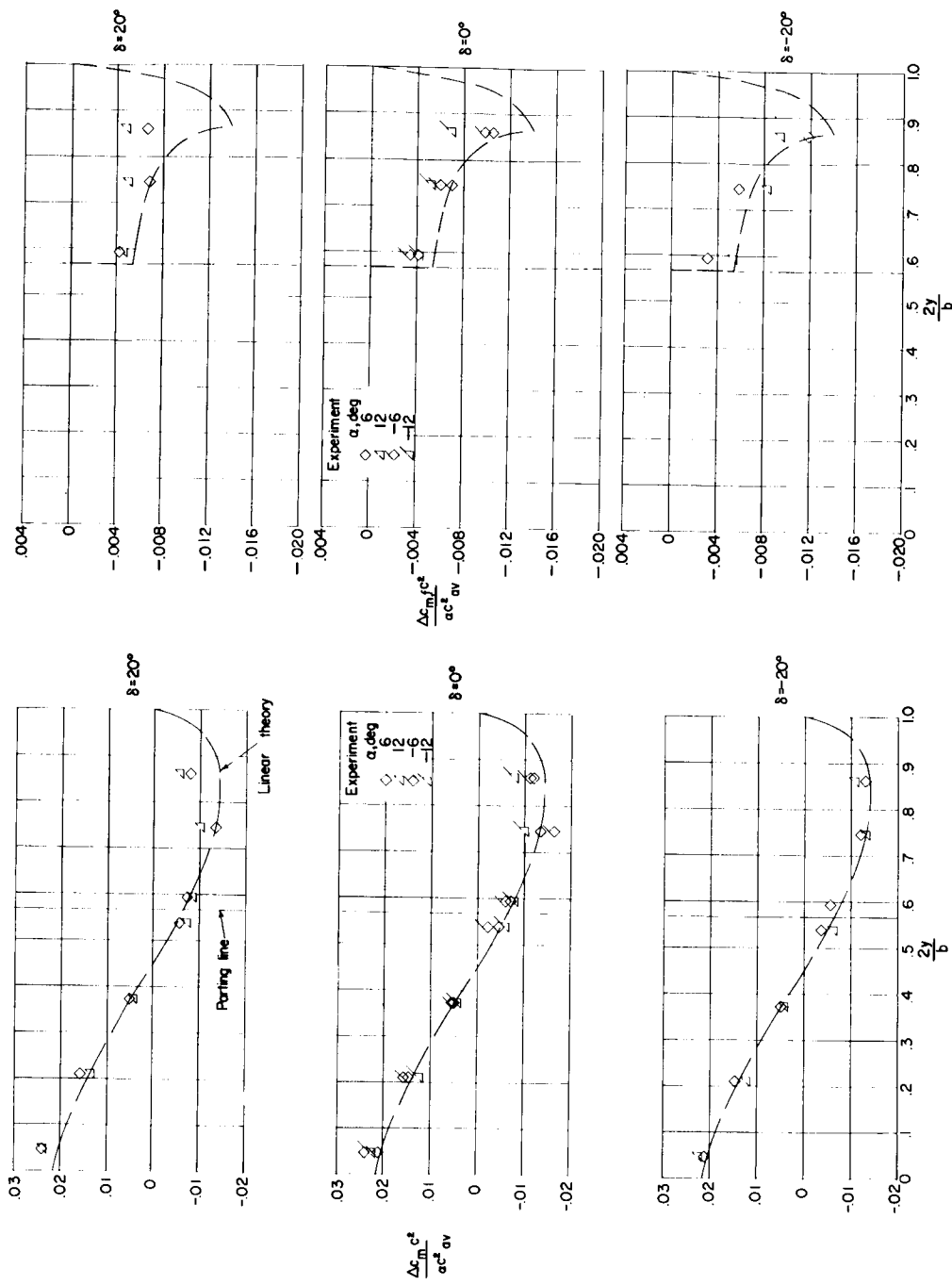
CONFIDENTIAL





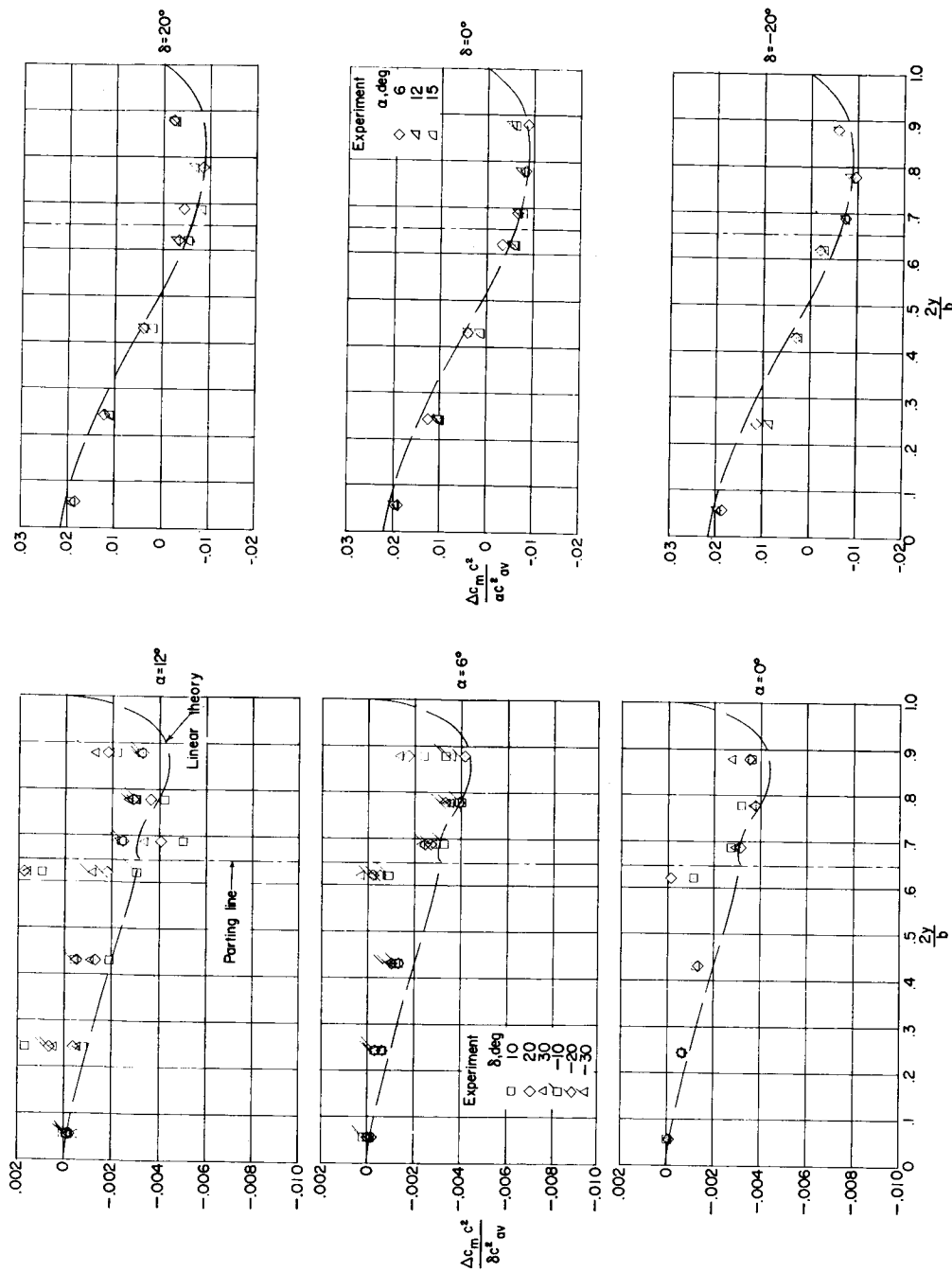
(a) Wing pitching-moment loading due to δ . (b) Control pitching-moment loading due to δ .

Figure 24.- Spanwise pitching-moment distributions for configuration A. $M = 1.61$.

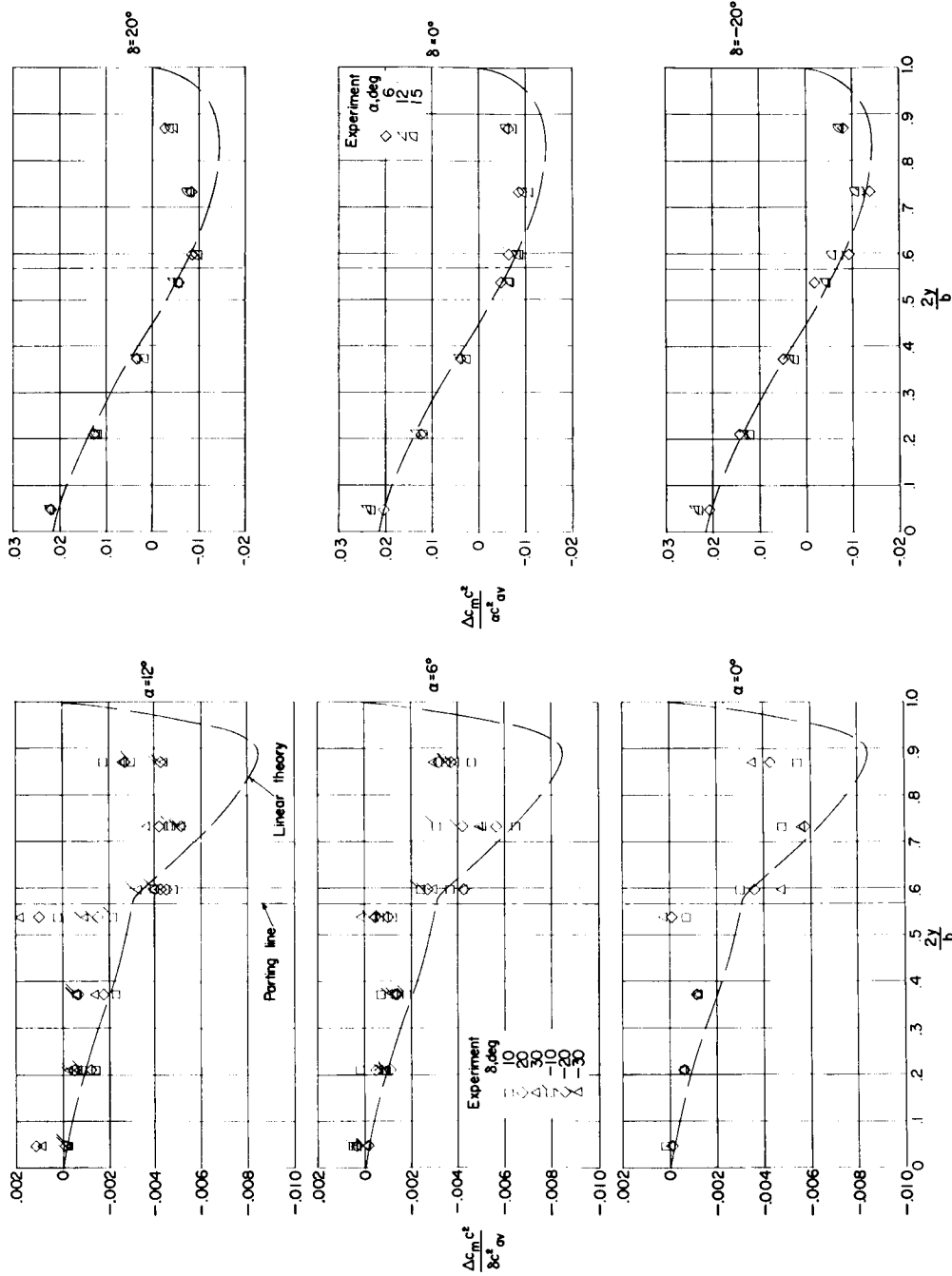


(c) Wing pitching-moment loading due to α . (d) Control pitching-moment loading due to α .

Figure 24.- Concluded.

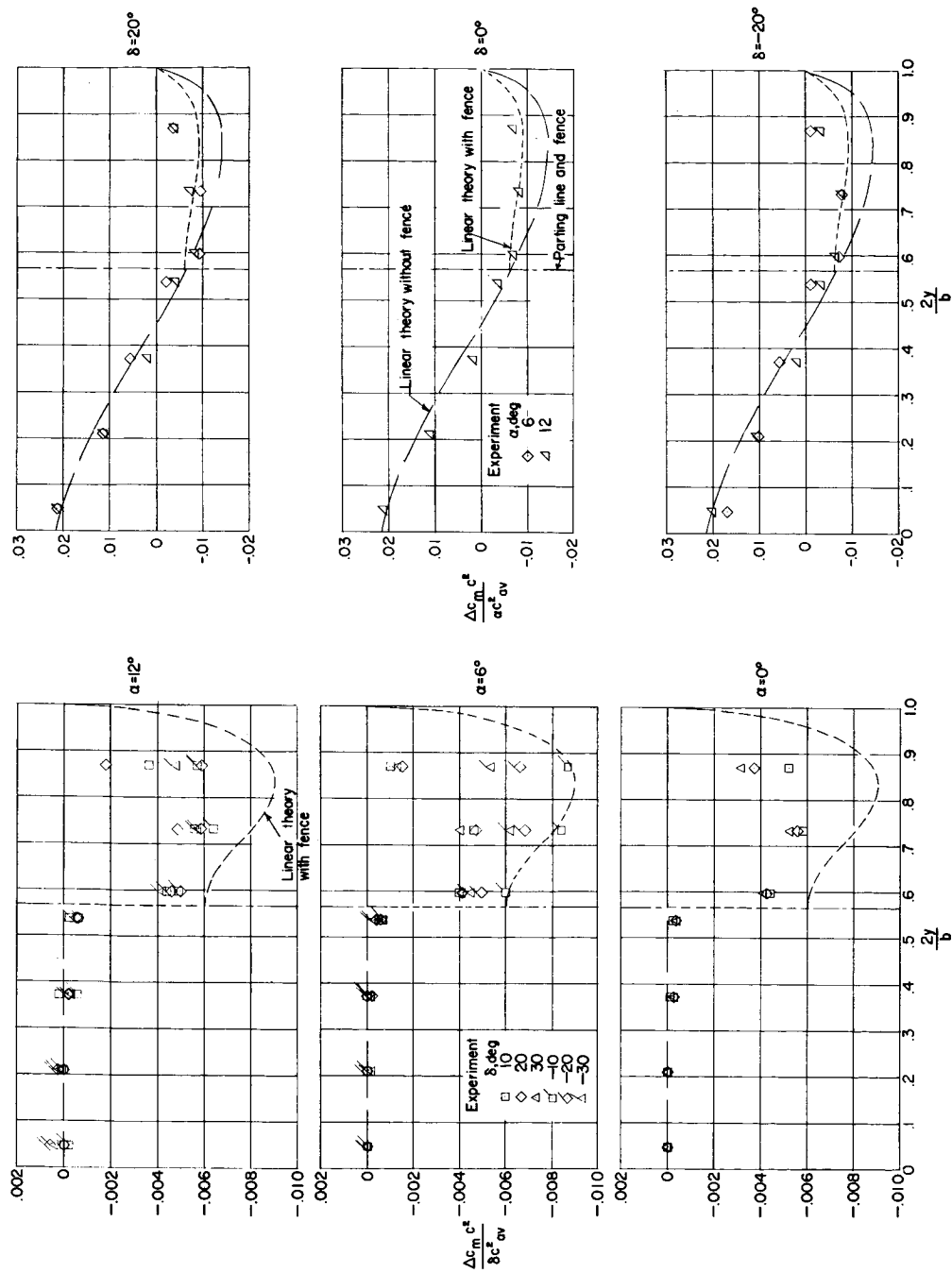


(a) Wing pitching-moment loading due to δ . (b) Wing pitching-moment loading due to α .
Figure 25.- Spanwise pitching-moment distributions for configuration D. $M = 1.61$.

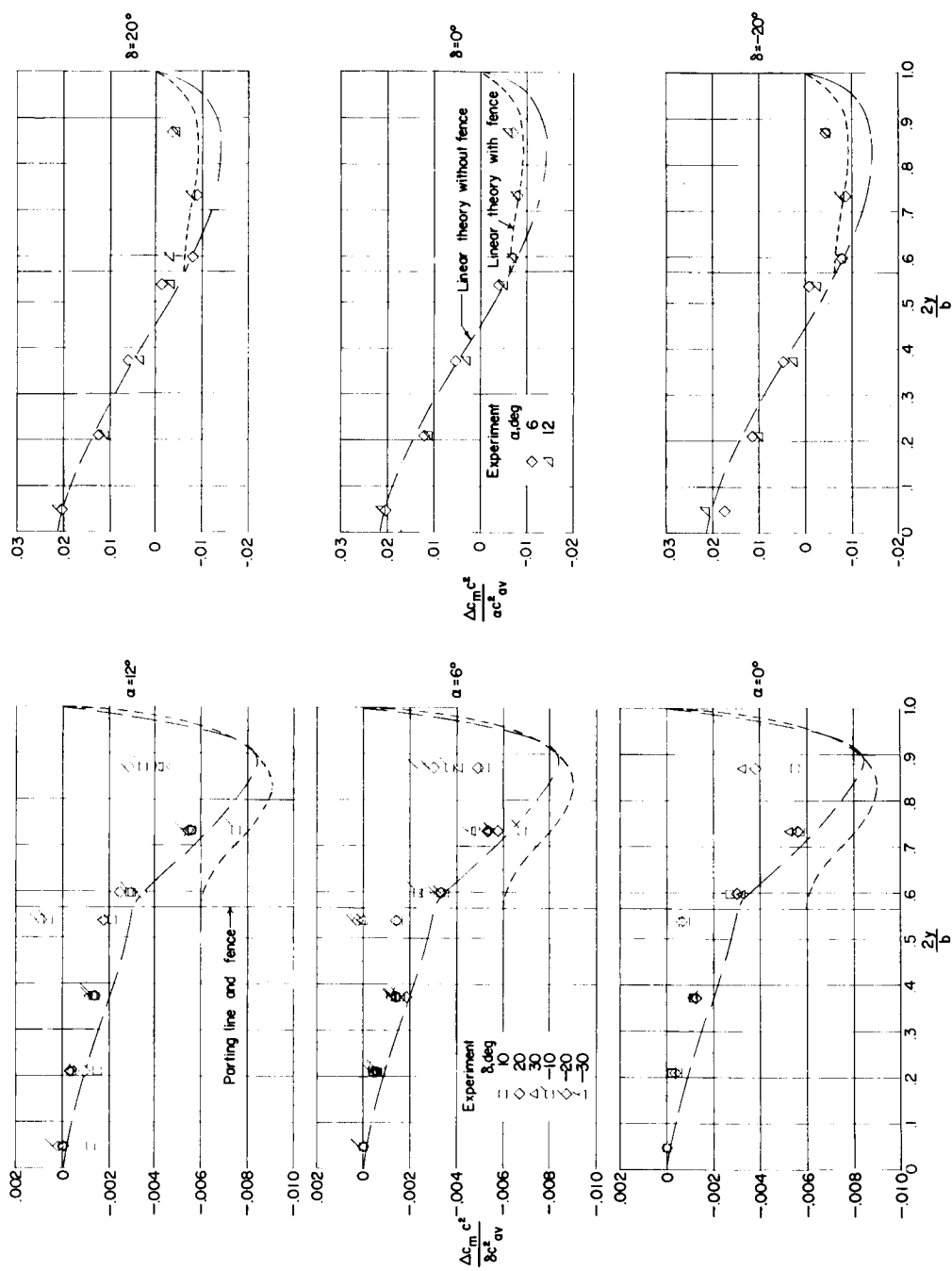


(a) Wing pitching-moment loading due to δ . (b) Wing pitching-moment loading due to α .

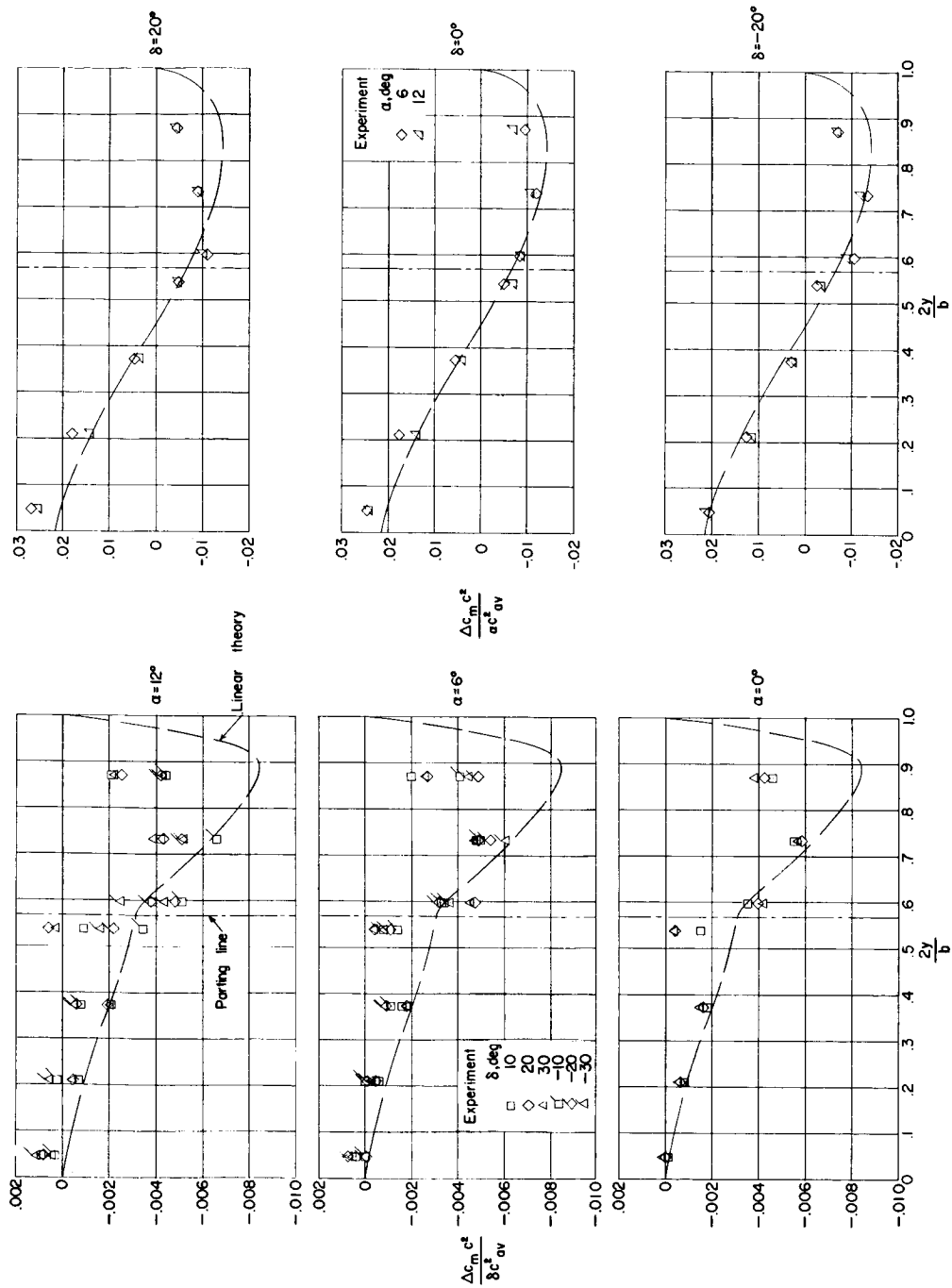
Figure 26.- Spanwise pitching-moment distributions for configuration E. $M = 1.61$.



(a) Wing pitching-moment loading due to δ . (b) Wing pitching-moment loading due to α .
Figure 27.- Spanwise pitching-moment distributions for configuration E2. $M = 1.61$.

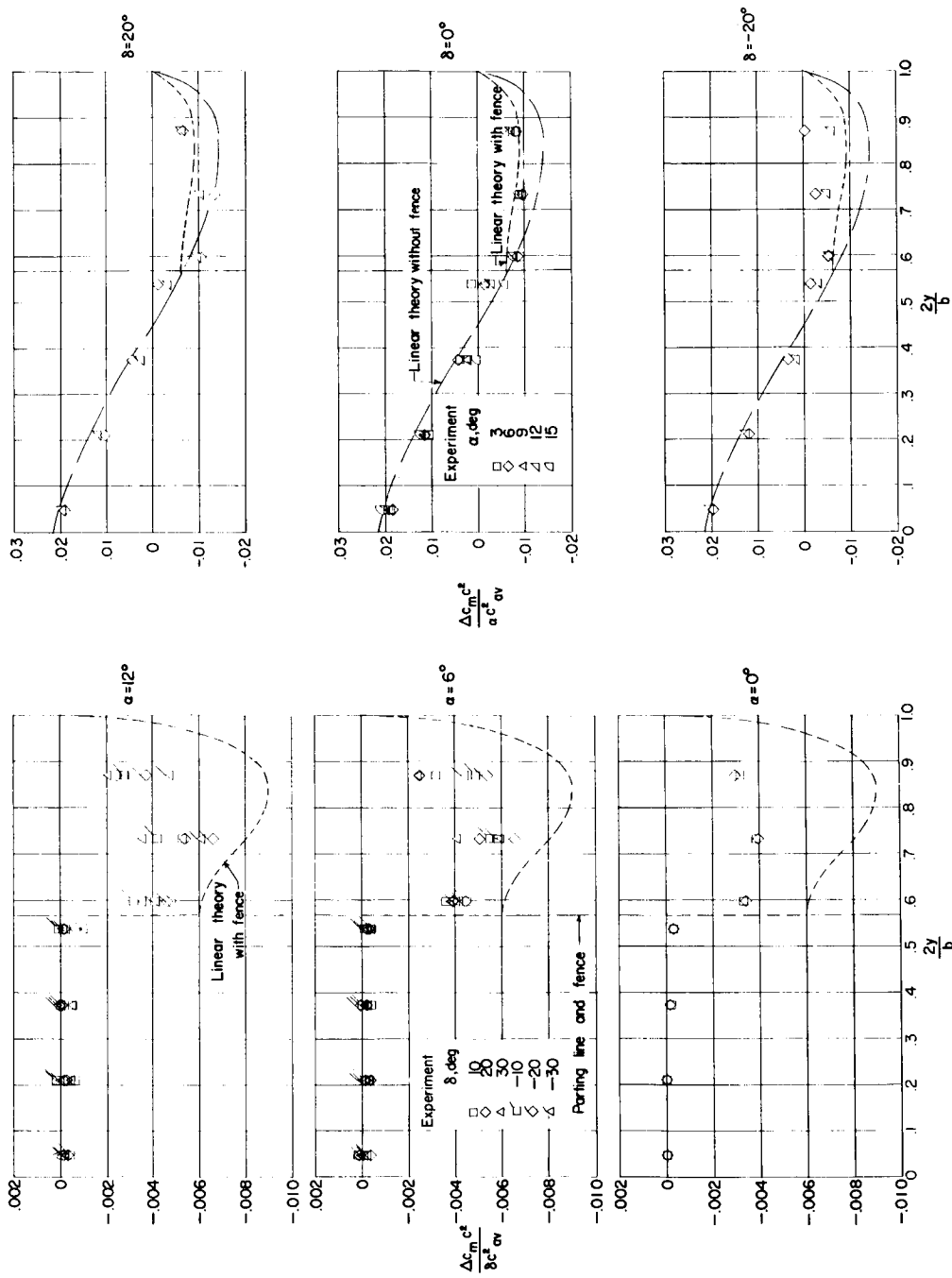


(a) Wing pitching-moment loading due to δ . (b) Wing pitching-moment loading due to α .
 Figure 28.- Spanwise pitching-moment distributions for configuration E3. $M = 1.61$.



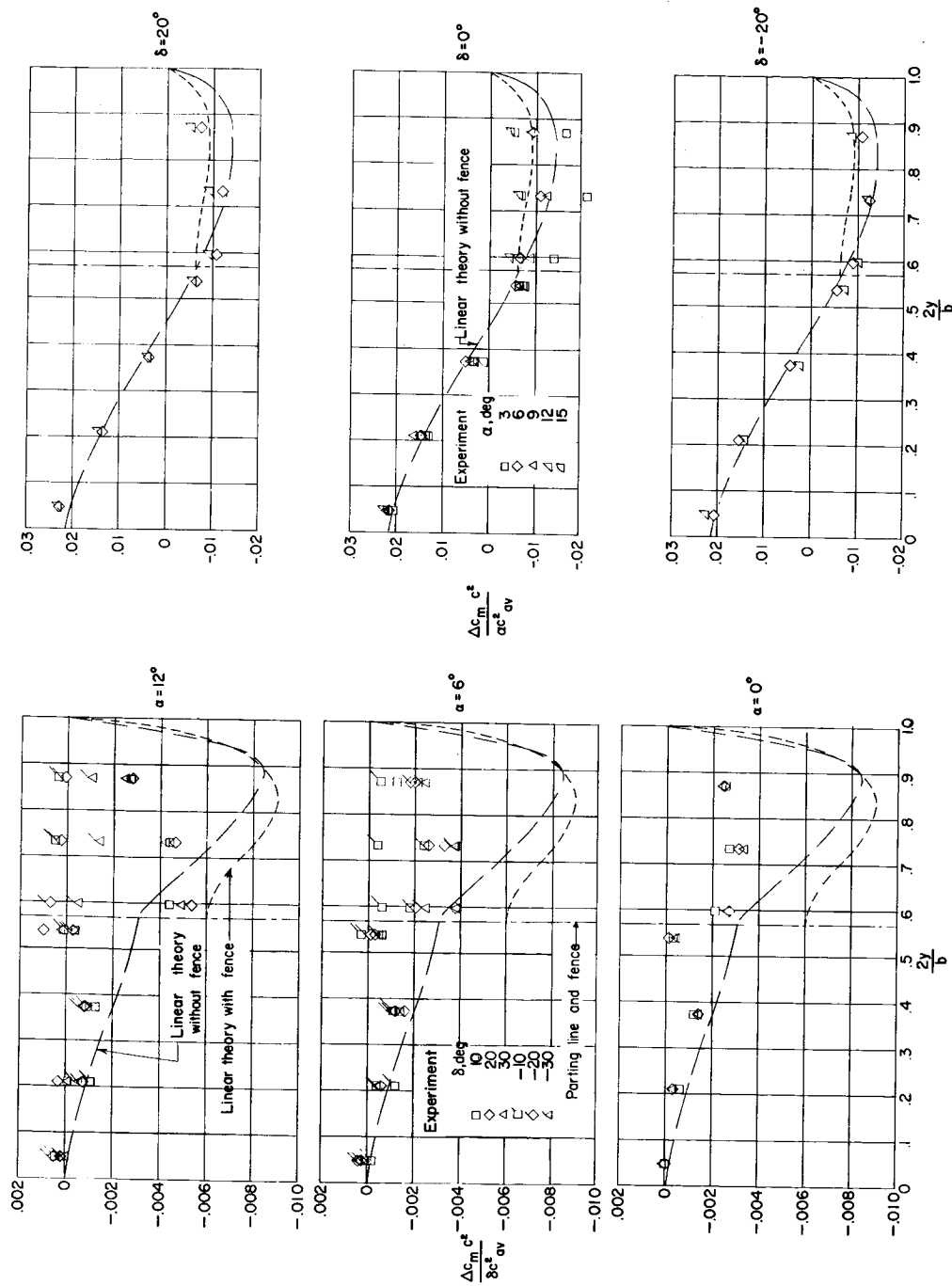
(a) Wing pitching-moment loading due to δ . (b) Wing pitching-moment loading due to α .

Figure 29.- Spanwise pitching-moment distribution for configuration F. $M = 1.61$.



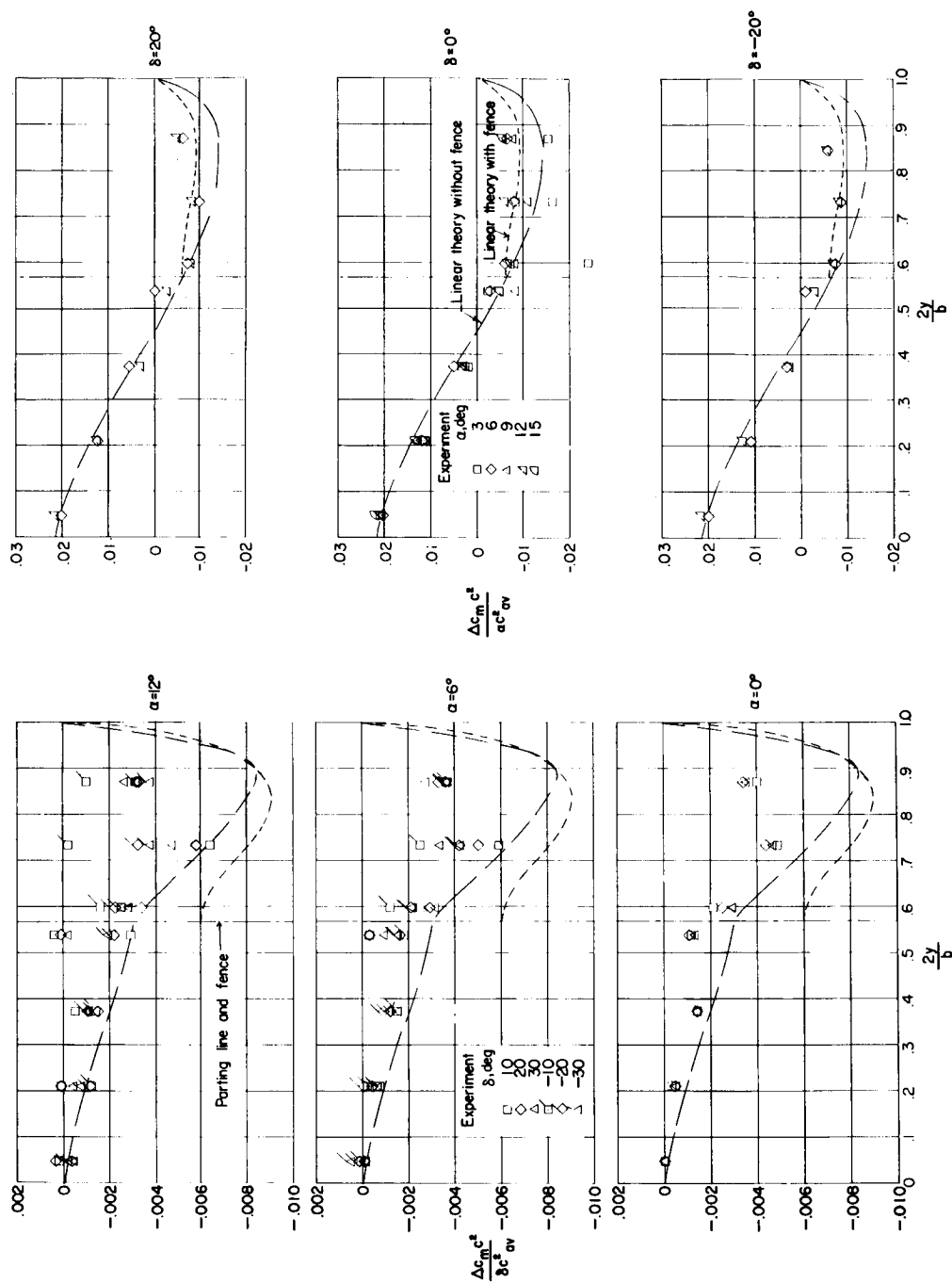
(a) Wing pitching-moment loading due to δ . (b) Wing pitching-moment loading due to α .

Figure 30.- Spanwise pitching-moment distributions for configuration Fl. $M = 1.61$.



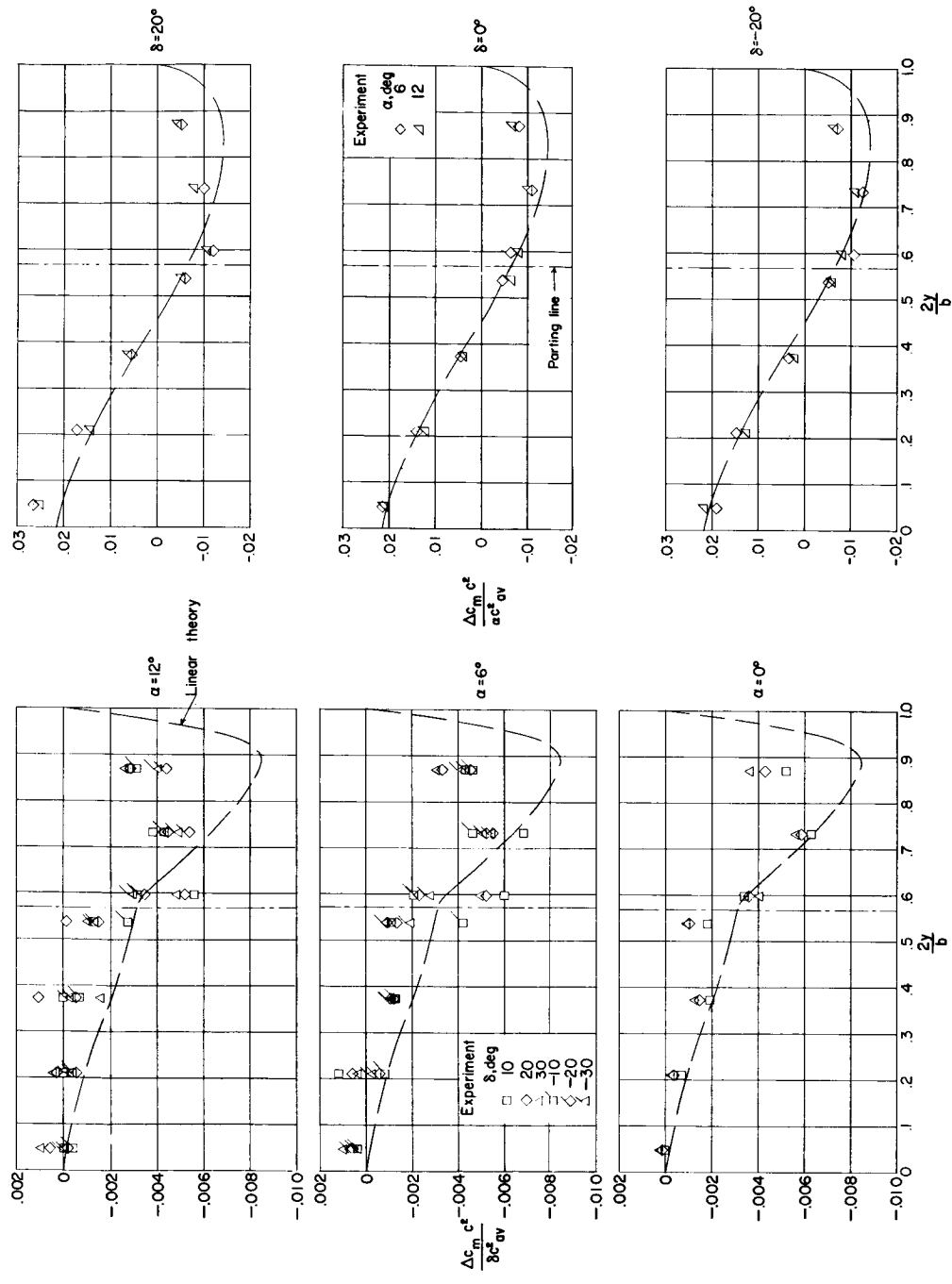
(a) Wing pitching-moment loading due to δ . (b) Wing pitching-moment loading due to α .

Figure 31.- Spanwise pitching-moment distributions for configuration F2. $M = 1.61$.



(a) Wing pitching-moment loading due to δ . (b) Wing pitching-moment loading due to α .

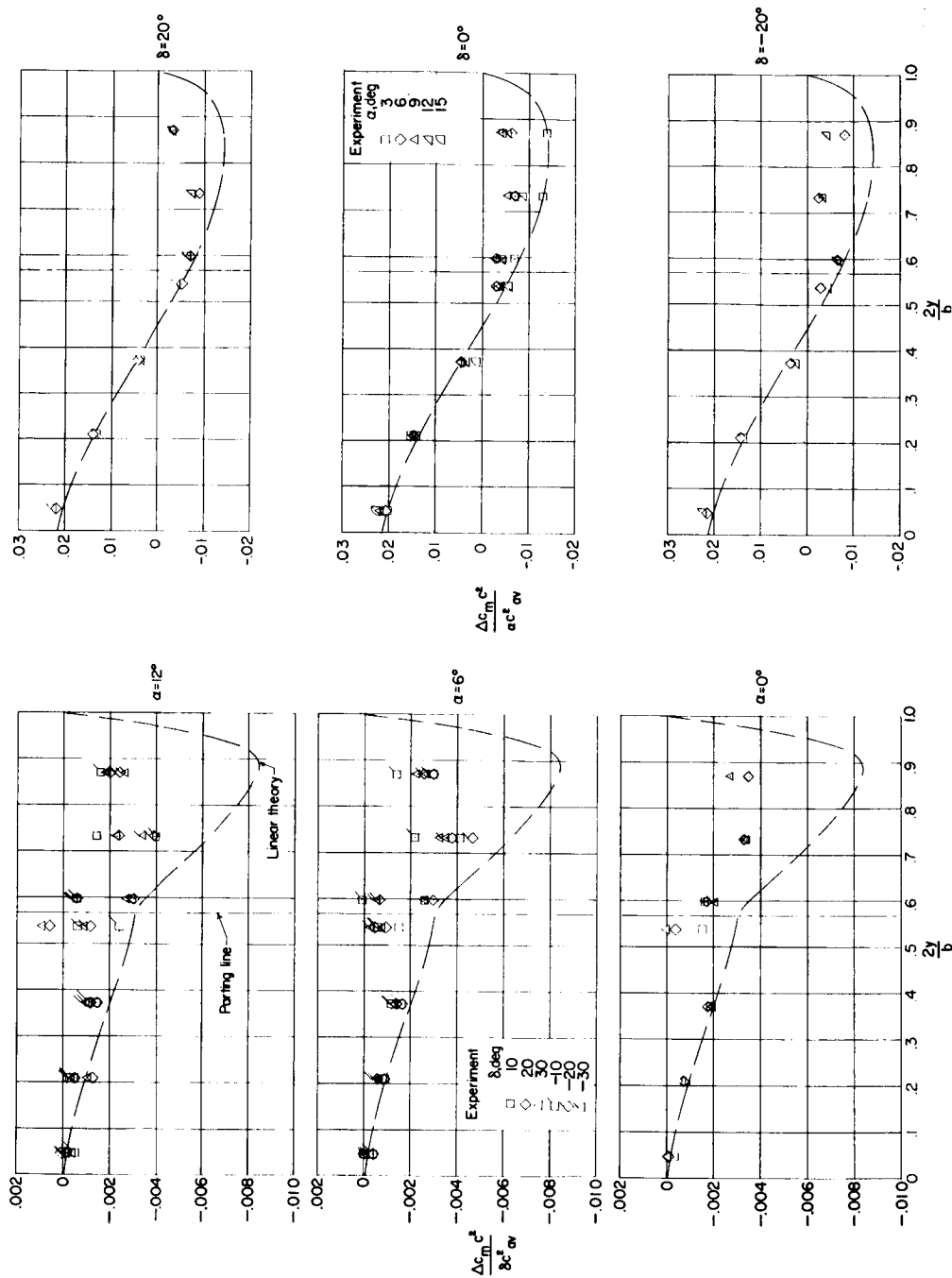
Figure 32.- Spanwise pitching-moment distributions for configuration F3. $M = 1.61$.



(a) Wing pitching-moment loading due to δ . (b) Wing pitching-moment loading due to α .

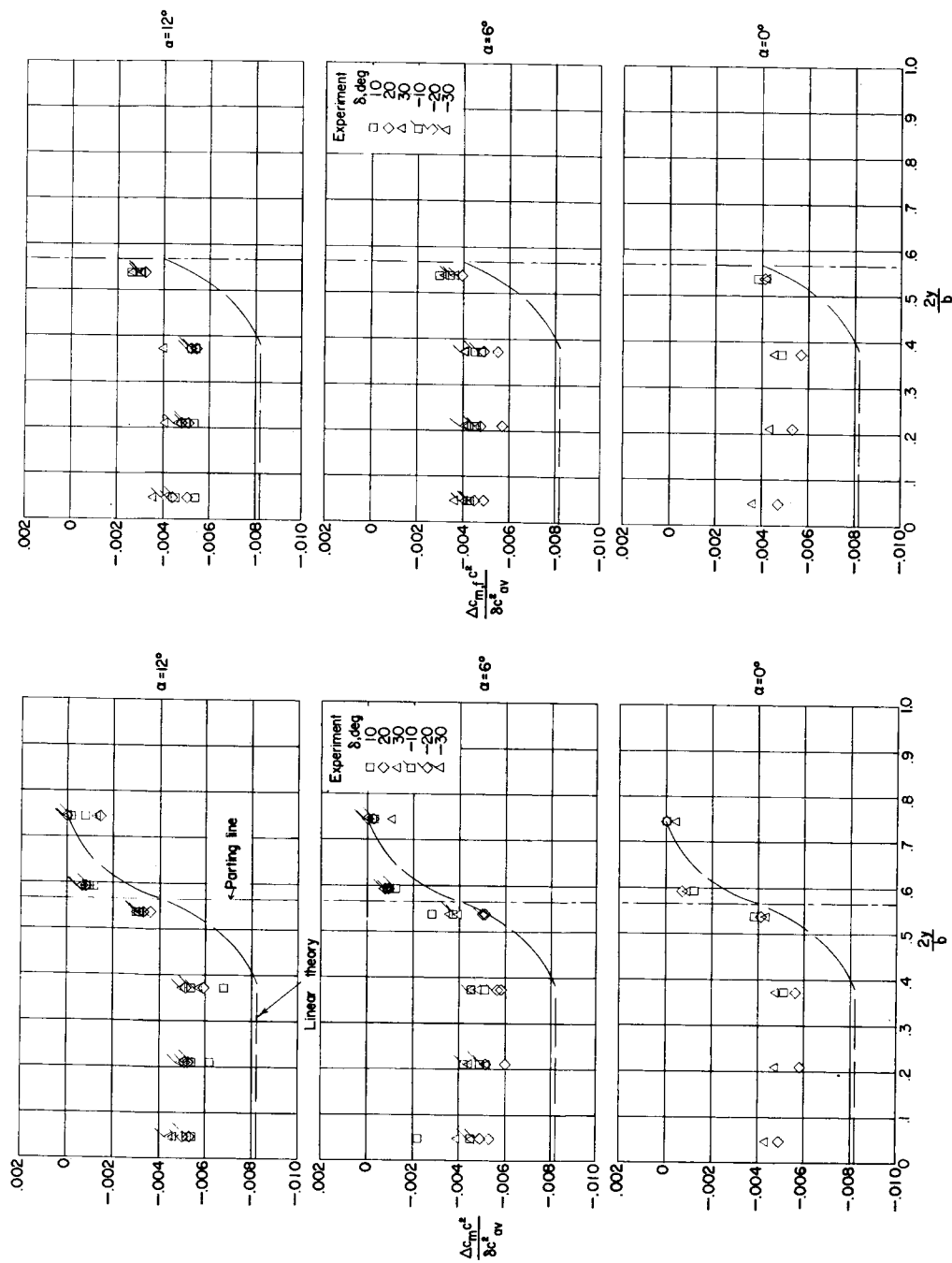
Figure 33.- Spanwise pitching-moment distributions for configuration G. $M = 1.61$.

CONFIDENTIAL



(a) Wing pitching-moment loading due to δ . (b) Wing pitching-moment loading due to α .

Figure 34.- Spanwise pitching-moment distributions for configuration H. $M = 1.61$.

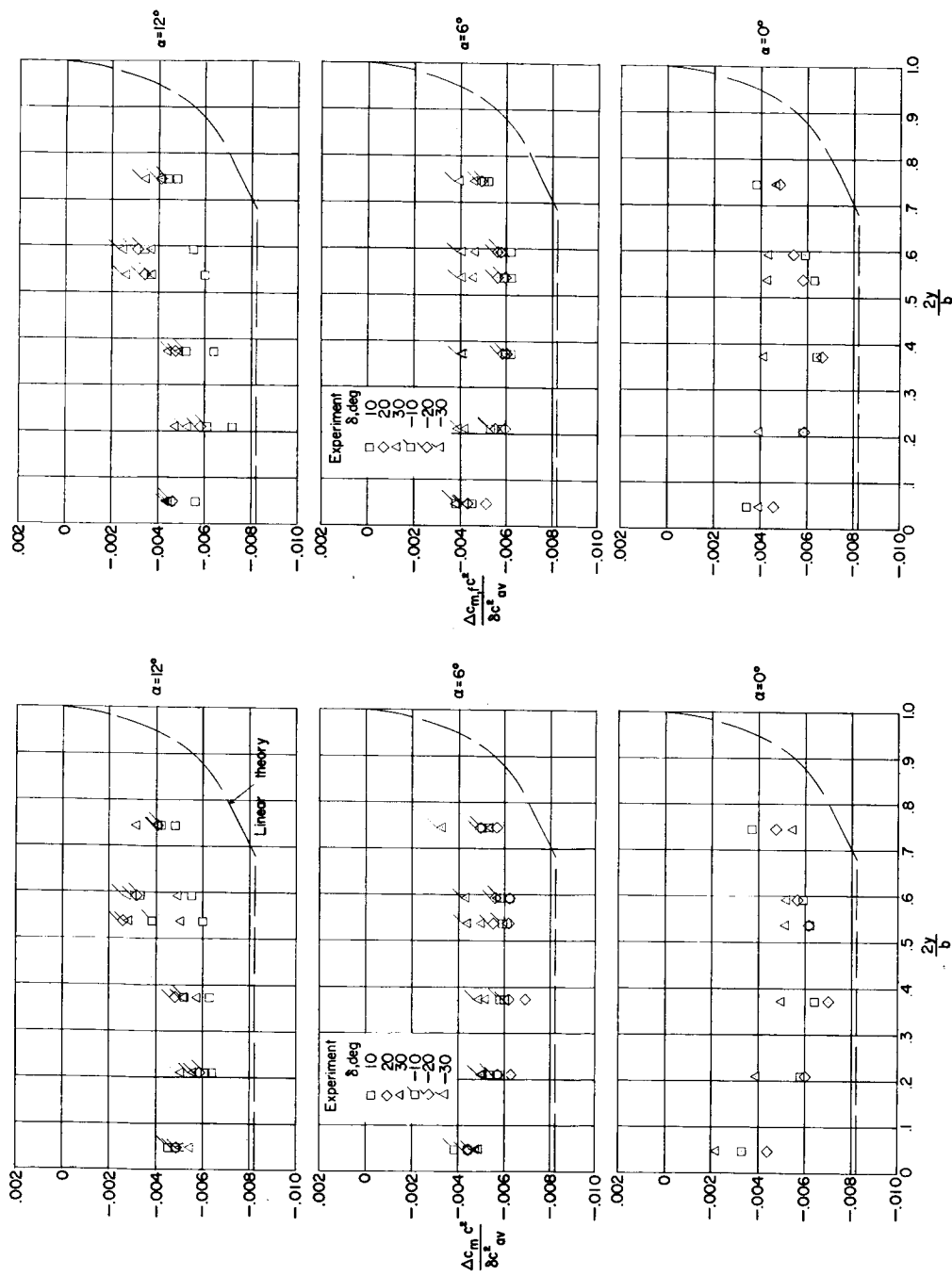


(a) Wing pitching-moment loading due to δ . (b) Control pitching-moment loading due to δ .

Figure 35.- Spanwise pitching-moment distributions for configuration I. $M = 1.61$.

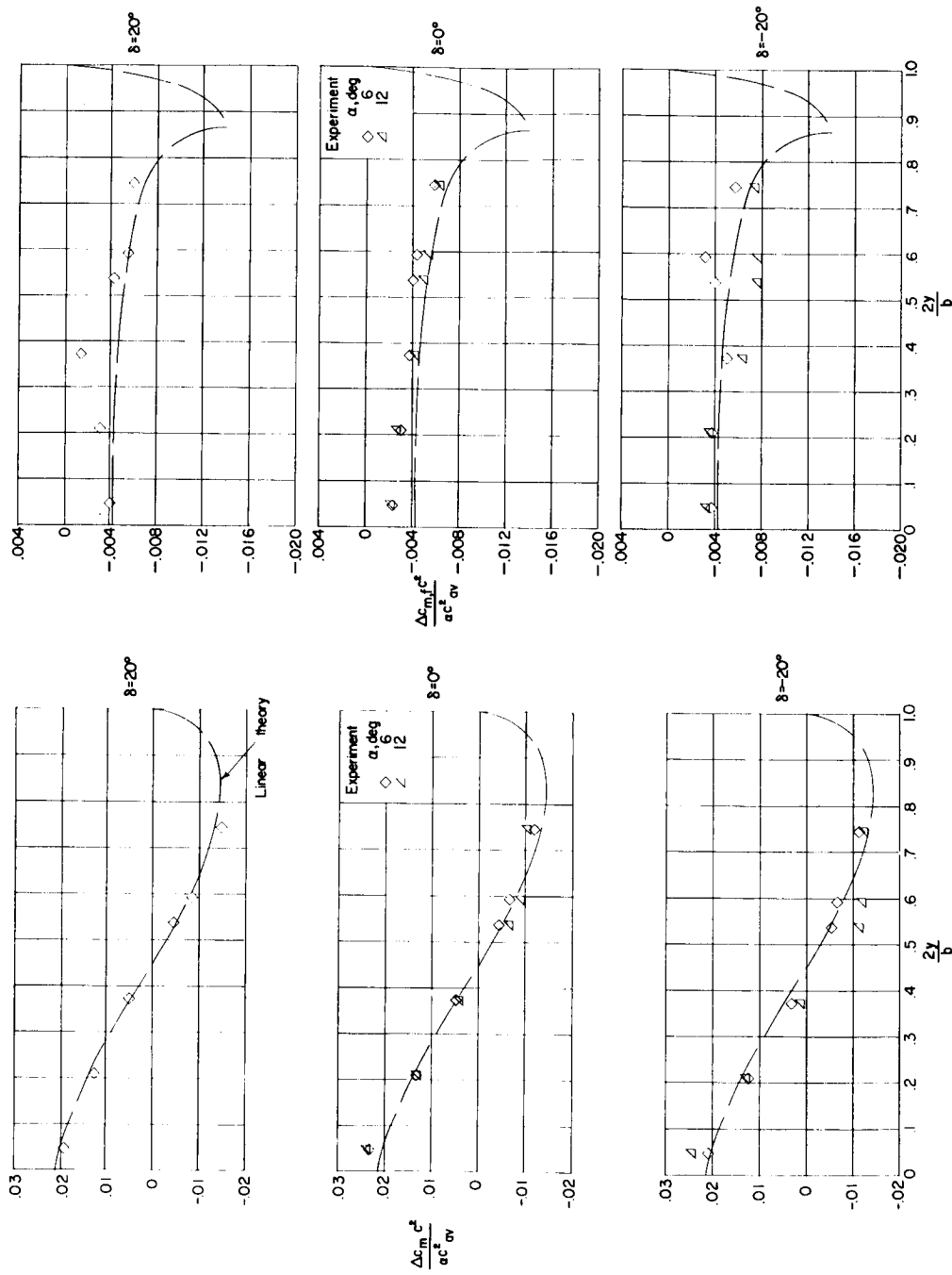


L-258



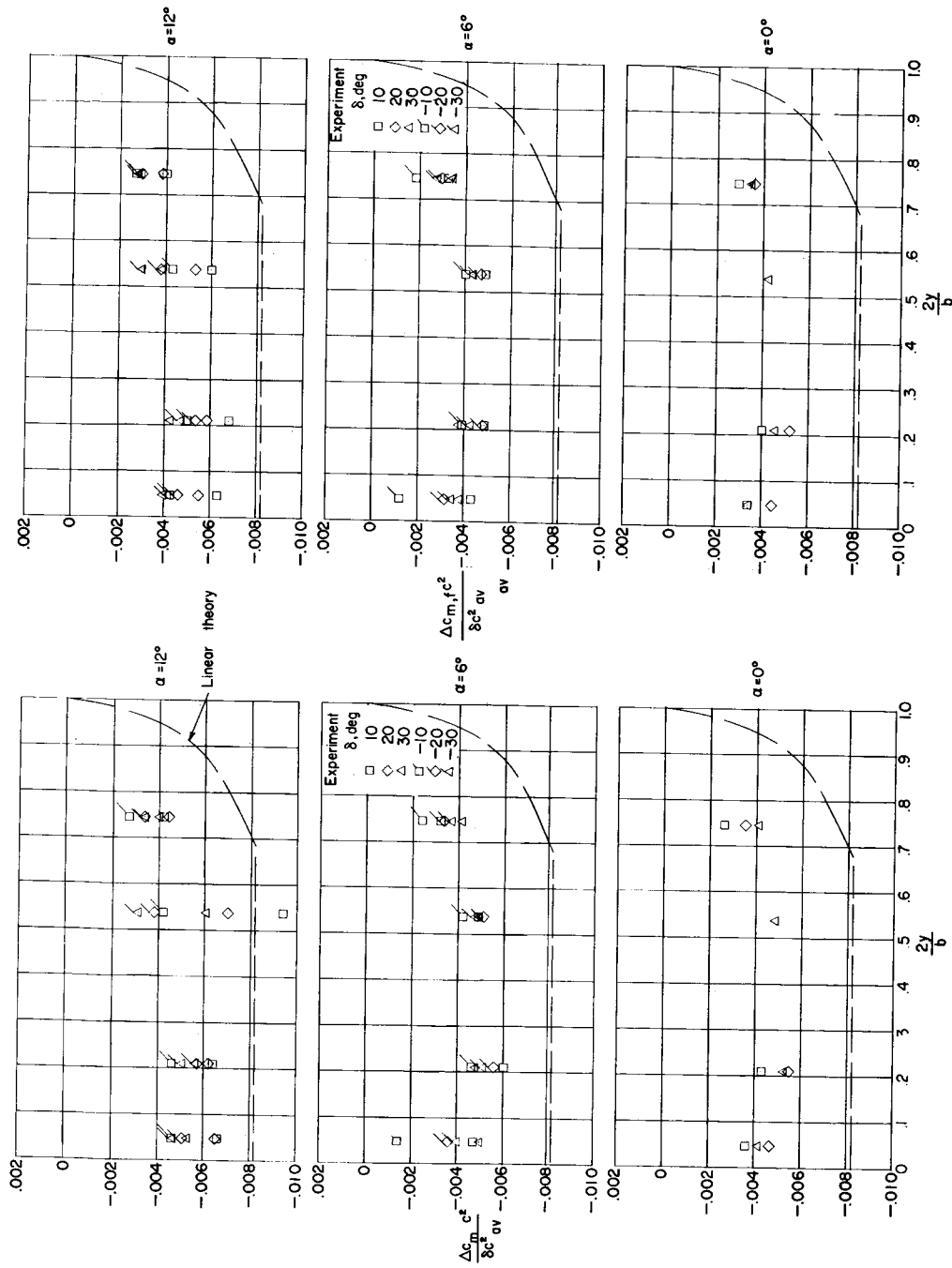
(a) Wing pitching-moment loading due to δ . (b) Control pitching-moment loading due to δ .

Figure 36.- Spanwise pitching-moment distributions for configuration J. $M = 1.61$.



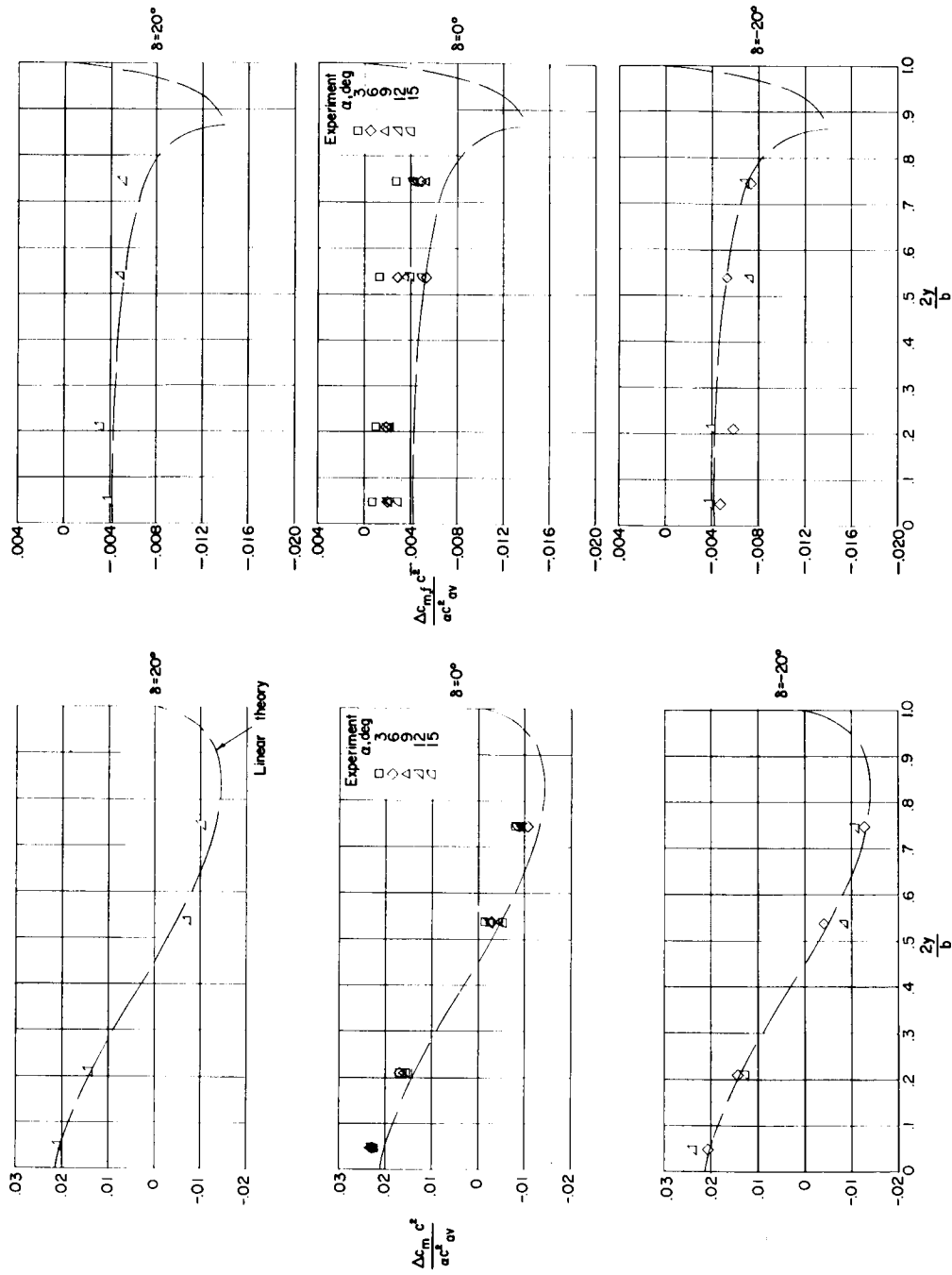
(c) Wing pitching-moment loading due to α . (d) Control pitching-moment loading due to α .

Figure 36.- Concluded.



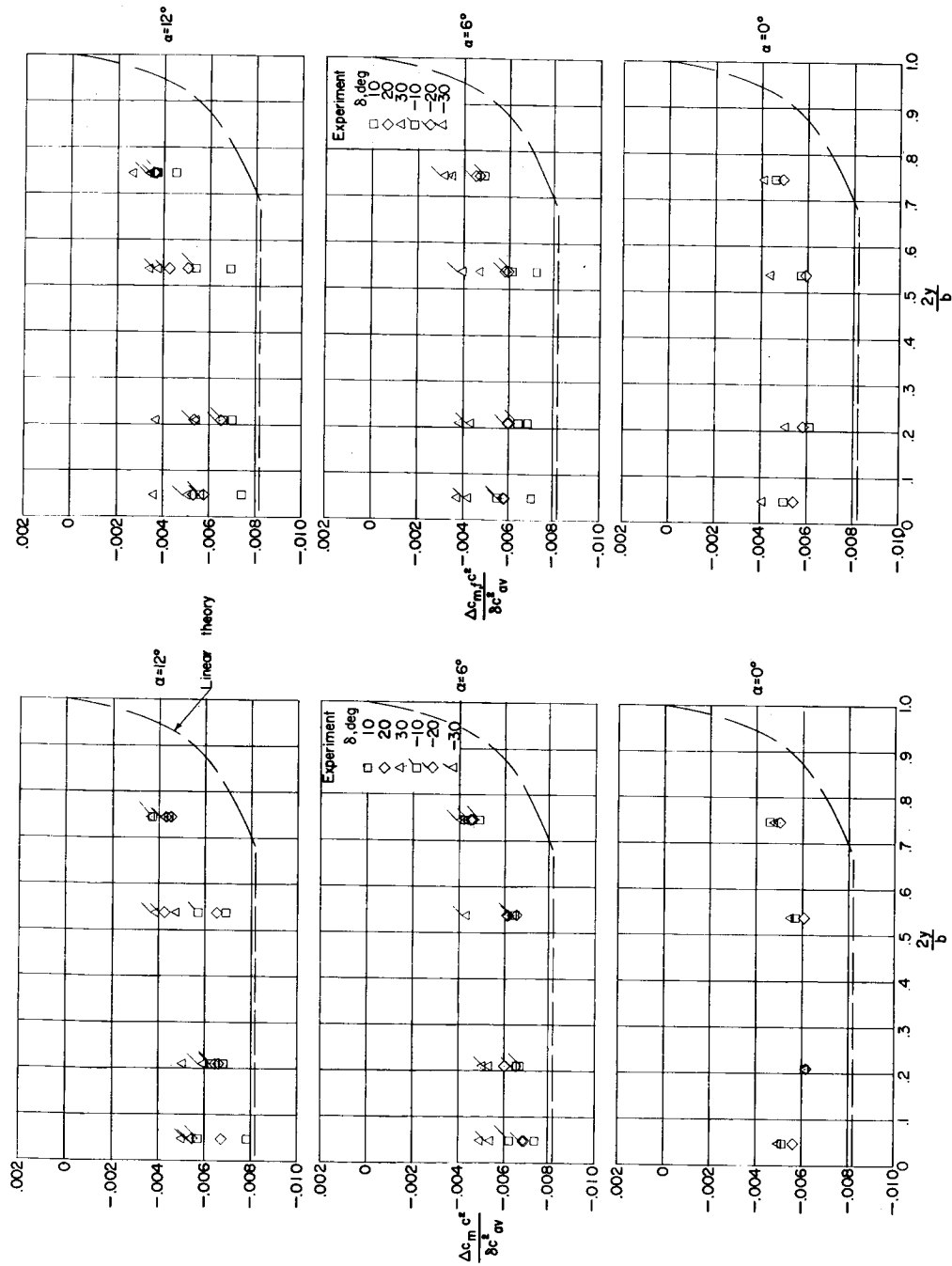
(a) Wing pitching-moment loading due to δ . (b) Control pitching-moment loading due to δ .

Figure 37.- Spanwise pitching-moment distributions for configuration J1. $M = 1.61$.



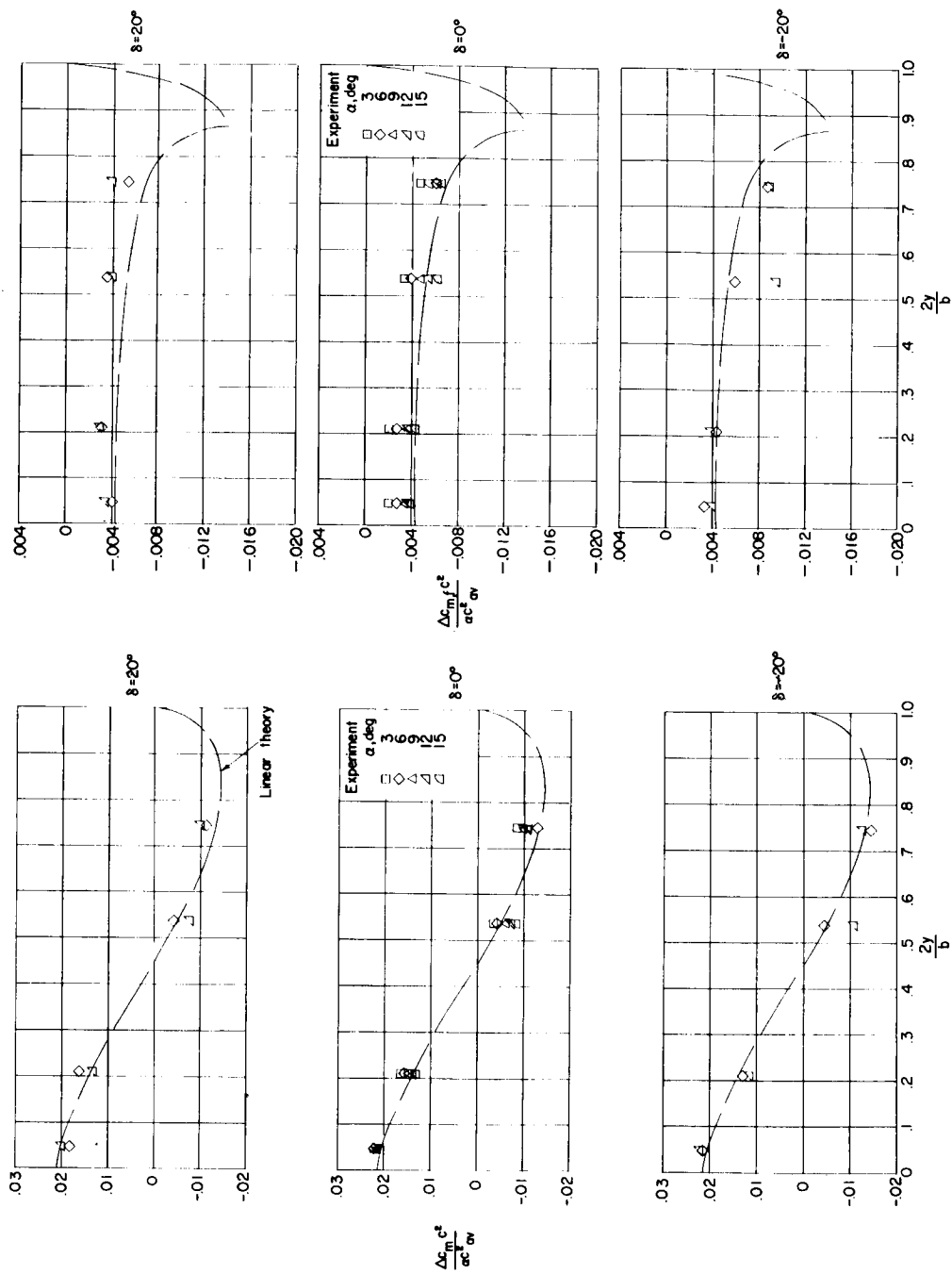
(c) Wing pitching-moment loading due to α . (d) Control pitching-moment loading due to α .

Figure 37.- Concluded.



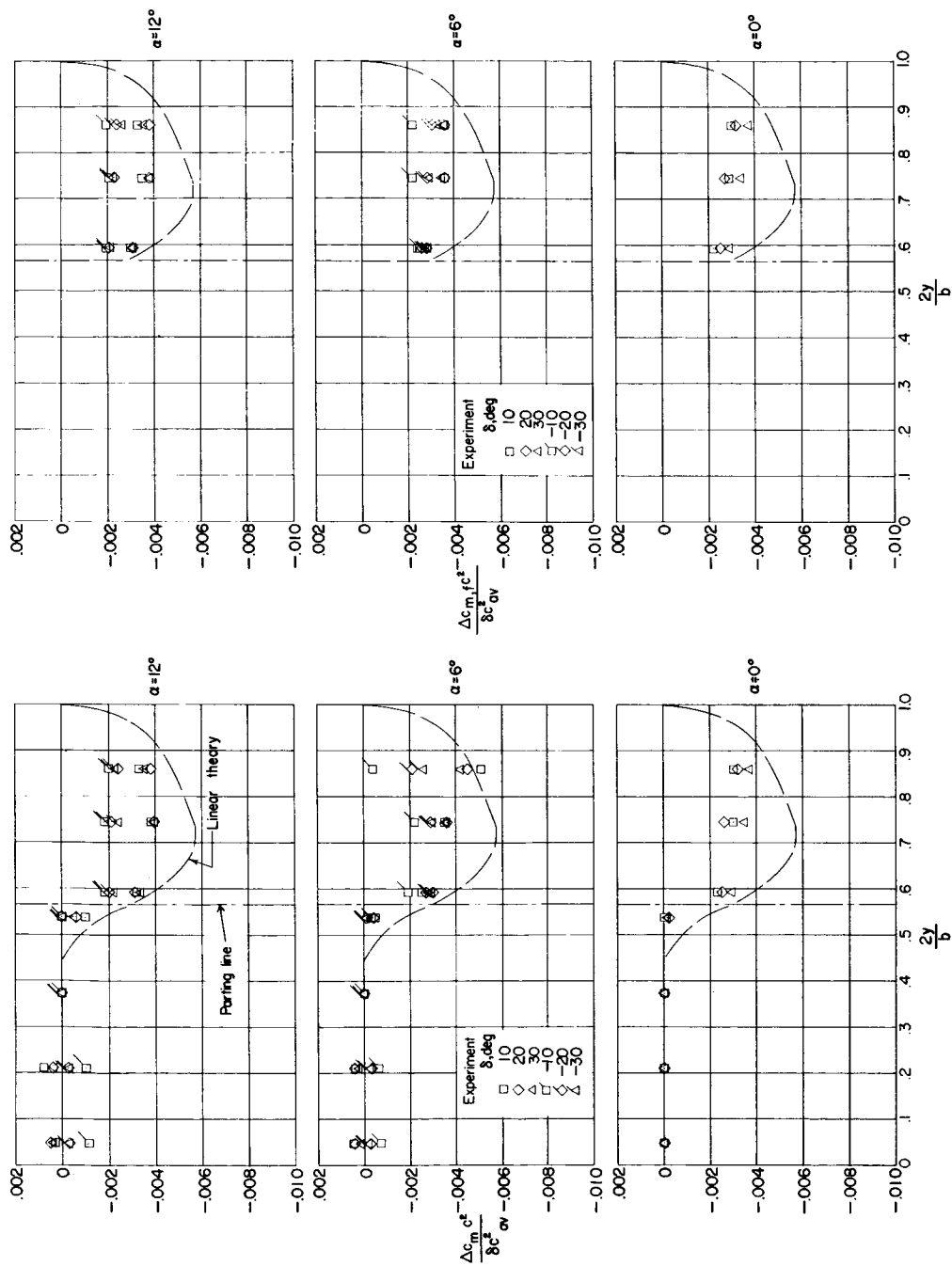
(a) Wing pitching-moment loading due to δ . (b) Control pitching-moment loading due to δ .
Figure 38.- Spanwise pitching-moment distribution for configuration J2. $M = 1.61$.

03 02 01 00 -01 -02 -03 -04 -05 -06 -07 -08 -09 -10 -11 -12 -13 -14 -15 -16 -17 -18 -19 -20 -21 -22 -23 -24 -25 -26 -27 -28 -29 -30 -31 -32 -33 -34 -35 -36 -37 -38 -39 -40 -41 -42 -43 -44 -45 -46 -47 -48 -49 -50 -51 -52 -53 -54 -55 -56 -57 -58 -59 -60 -61 -62 -63 -64 -65 -66 -67 -68 -69 -70 -71 -72 -73 -74 -75 -76 -77 -78 -79 -80 -81 -82 -83 -84 -85 -86 -87 -88 -89 -90 -91 -92 -93 -94 -95 -96 -97 -98 -99 -100



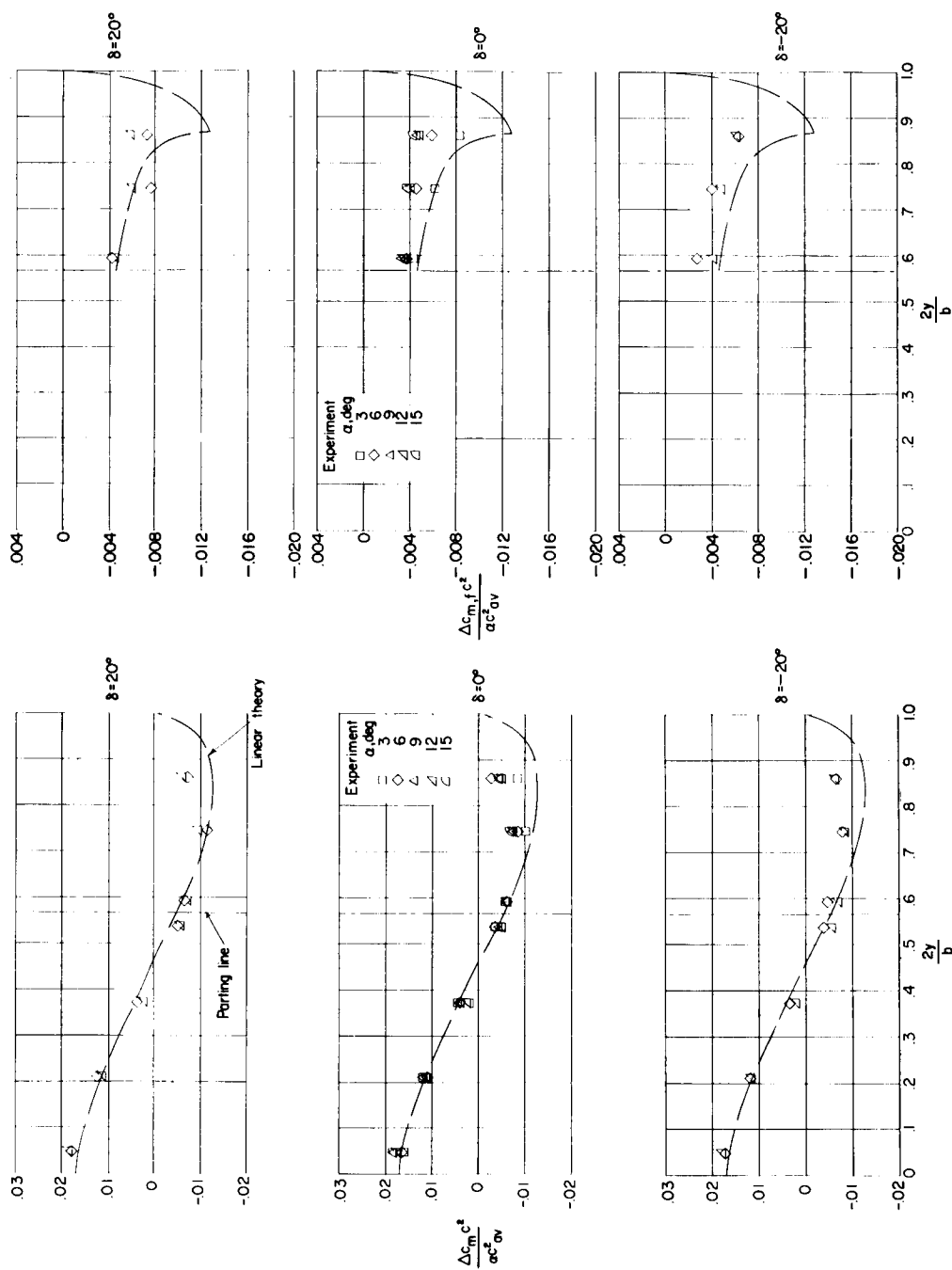
(c) Wing pitching-moment loading due to α . (d) Control pitching-moment loading due to α .

Figure 38.- Concluded.



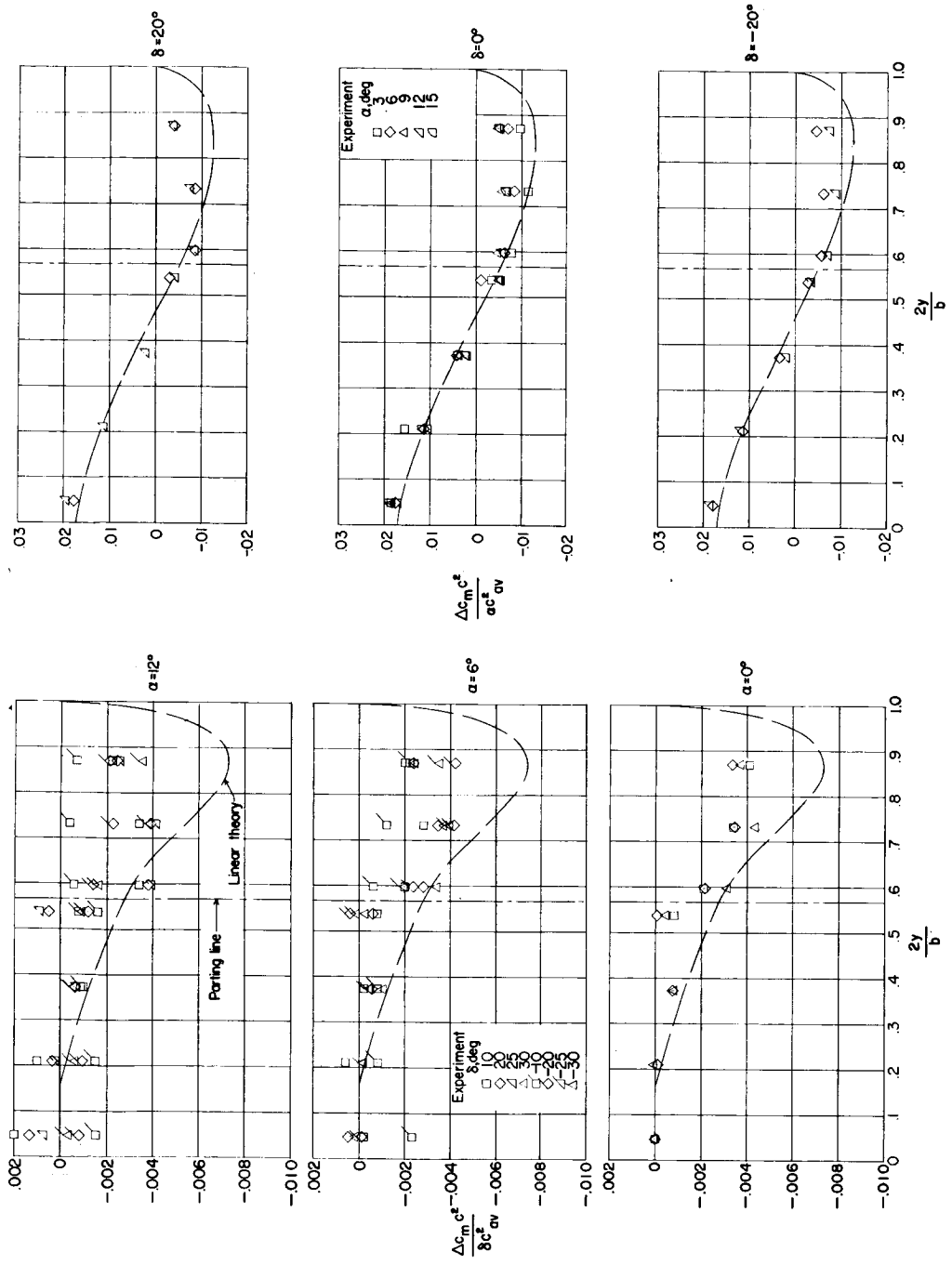
(a) Wing pitching-moment loading due to δ . (b) Control pitching-moment loading due to δ .

Figure 39.- Spanwise pitching-moment distributions for configuration A. $M = 2.01$.

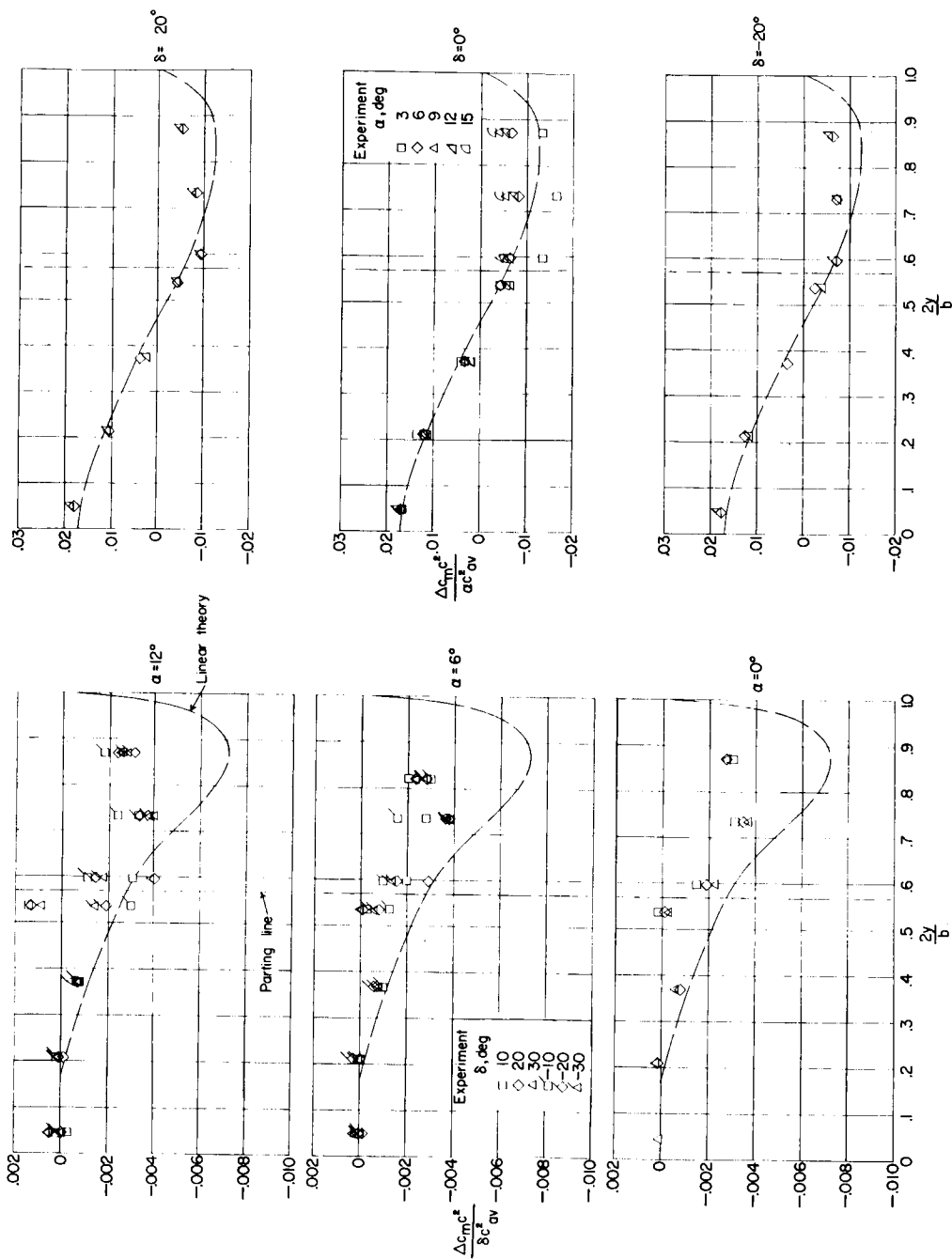


(c) Wing pitching-moment loading due to α . (d) Control pitching-moment loading due to α .

Figure 39.- Concluded.

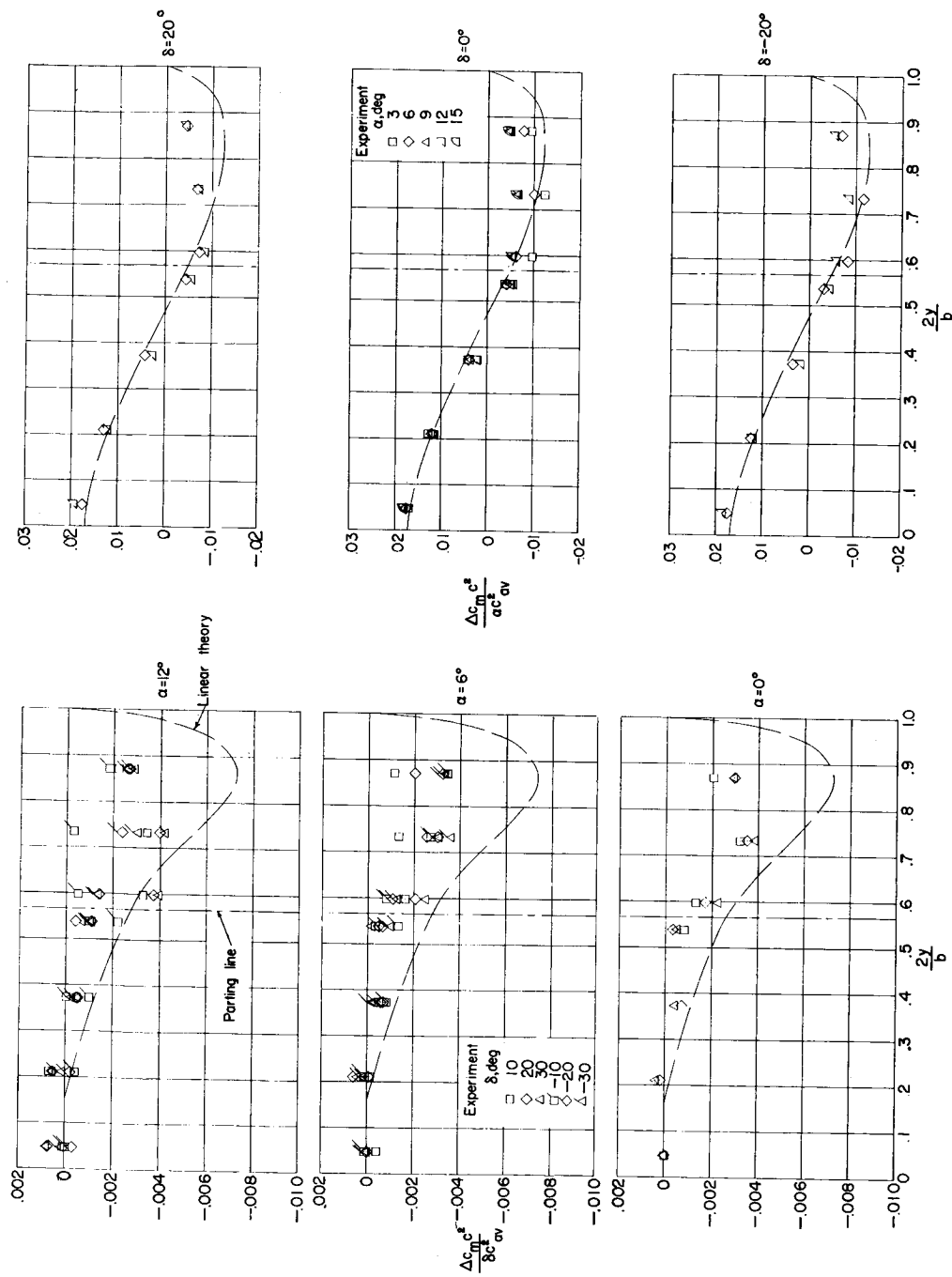


(a) Wing pitching-moment loading due to δ . (b) Wing pitching-moment loading due to α .
Figure 40.- Spanwise pitching-moment distributions for configuration E. $M = 2.01$.



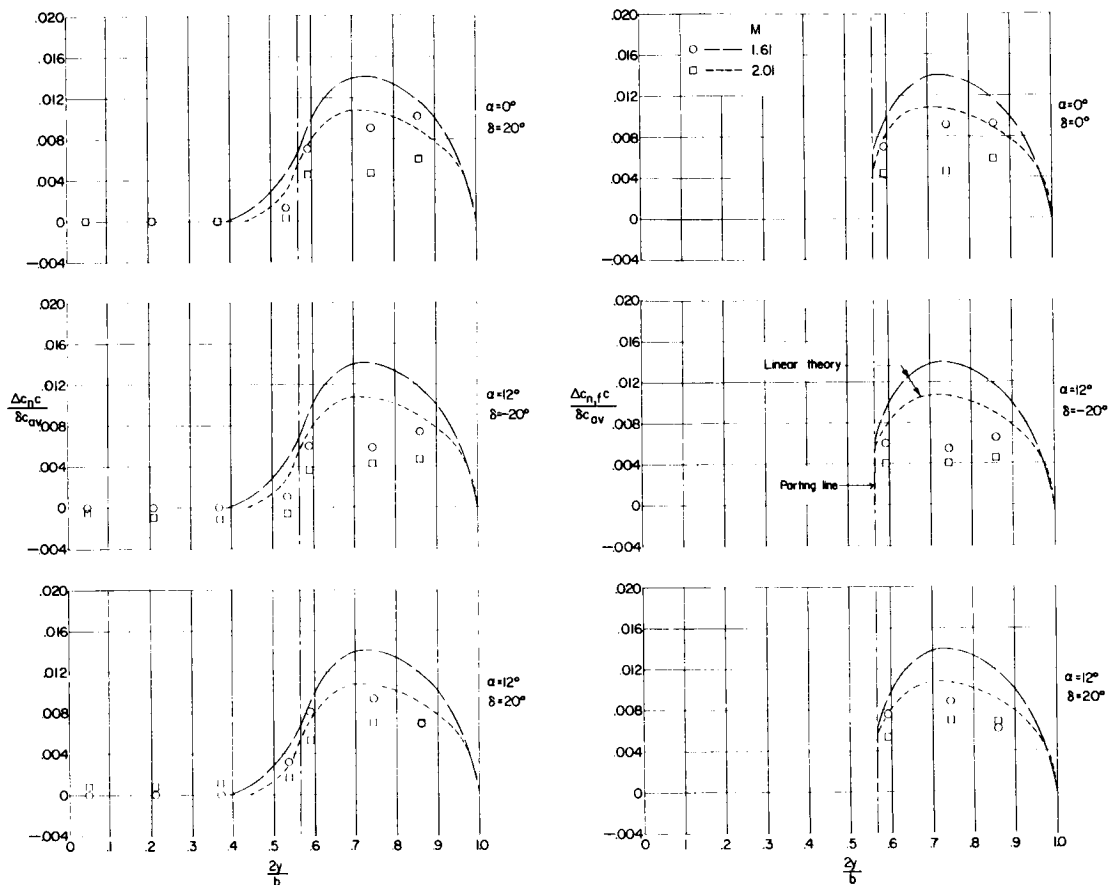
(a) Wing pitching-moment loading due to δ . (b) Wing pitching-moment loading due to α .

Figure 41.- Spanwise pitching-moment distributions for configuration F. $M = 2.01$.



(a) Wing pitching-moment loading due to δ . (b) Wing pitching-moment loading due to α .
 Figure 42.- Spanwise pitching-moment distributions for configuration G. $M = 2.01$.

CONFIDENTIAL

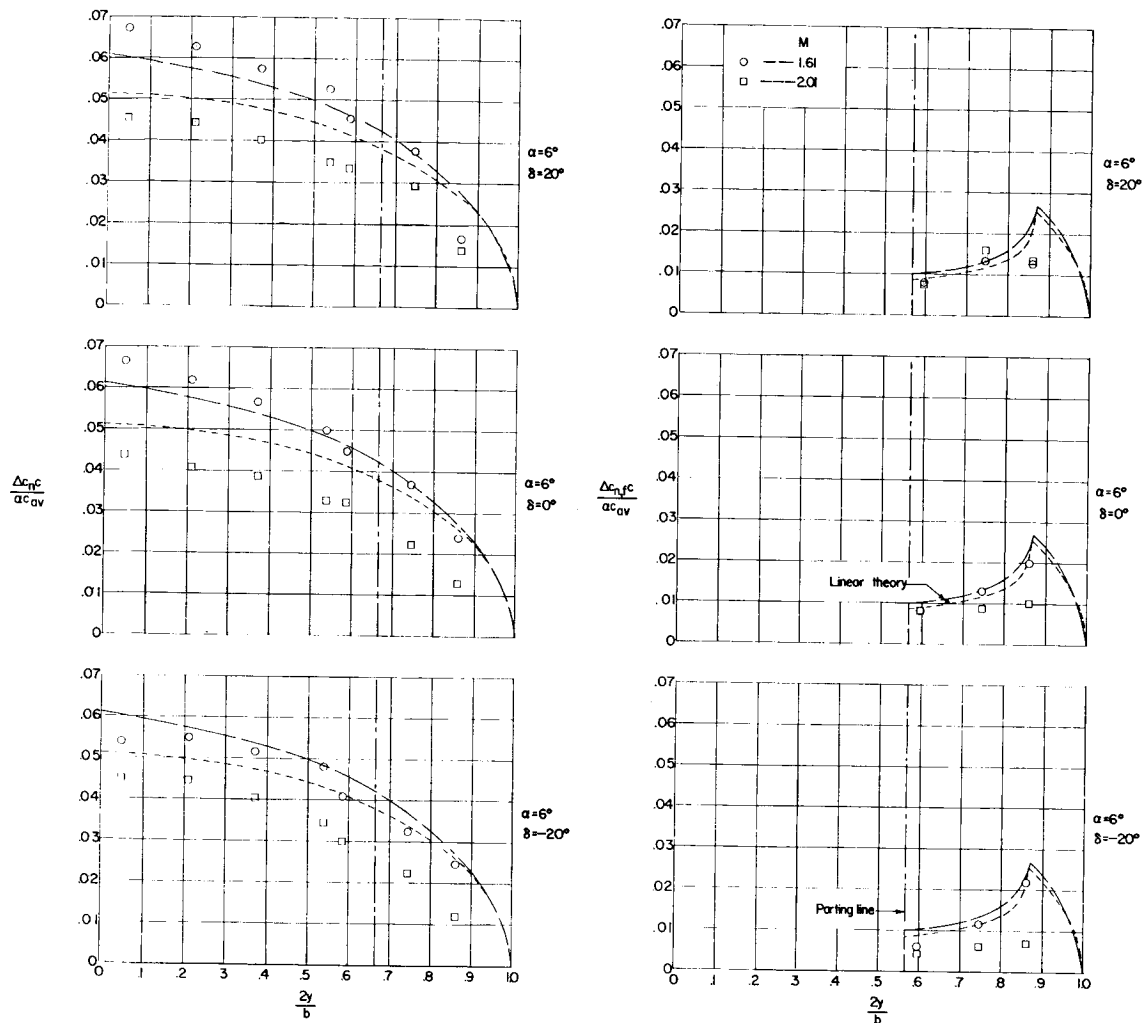


(a) Wing normal-force loading
due to δ .

(b) Control normal-force loading
due to δ .

Figure 43.- Effect of Mach number on spanwise normal-force loading distributions for configuration A.

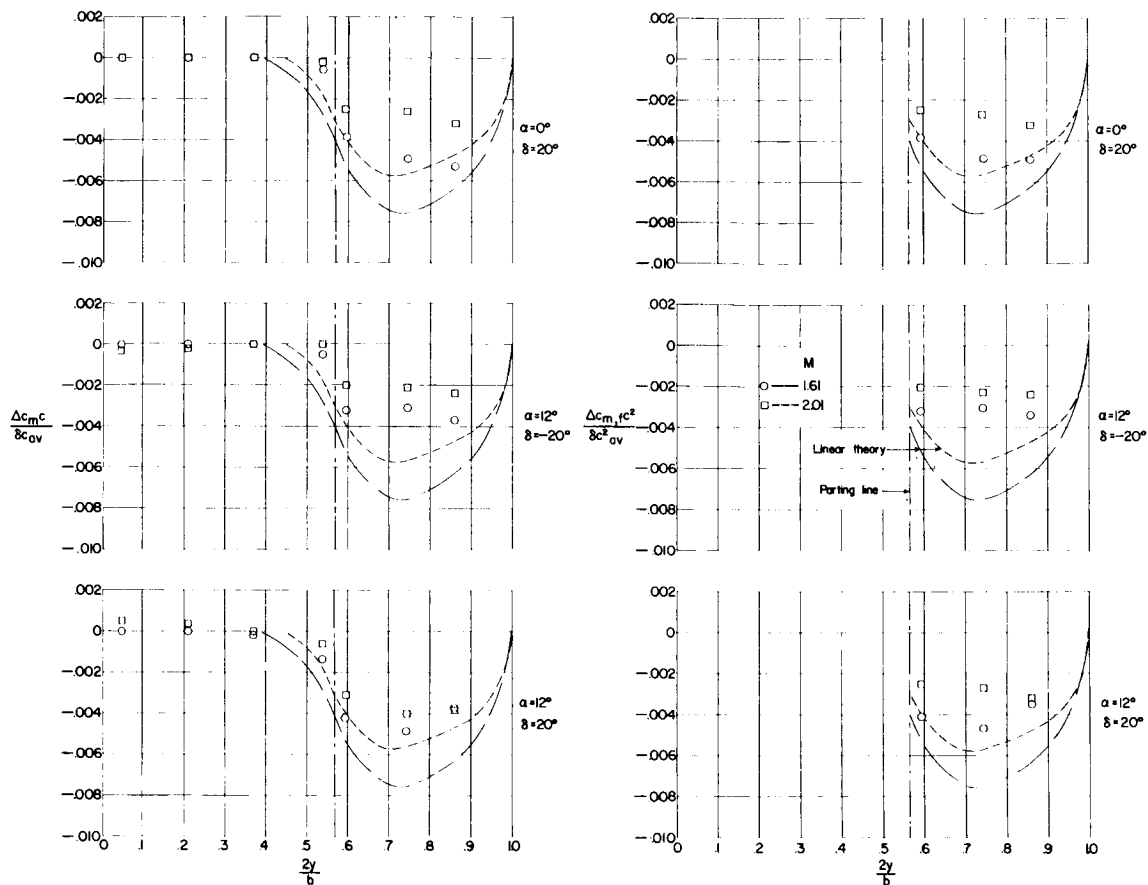
I-258



(c) Wing normal-force loading due to α .

(d) Control normal-force loading due to α .

Figure 43.- Concluded.



(a) Wing pitching-moment loading due to δ . (b) Control pitching-moment loading due to δ .

Figure 44.- Effect of Mach number on spanwise pitching-moment loading distribution for configuration A.

[REDACTED]

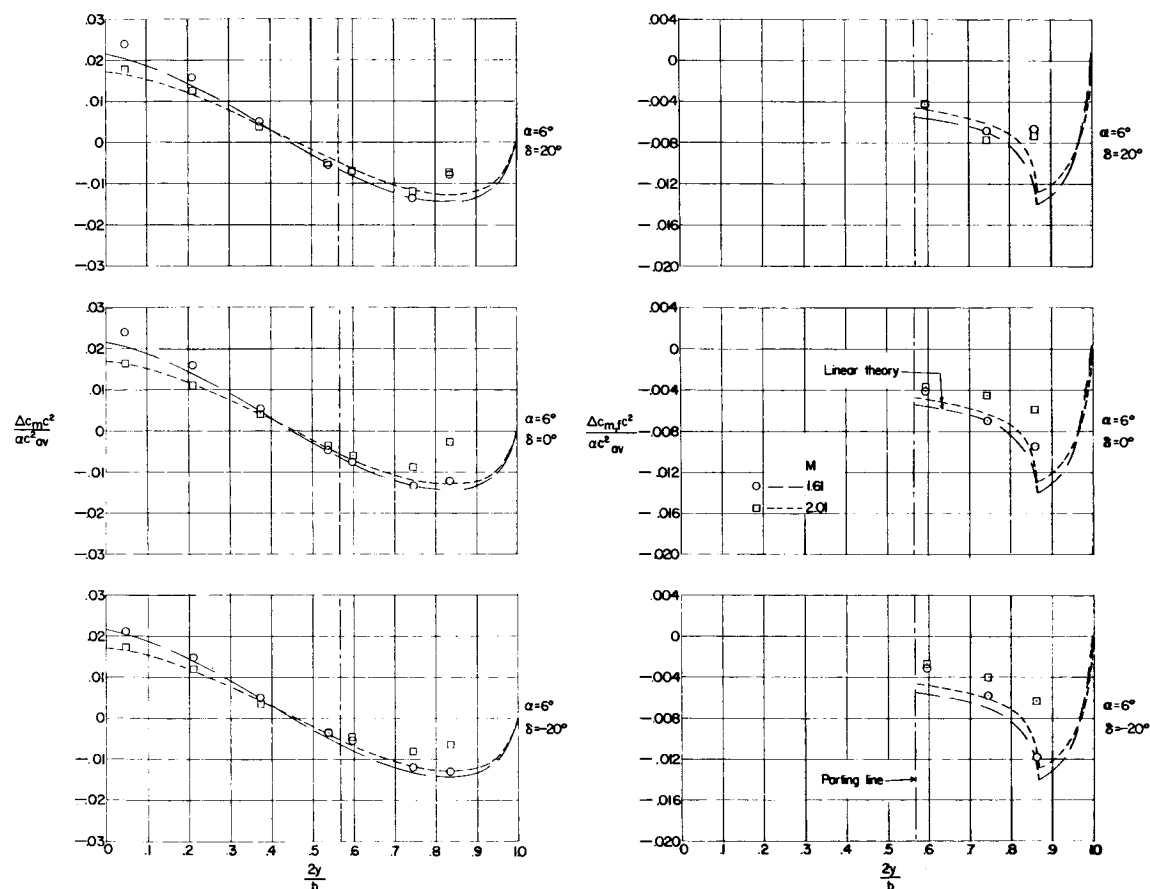
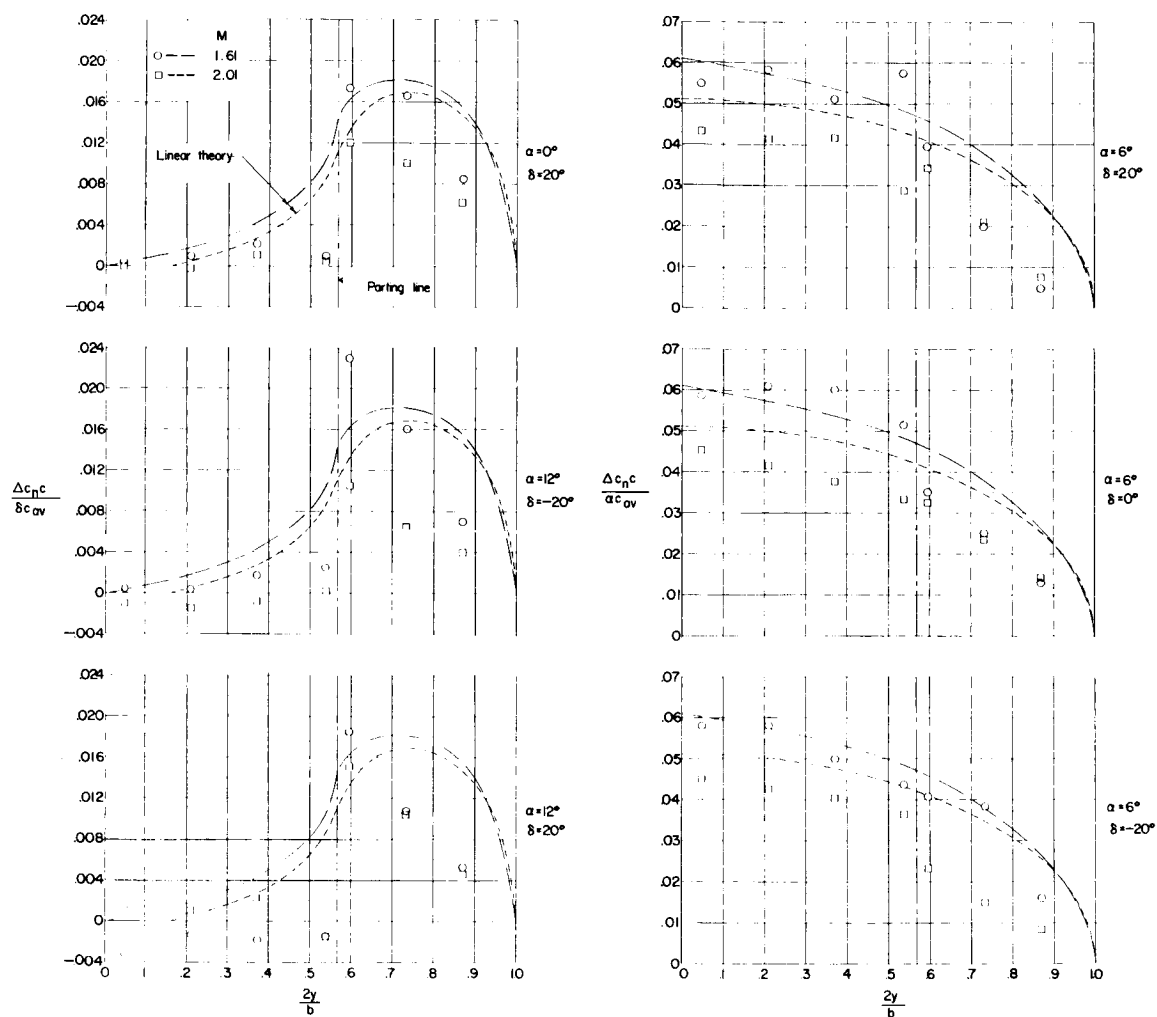


Figure 44.- Concluded.

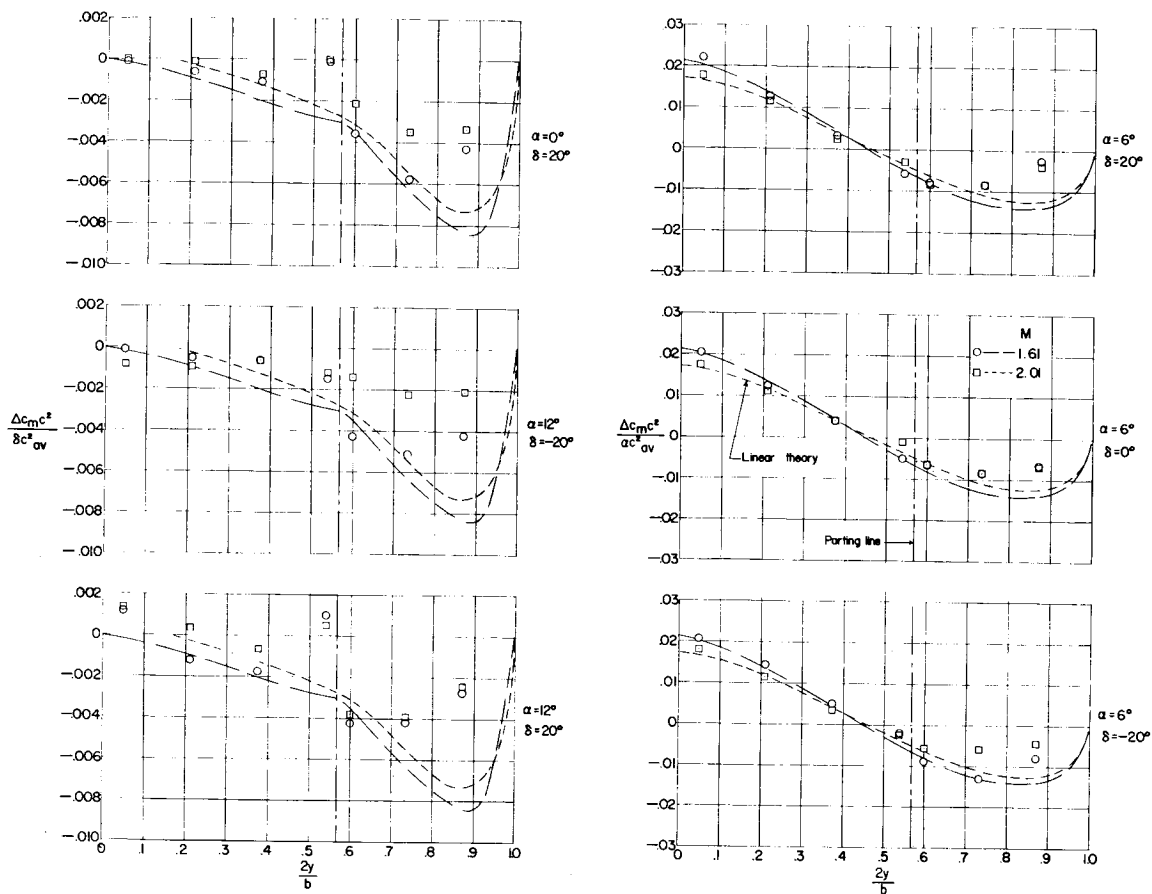
CONFIDENTIAL



(a) Wing normal-force loading
due to δ .

(b) Wing normal-force loading
due to α .

Figure 45.- Effect of Mach number on spanwise normal-force loading distributions for configuration E.

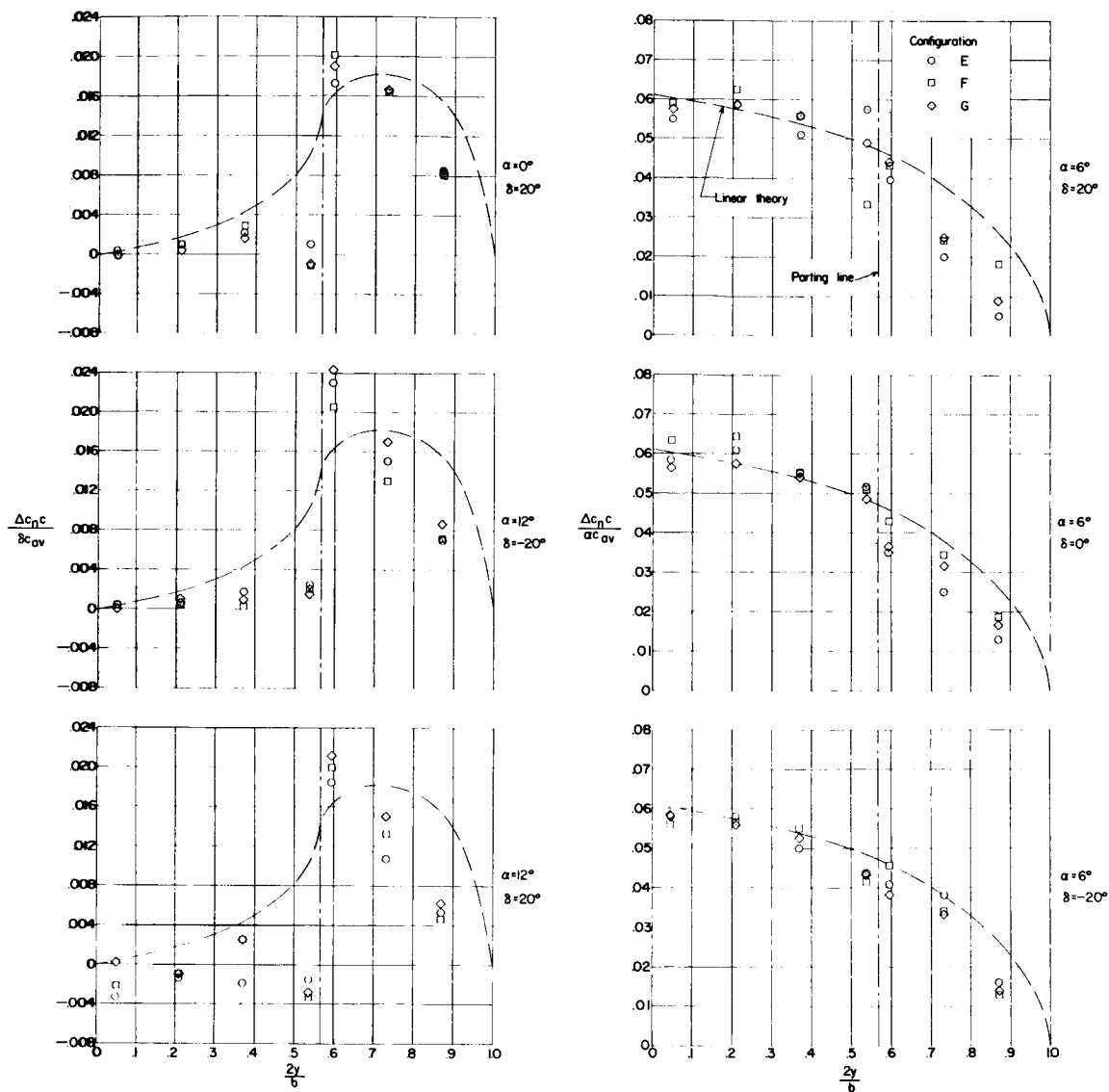


(a) Wing pitching-moment loading due to δ .

(b) Wing pitching-moment loading due to α .

Figure 46.- Effect of Mach number on spanwise pitching-moment loading distribution for configuration E.

037122

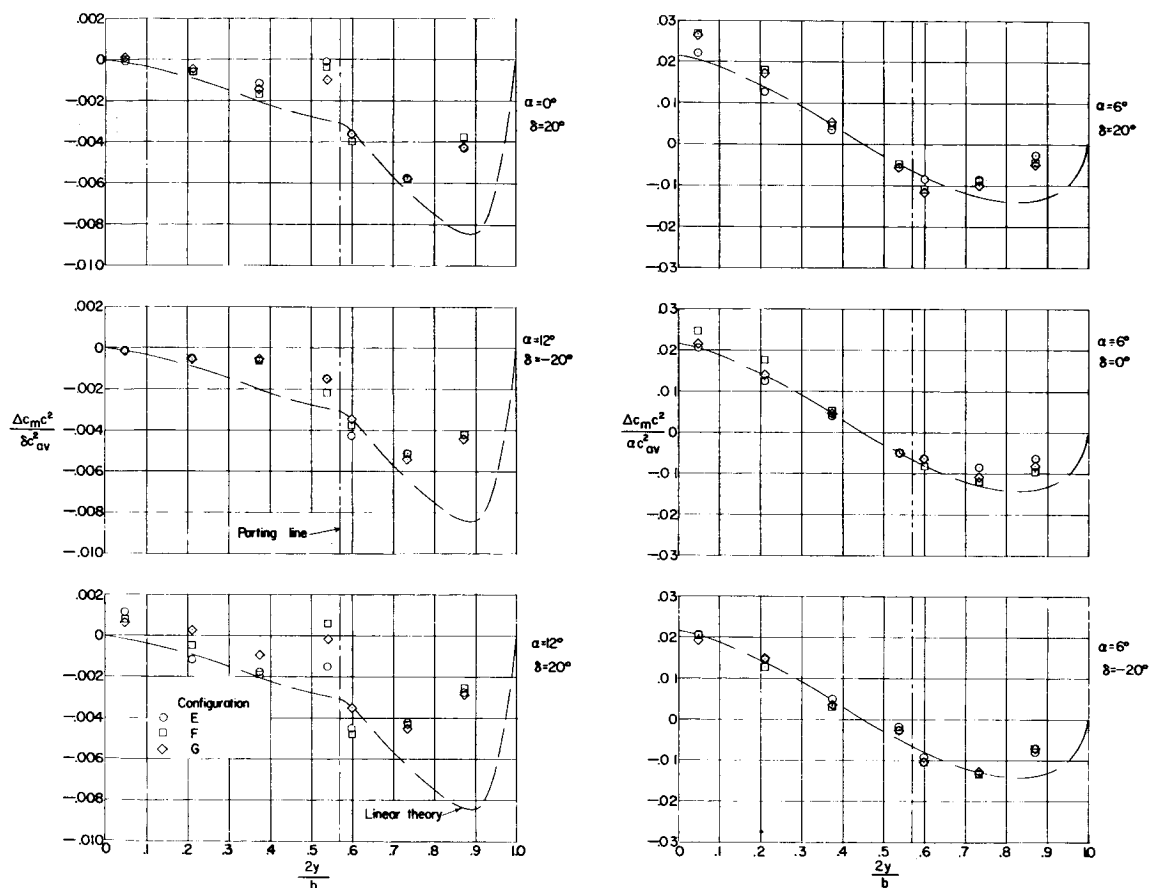


(a) Wing normal-force loading due to δ .

(b) Wing normal-force loading due to α .

Figure 47.- Effect of hinge-line location on spanwise normal-force loading distributions. $M = 1.61$.

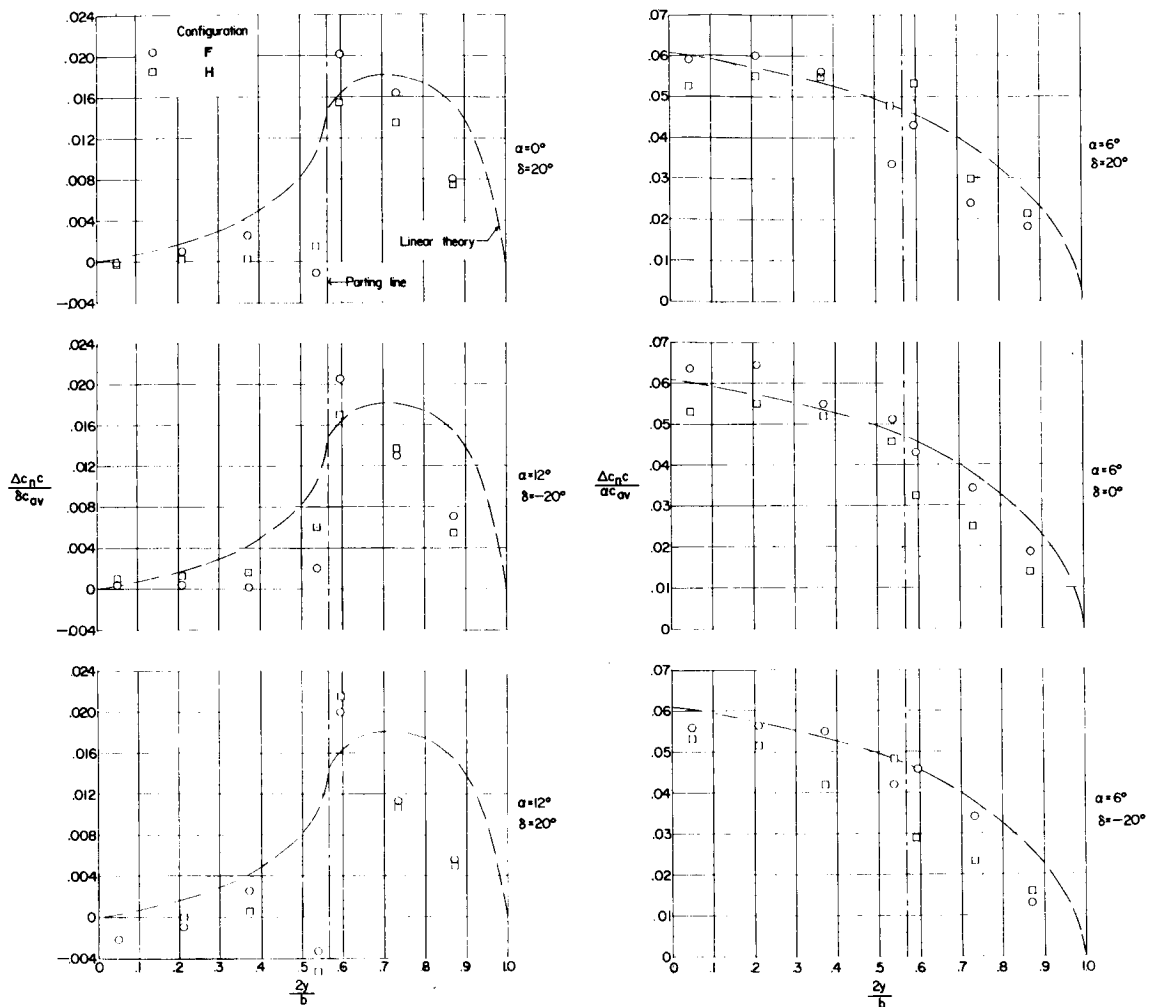
L-258



(a) Wing pitching-moment loading due to δ .

(b) Wing pitching-moment loading due to α .

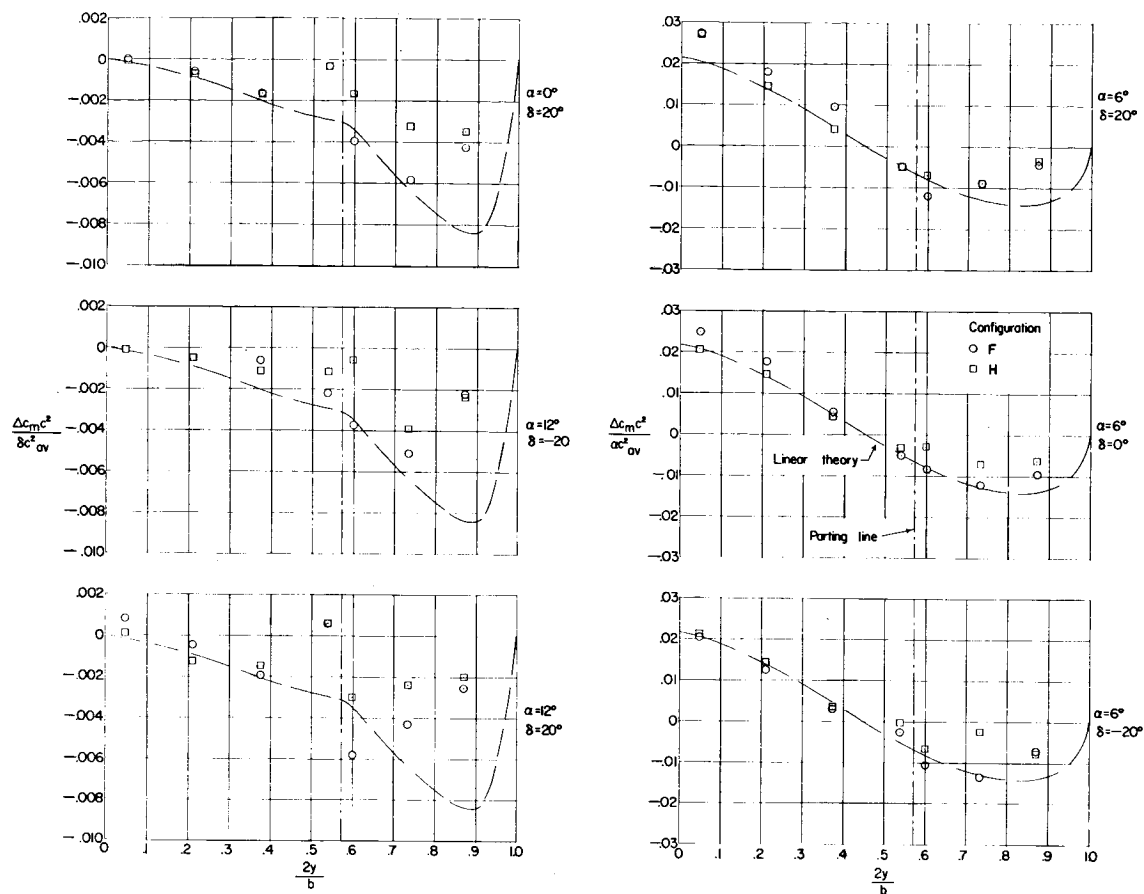
Figure 48.- Effect of hinge-line location on spanwise pitching-moment loading distributions. $M = 1.61$.



(a) Wing normal-force loading due to δ .

(b) Wing normal-force loading due to α .

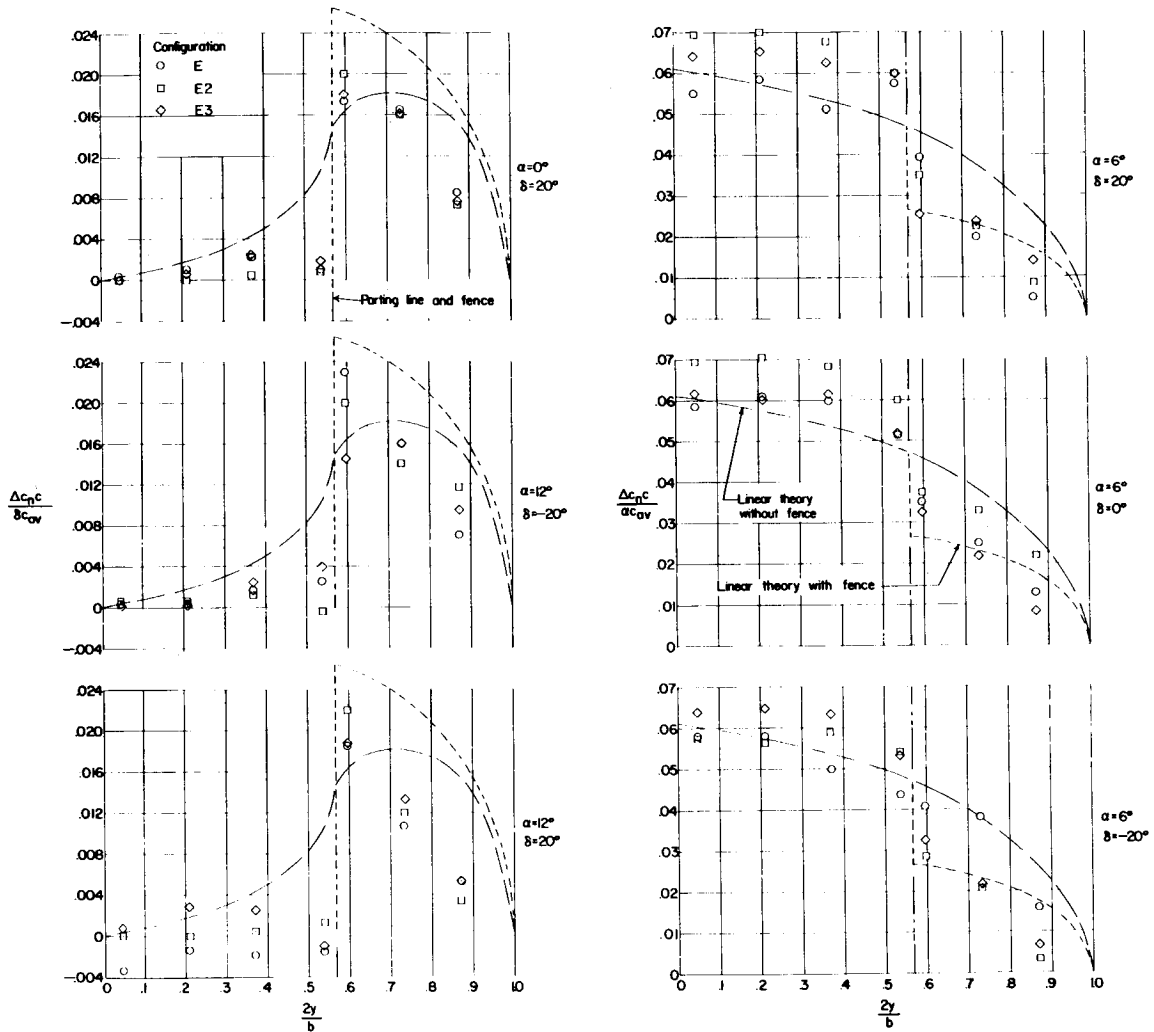
Figure 49.- Effect of offsetting a half-delta tip control with respect to wing on spanwise normal-force loading distributions. $M = 1.61$.



(a) Wing pitching-moment loading due to δ . (b) Wing pitching-moment loading due to α .

Figure 50.- Effect of offsetting a half-delta tip control with respect to wing on spanwise pitching-moment loading distributions. $M = 1.61$.

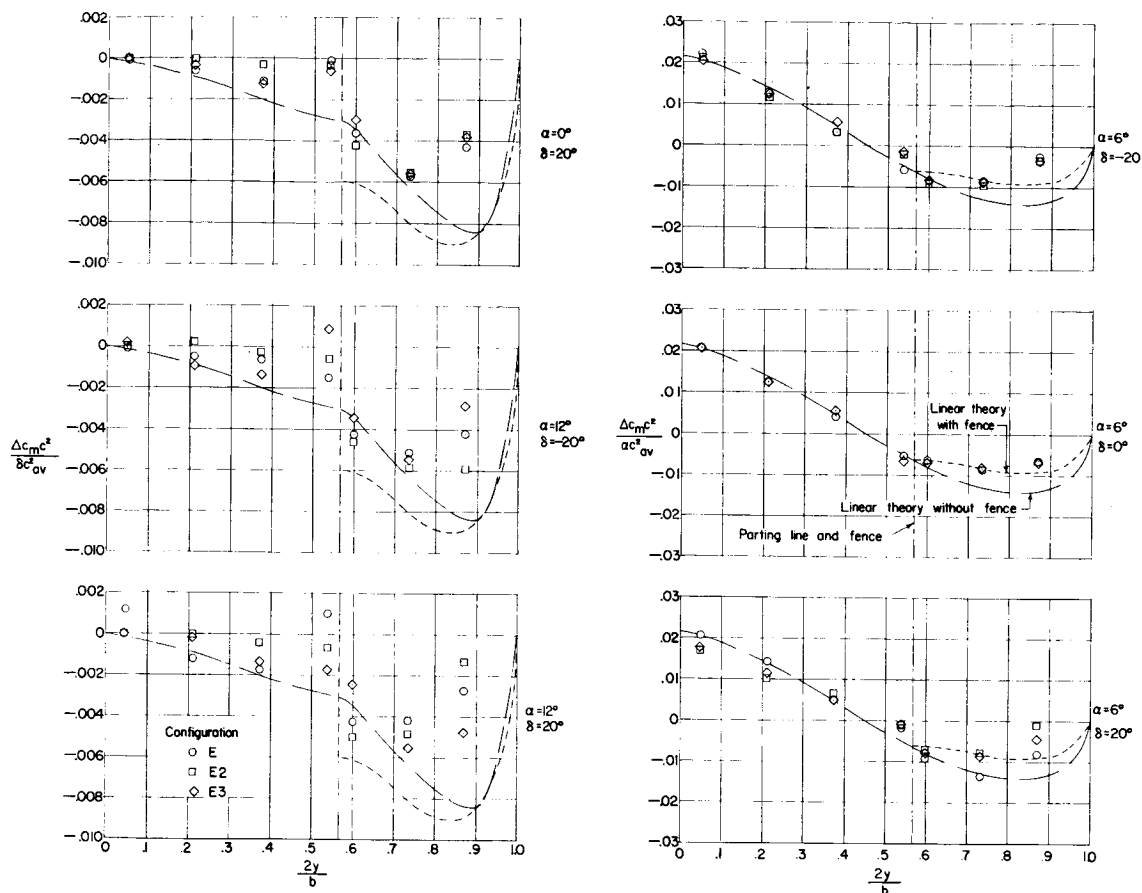
03712 [REDACTED]



(a) Wing normal-force loading due to δ . (b) Wing normal-force loading due to α .

Figure 51.- Effect of fences on spanwise normal-force loading distributions for configuration E. $M = 1.61$.

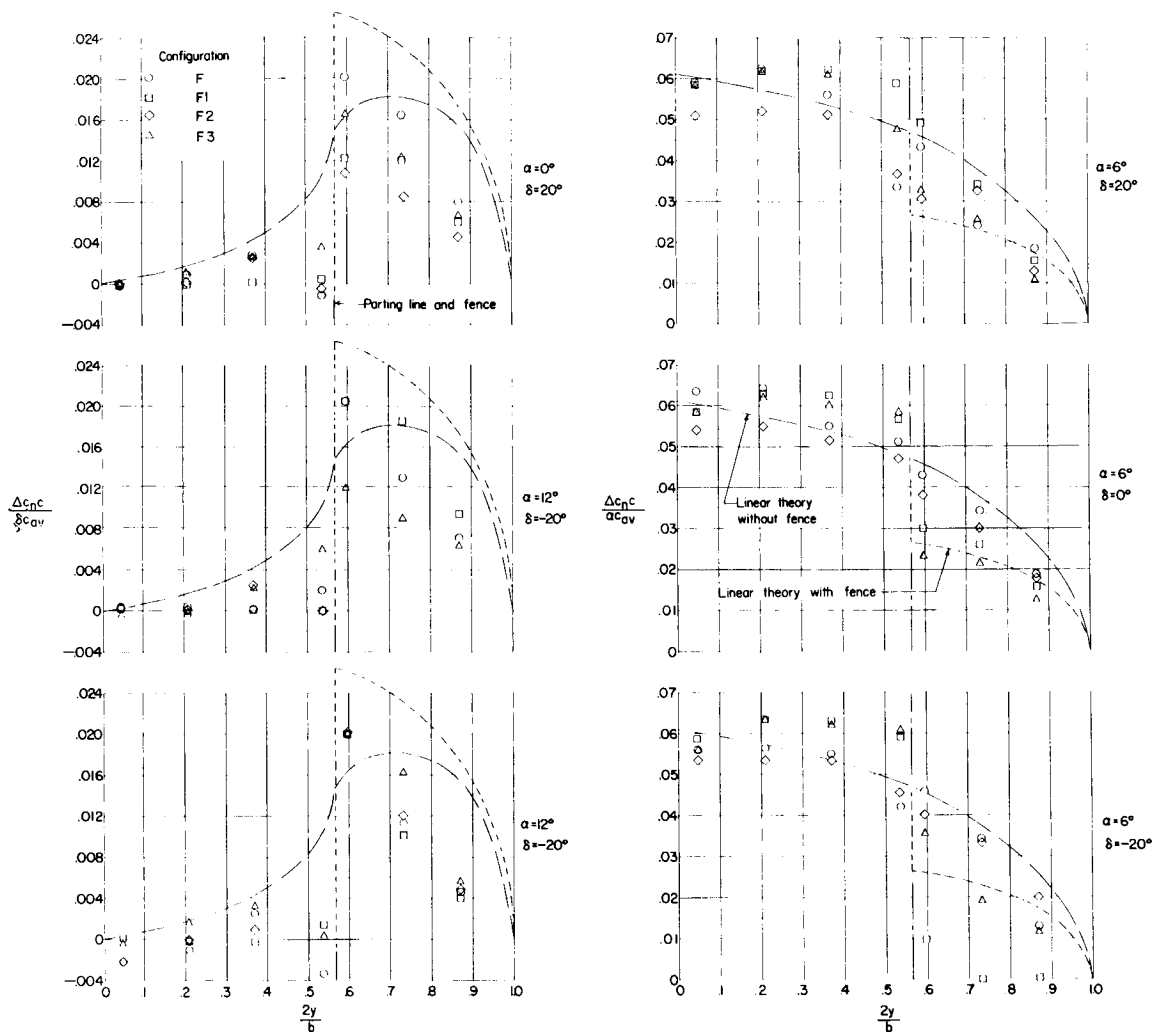
CONFIDENTIAL



(a) Wing pitching-moment loading due to δ .

(b) Wing pitching-moment loading due to α .

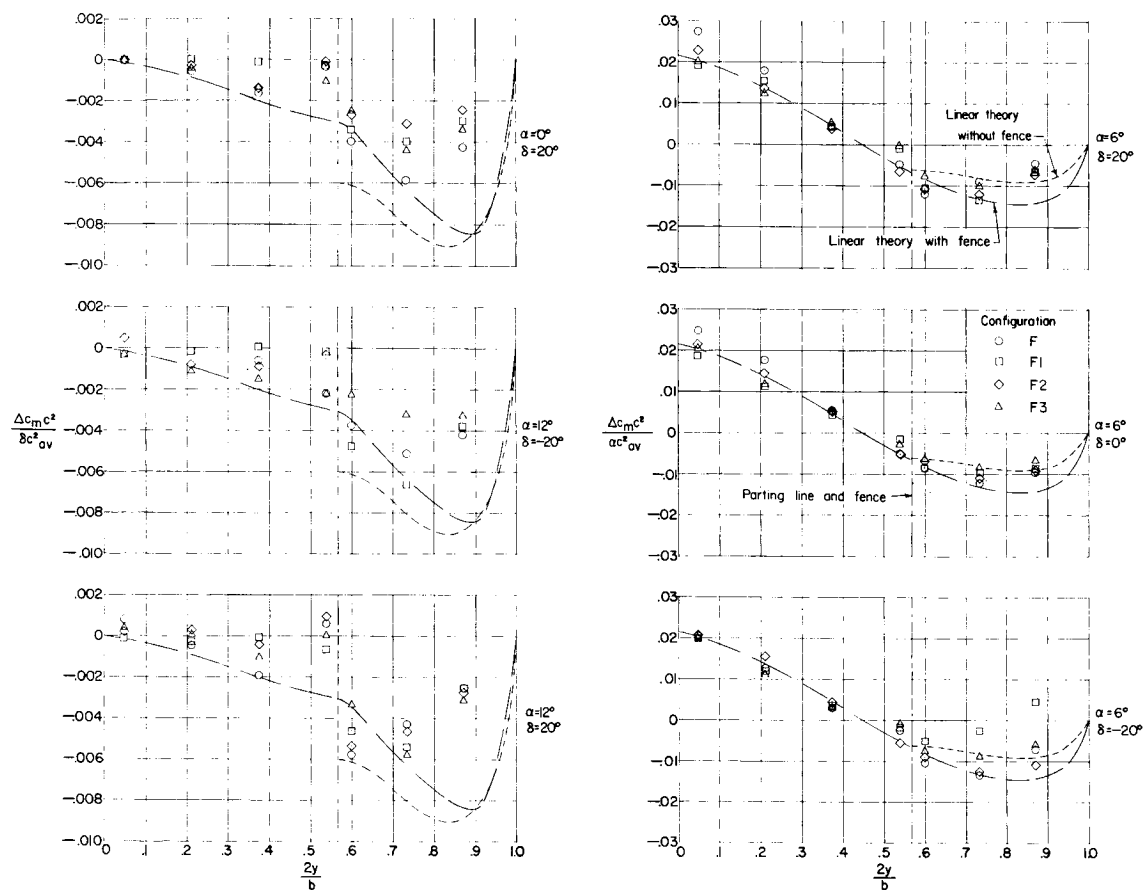
Figure 52.- Effect of fences on spanwise pitching-moment distributions for configuration E. $M = 1.61$.



(a) Wing normal-force loading
due to δ .

(b) Wing normal-force loading
due to α .

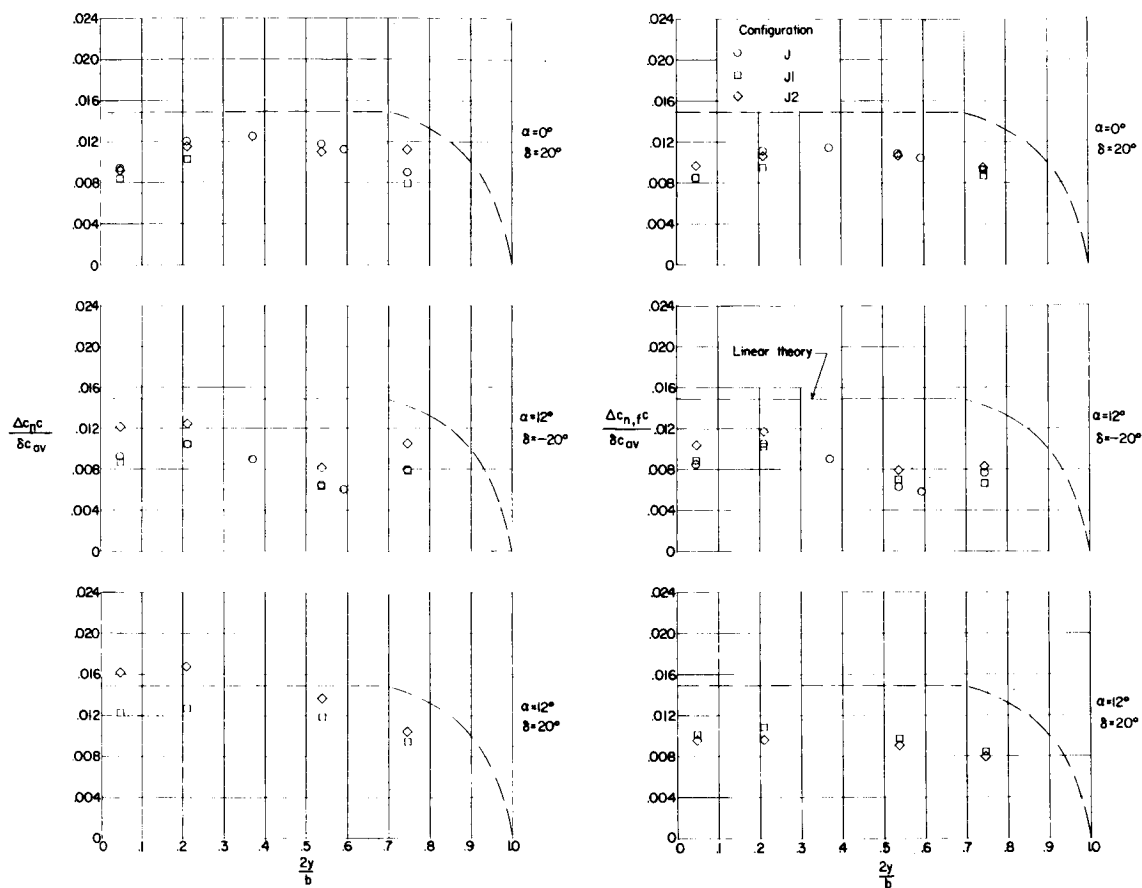
Figure 53.- Effect of fences on spanwise normal-force loading distributions for configuration F. $M = 1.61$.



(a) Wing pitching-moment loading due to δ . (b) Wing pitching-moment loading due to α .

Figure 54.- Effect of fences on spanwise pitching-moment distributions for configuration F. $M = 1.61$.

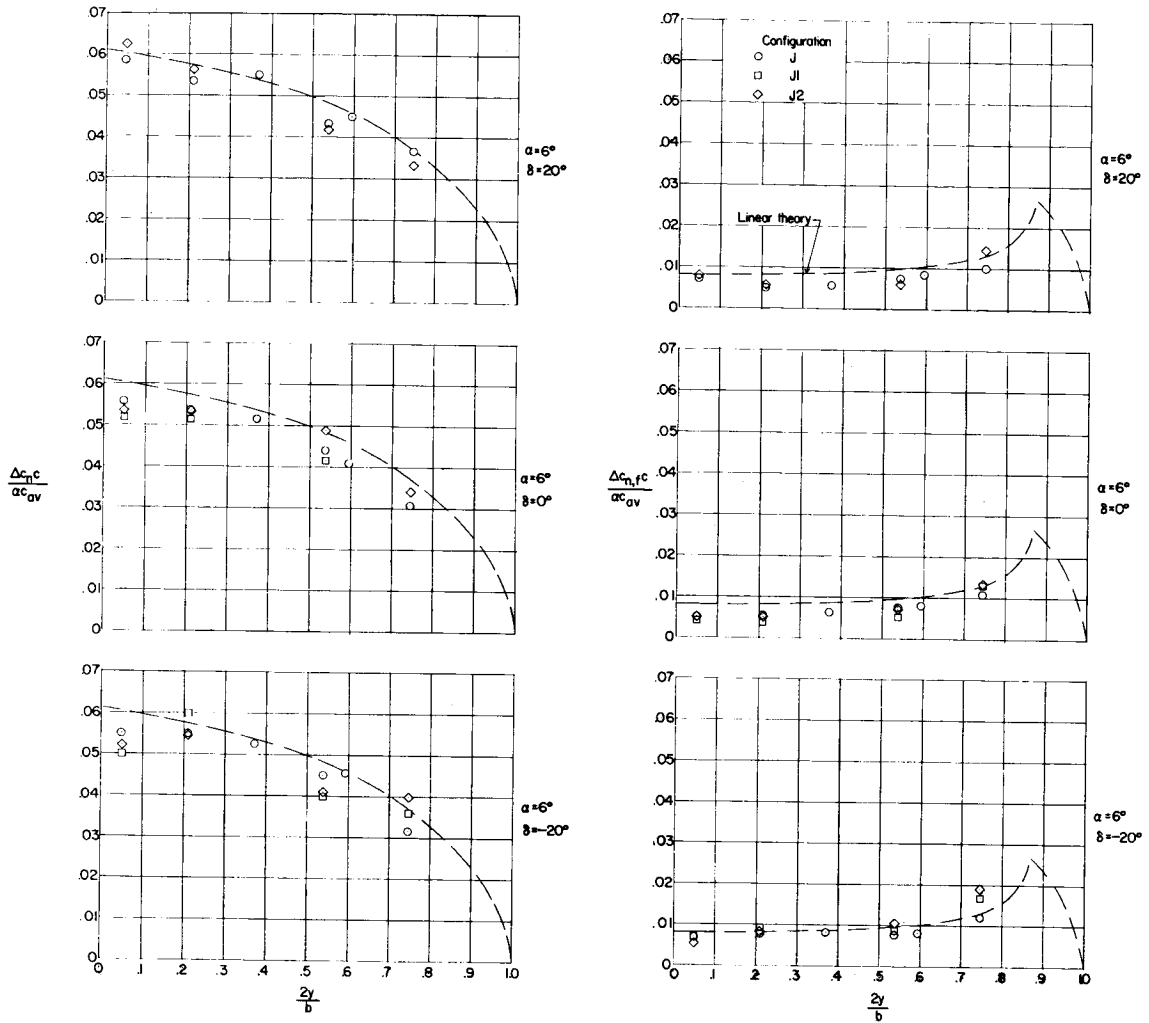
03712 [REDACTED]



(a) Wing normal-force loading
due to δ .

(b) Control normal-force loading
due to δ .

Figure 55.- Effect of trailing-edge thickness on the spanwise normal-force loading distributions for configuration J. $M = 1.61$.

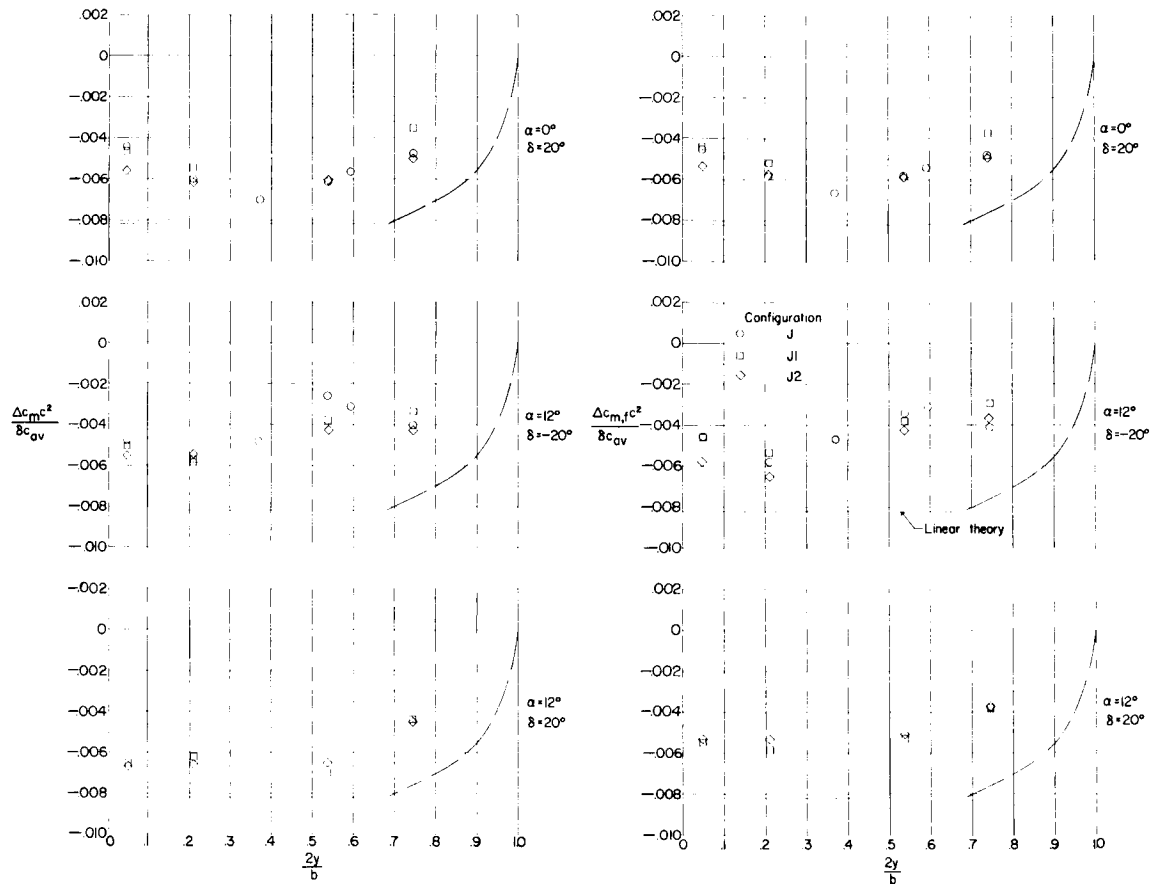


(c) Wing normal-force loading due to α .

(d) Control normal-force loading due to α .

Figure 55.- Concluded.

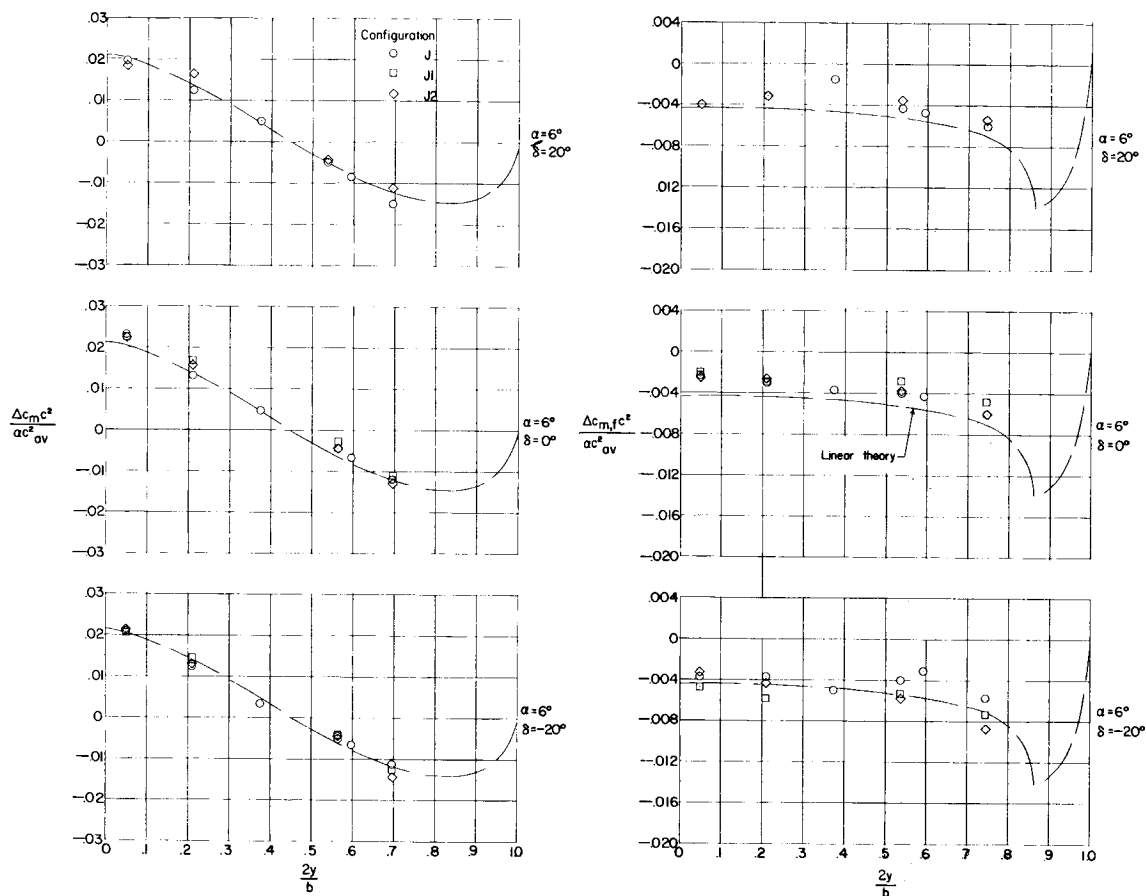
CONFIDENTIAL



(a) Wing pitching-moment loading due to δ .

(b) Control pitching-moment loading due to δ .

Figure 56.- Effect of trailing-edge thickness on the spanwise pitching-moment loading distributions for configuration J. $M = 1.61$.

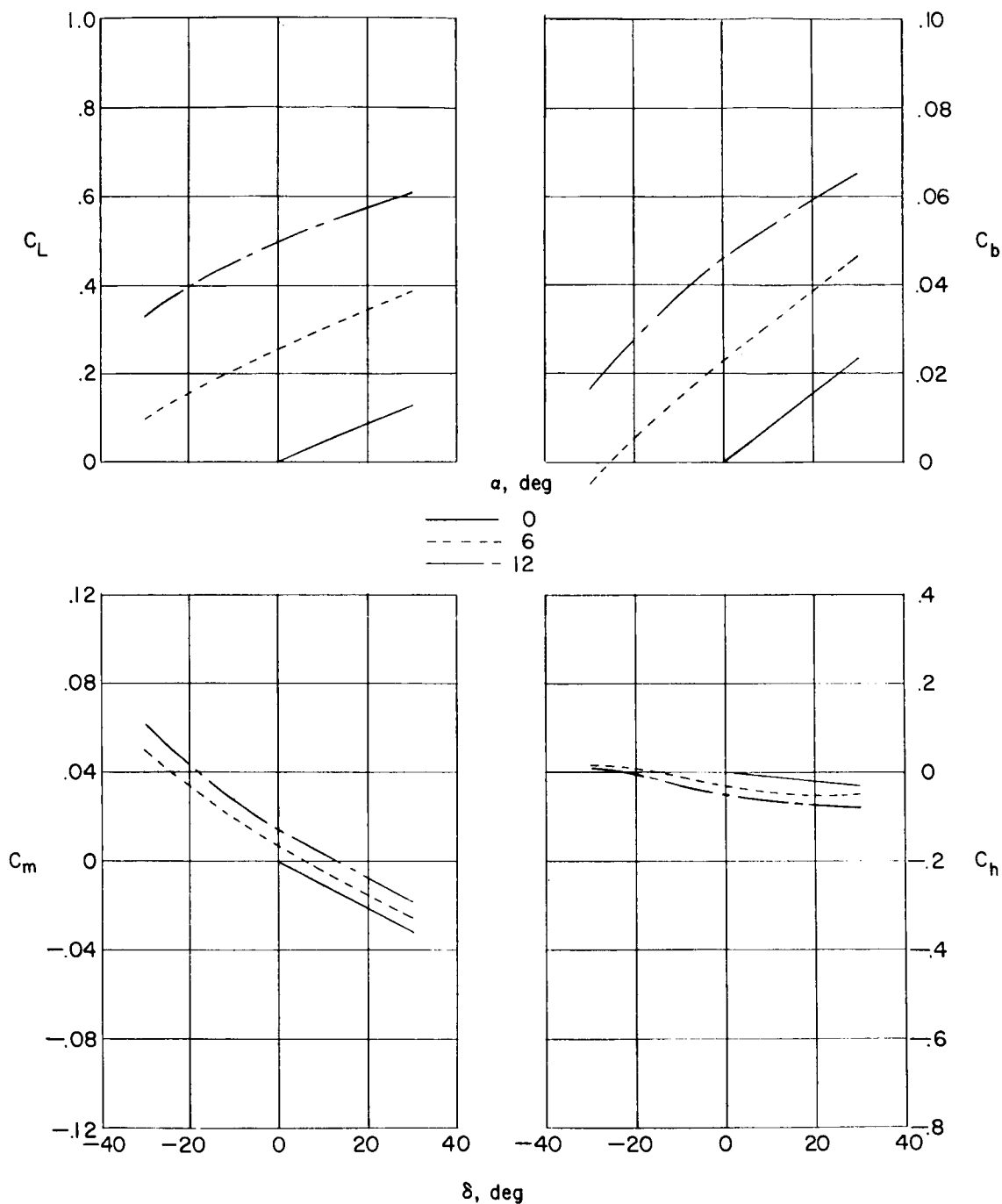


(c) Wing pitching-moment loading due to α .

(b) Control pitching-moment loading due to α .

Figure 56.- Concluded.

03712 ~~SECRET~~ 30



L-258

Figure 57.- Variation of lift, pitching moment, root bending moment, and hinge moment with control deflection and angle of attack for configuration F1. $M = 1.61$.

SECRET

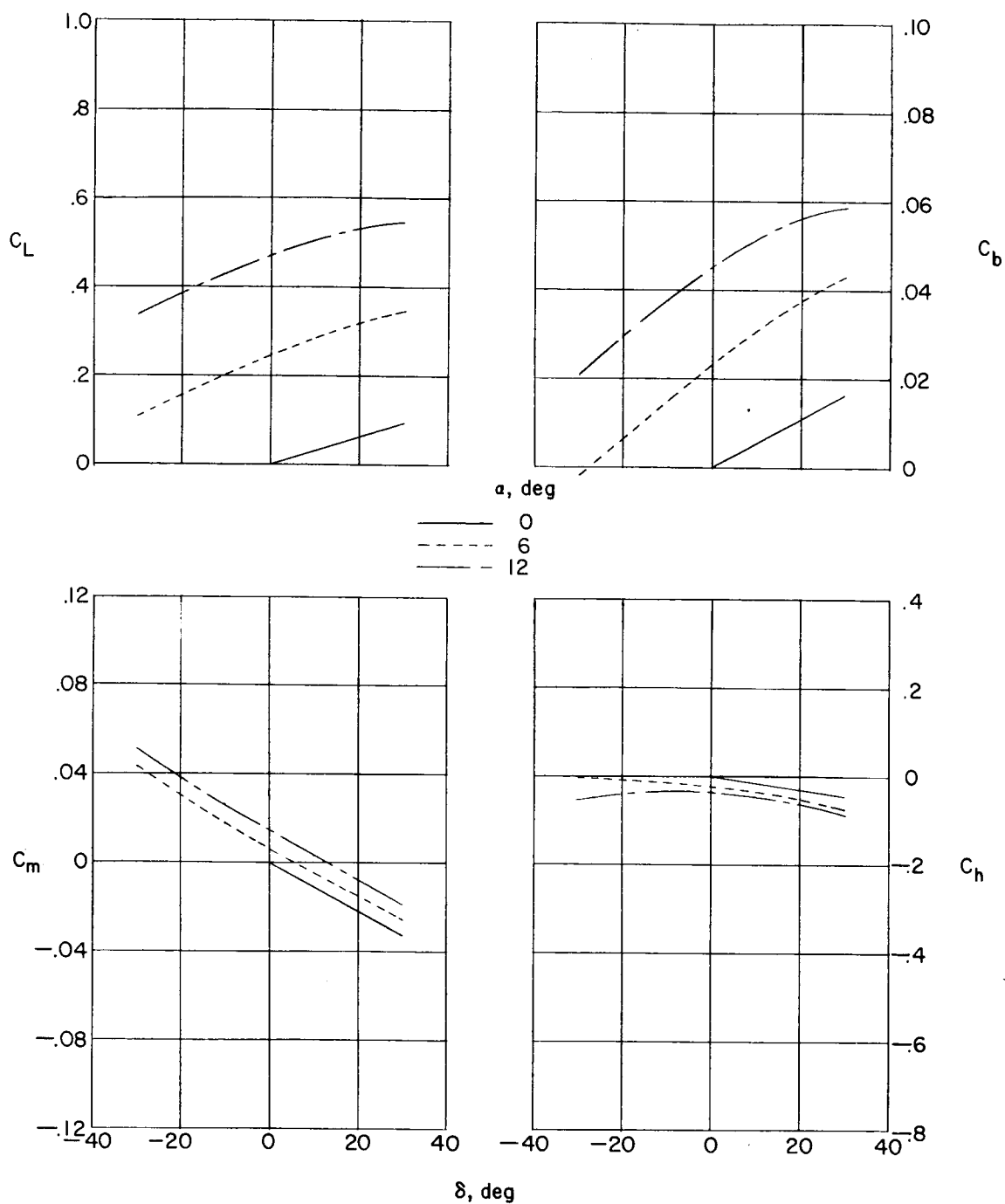


Figure 58.- Variation of lift, pitching moment, root bending moment, and hinge moment with control deflection and angle of attack for configuration F2. $M = 1.61$.

03712-1030

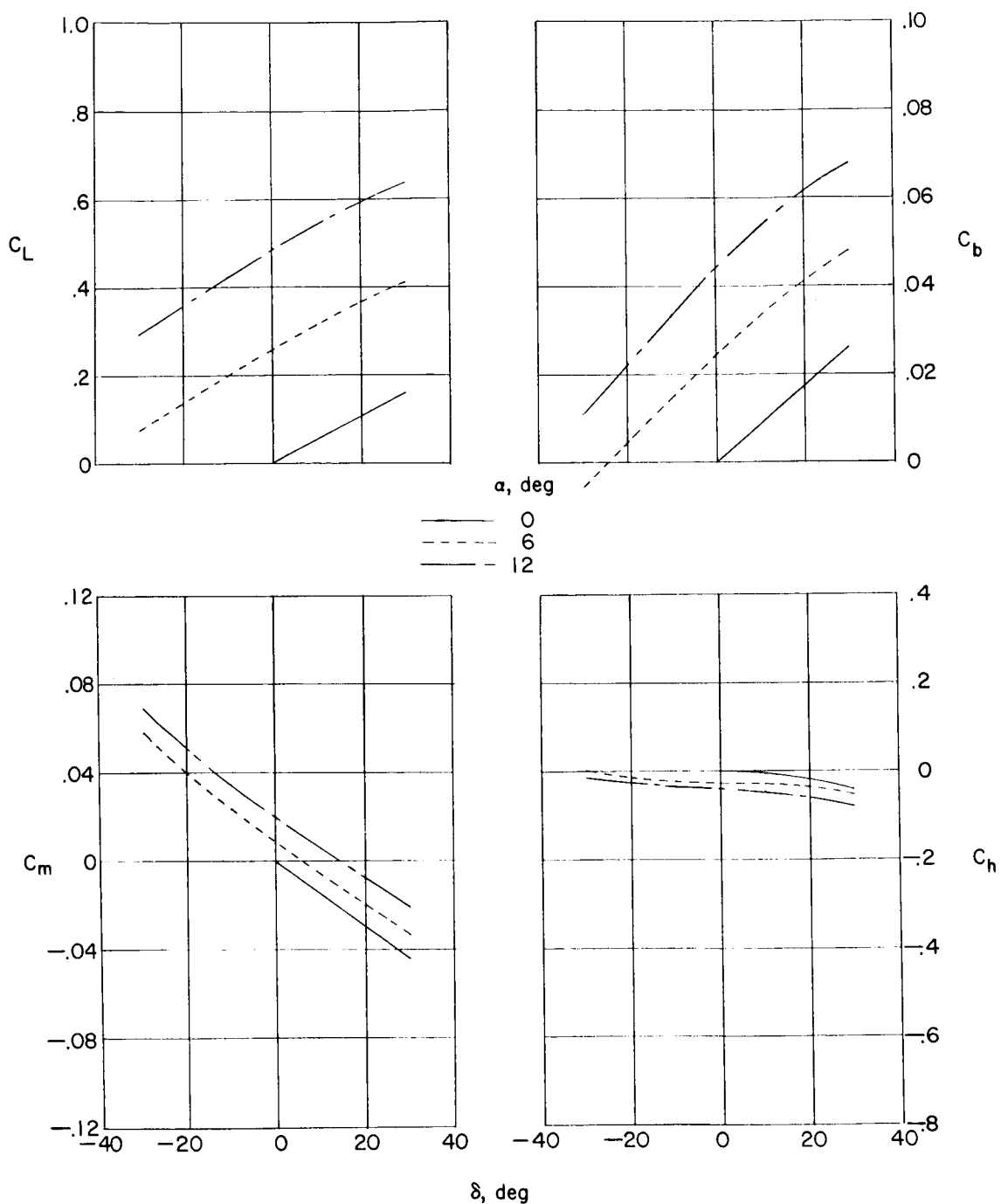


Figure 59.- Variation of lift, pitching moment, root bending moment, and hinge moment with control deflection and angle of attack for configuration F3. $M = 1.61$.

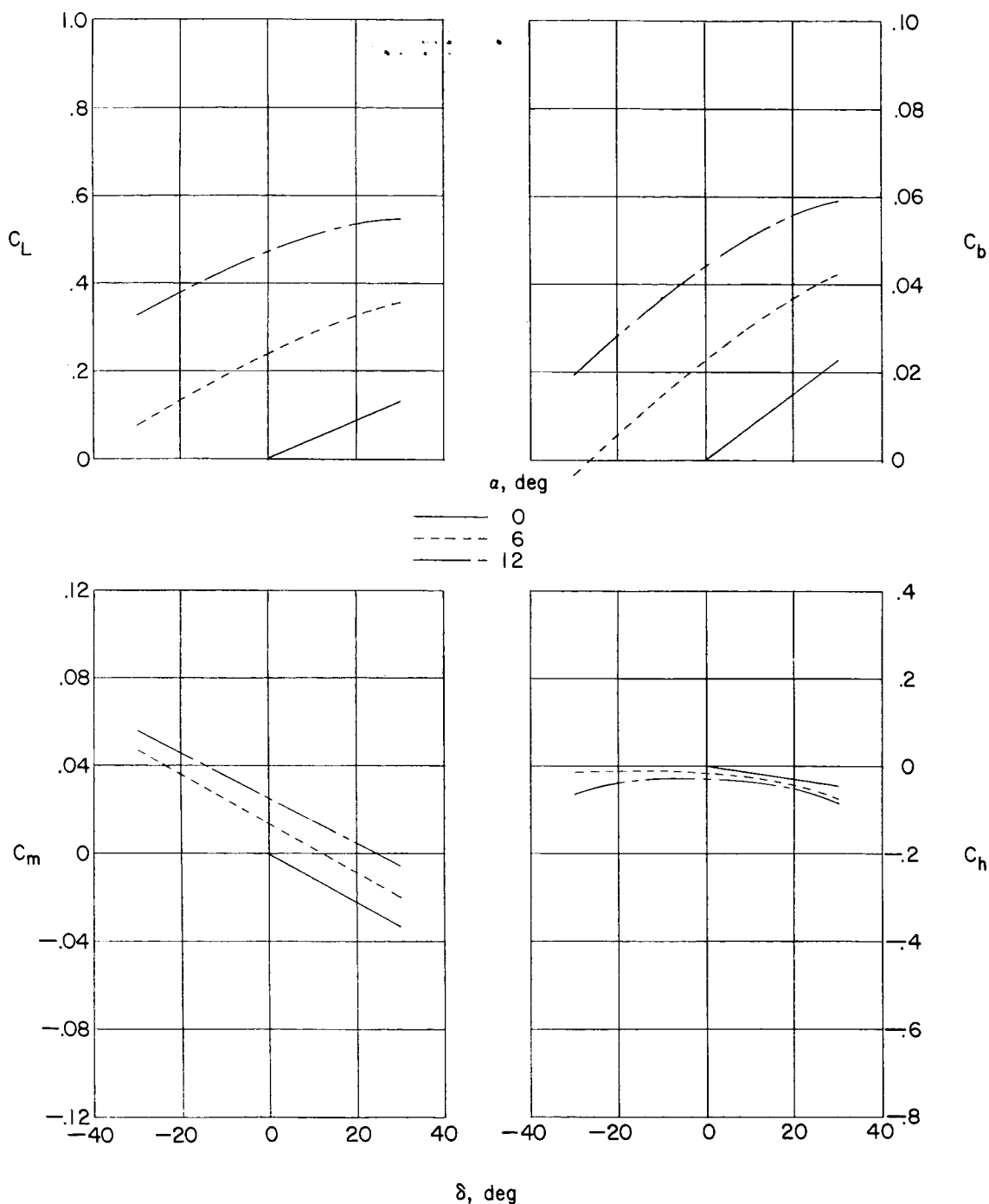


Figure 60.- Variation of lift, pitching moment, root bending moment, and hinge moment with control deflection and angle of attack for configuration H. $M = 1.61$.

03713 [REDACTED] 30

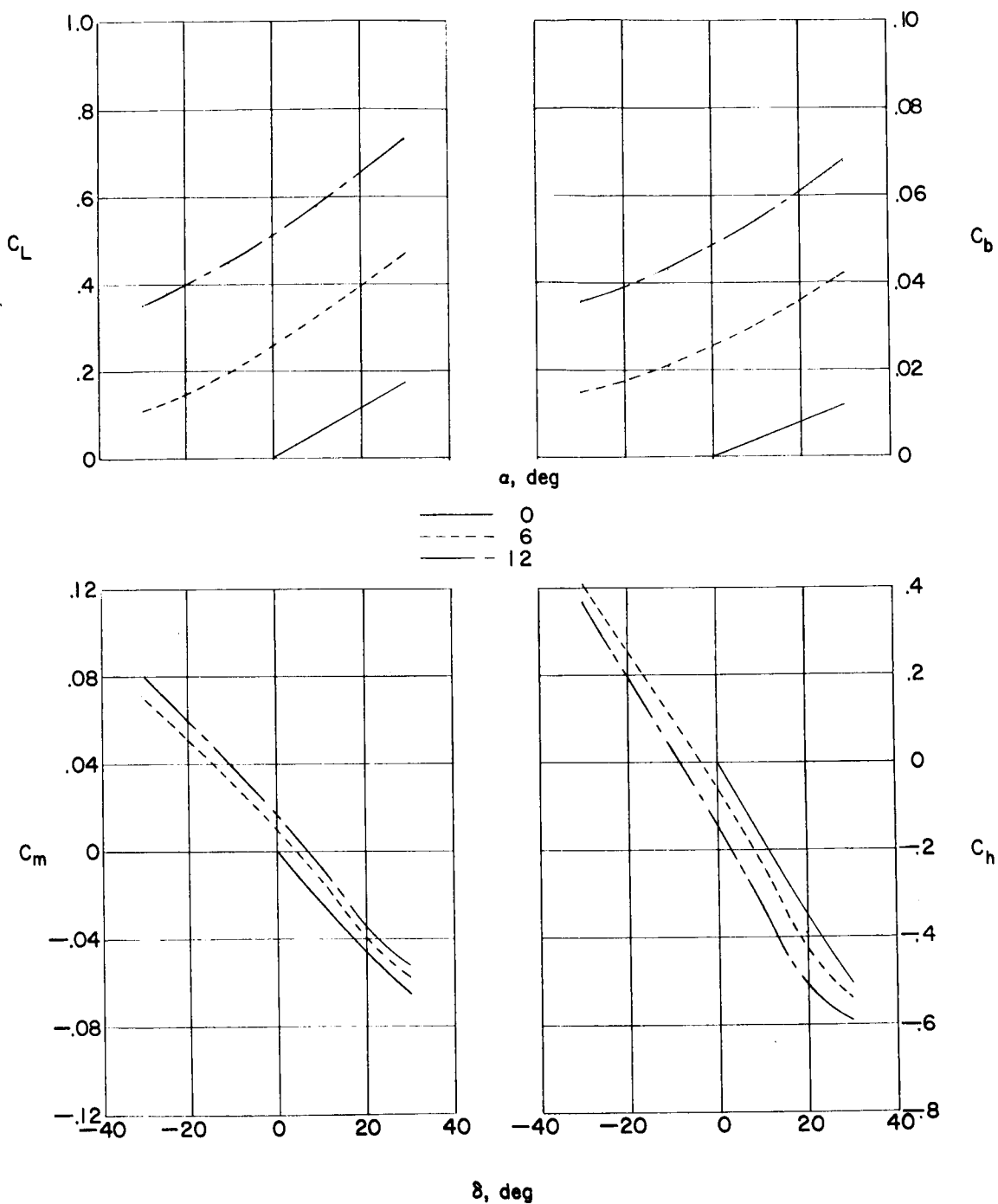


Figure 61.- Variation of lift, pitching moment, root bending moment, and hinge moment with control deflection and angle of attack for configuration I. $M = 1.61$.

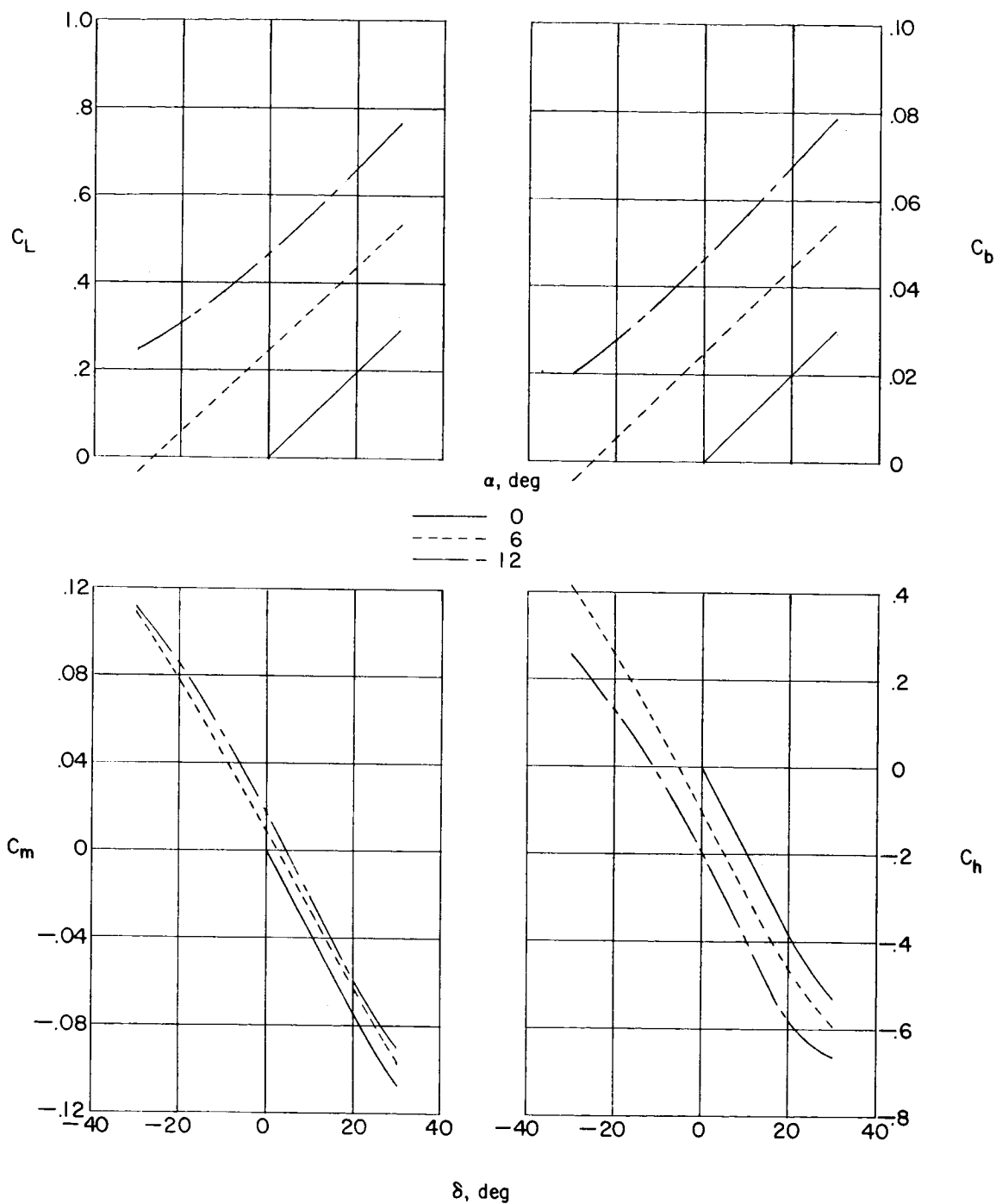


Figure 62.- Variation of lift, pitching moment, root bending moment, and hinge moment with control deflection and angle of attack for configuration J1. $M = 1.61$.

[REDACTED]

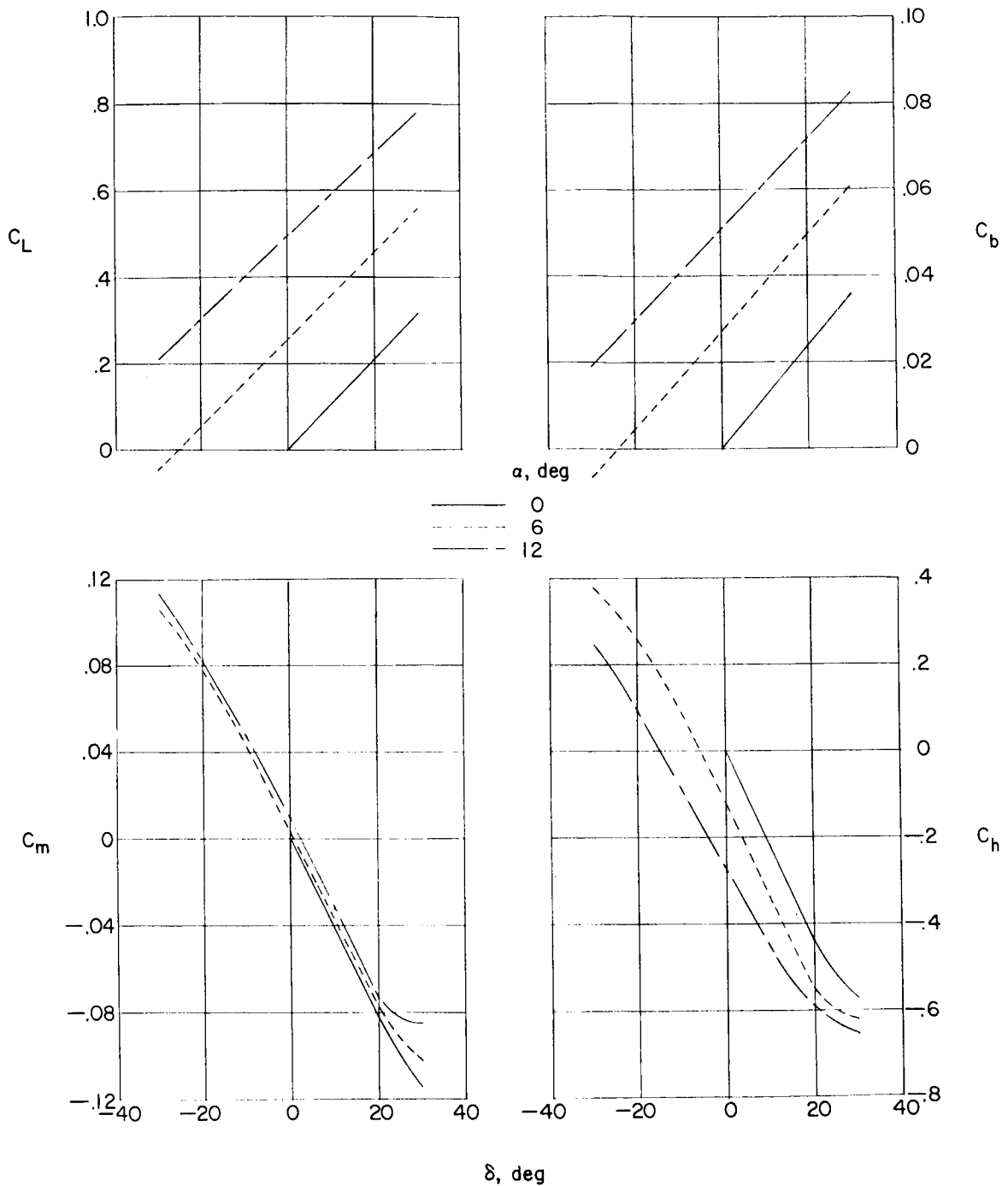


Figure 63.- Variation of lift, pitching moment, root bending moment, and hinge moment with control deflection and angle of attack for configuration J2. $M = 1.61$.

[REDACTED]

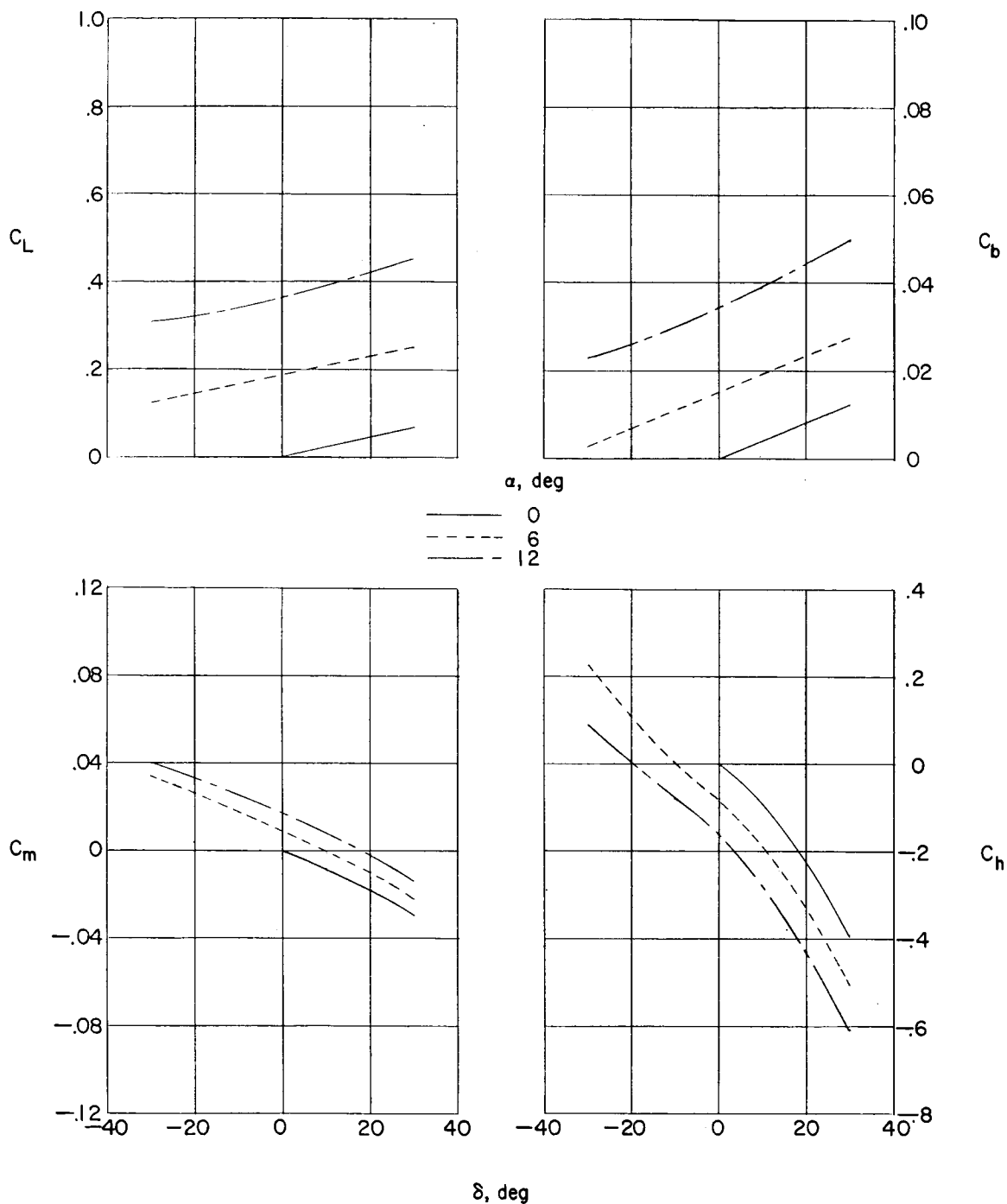


Figure 64.- Variation of lift, pitching moment, root bending moment, and hinge moment with control deflection and angle of attack for configuration A. $M = 2.01$.

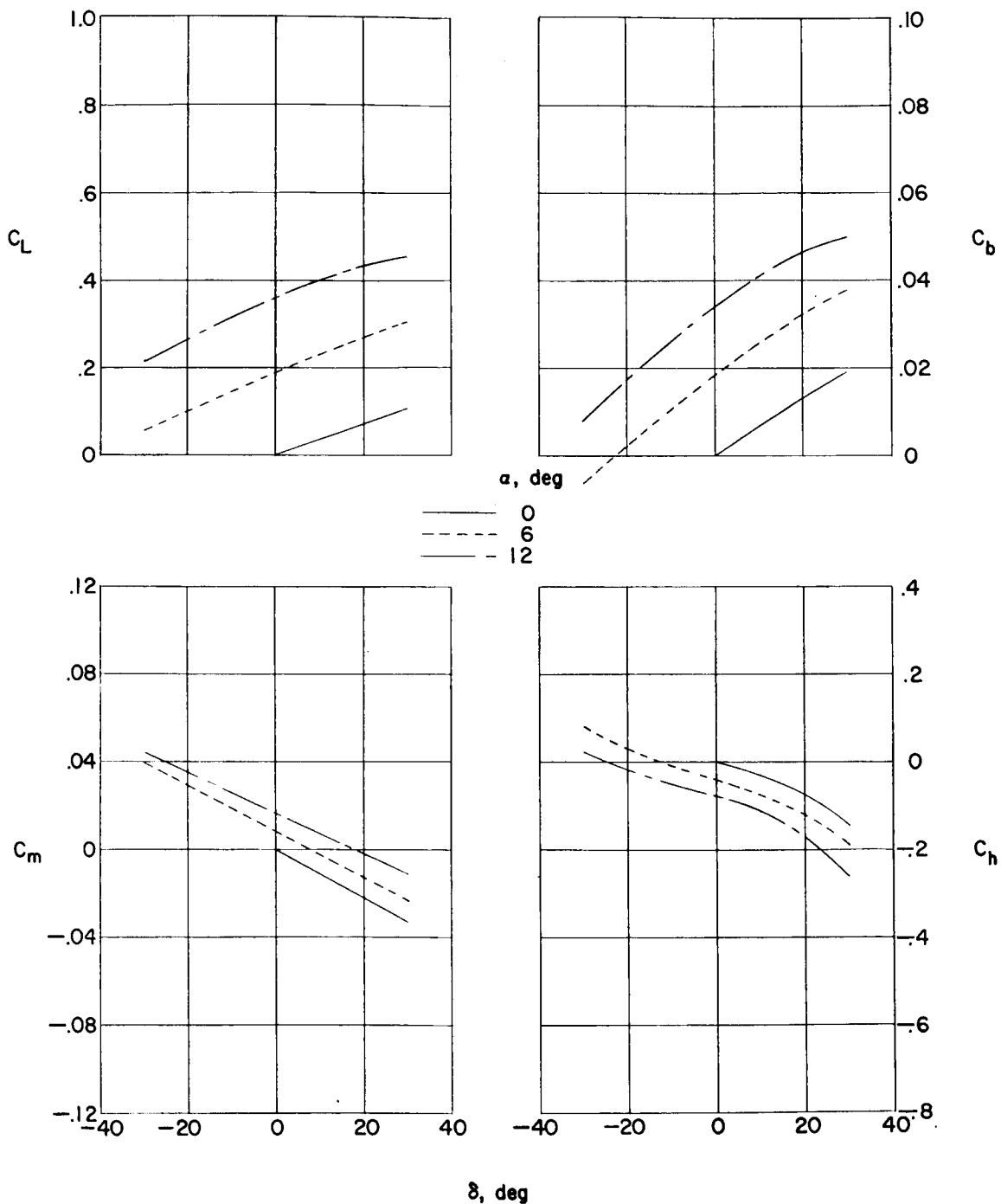


Figure 65.- Variation of lift, pitching moment, root bending moment, and hinge moment with control deflection and angle of attack for configuration E. $M = 2.01$.

SECRET

111

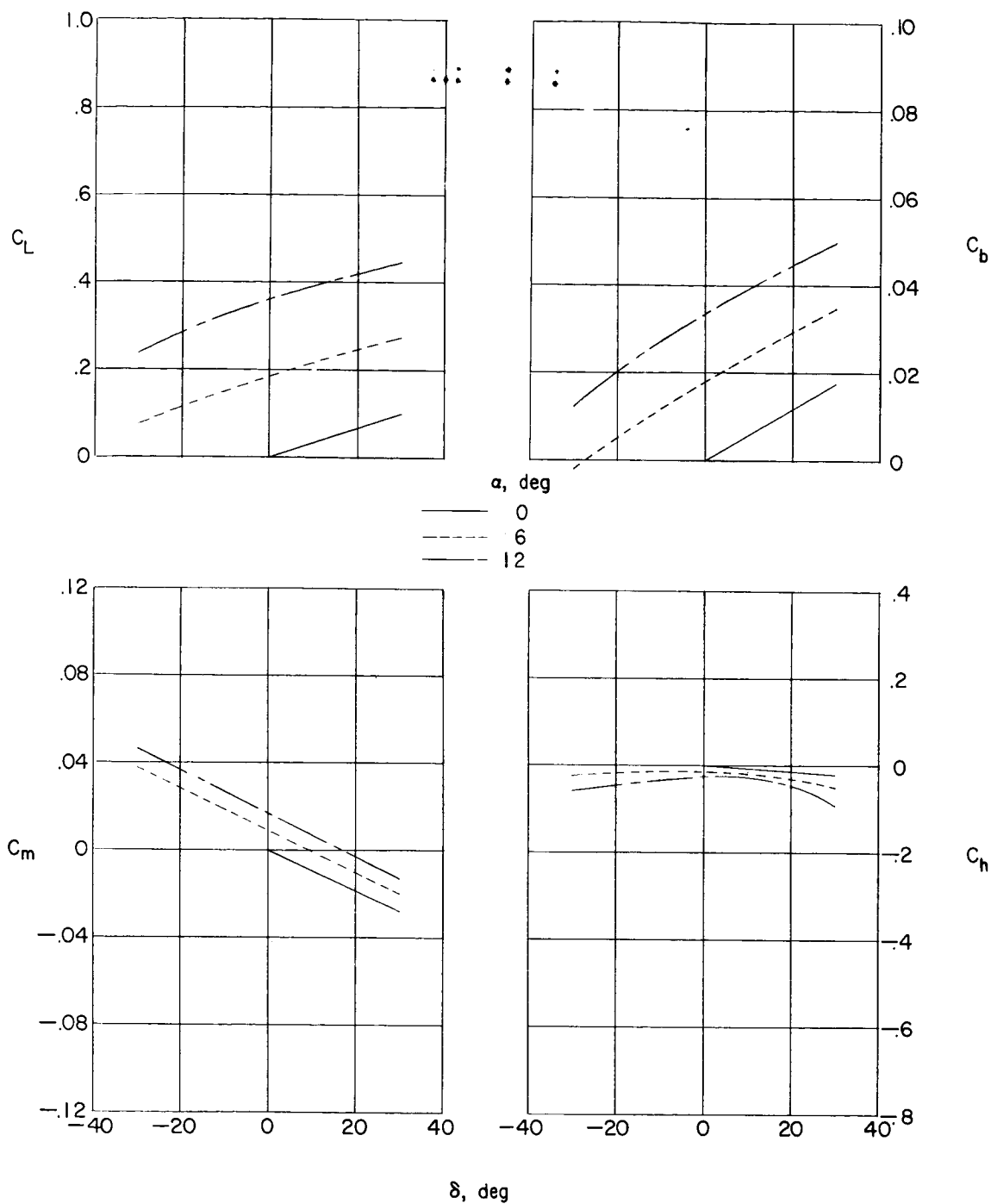


Figure 66.- Variation of lift, pitching moment, root bending moment, and hinge moment with control deflection and angle of attack for configuration F. $M = 2.01$.

03713 [REDACTED]

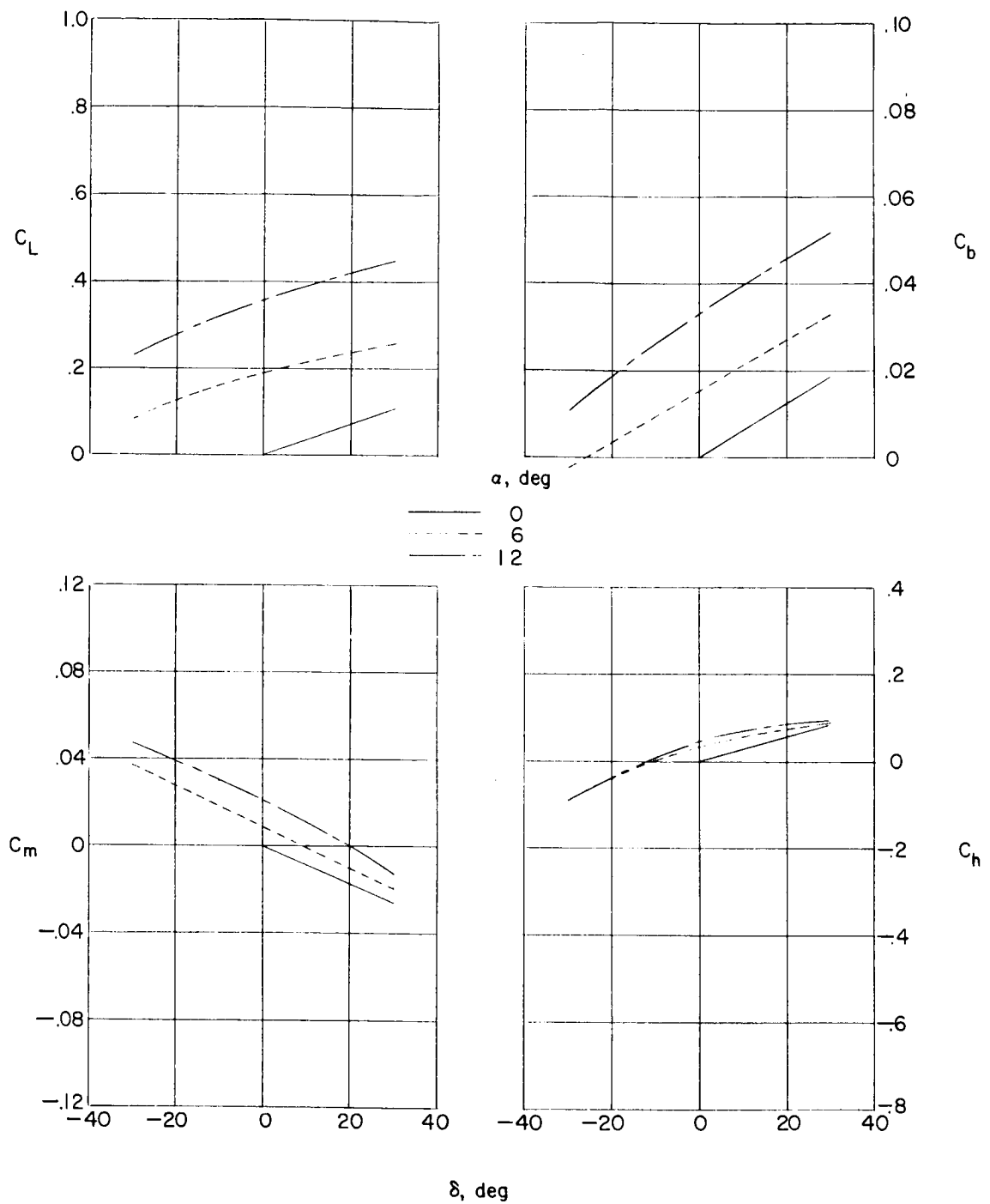


Figure 67.- Variation of lift, pitching moment, root bending moment, and hinge moment with control deflection and angle of attack for configuration G. $M = 2.01$.

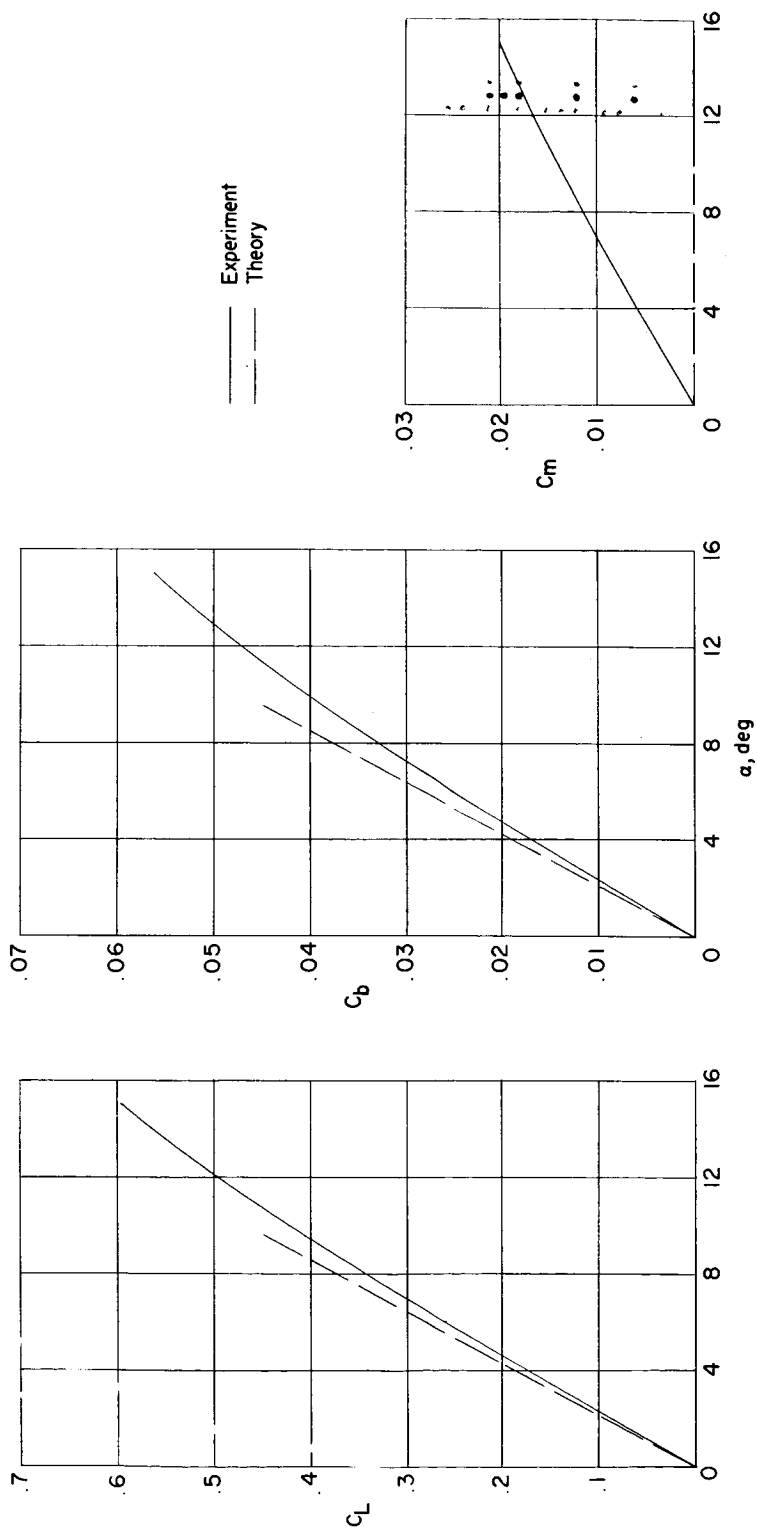


Figure 68.- Variations of wing lift, bending-moment, and pitching-moment coefficients with angle of attack. $M = 1.61$; $\delta = 0^\circ$.

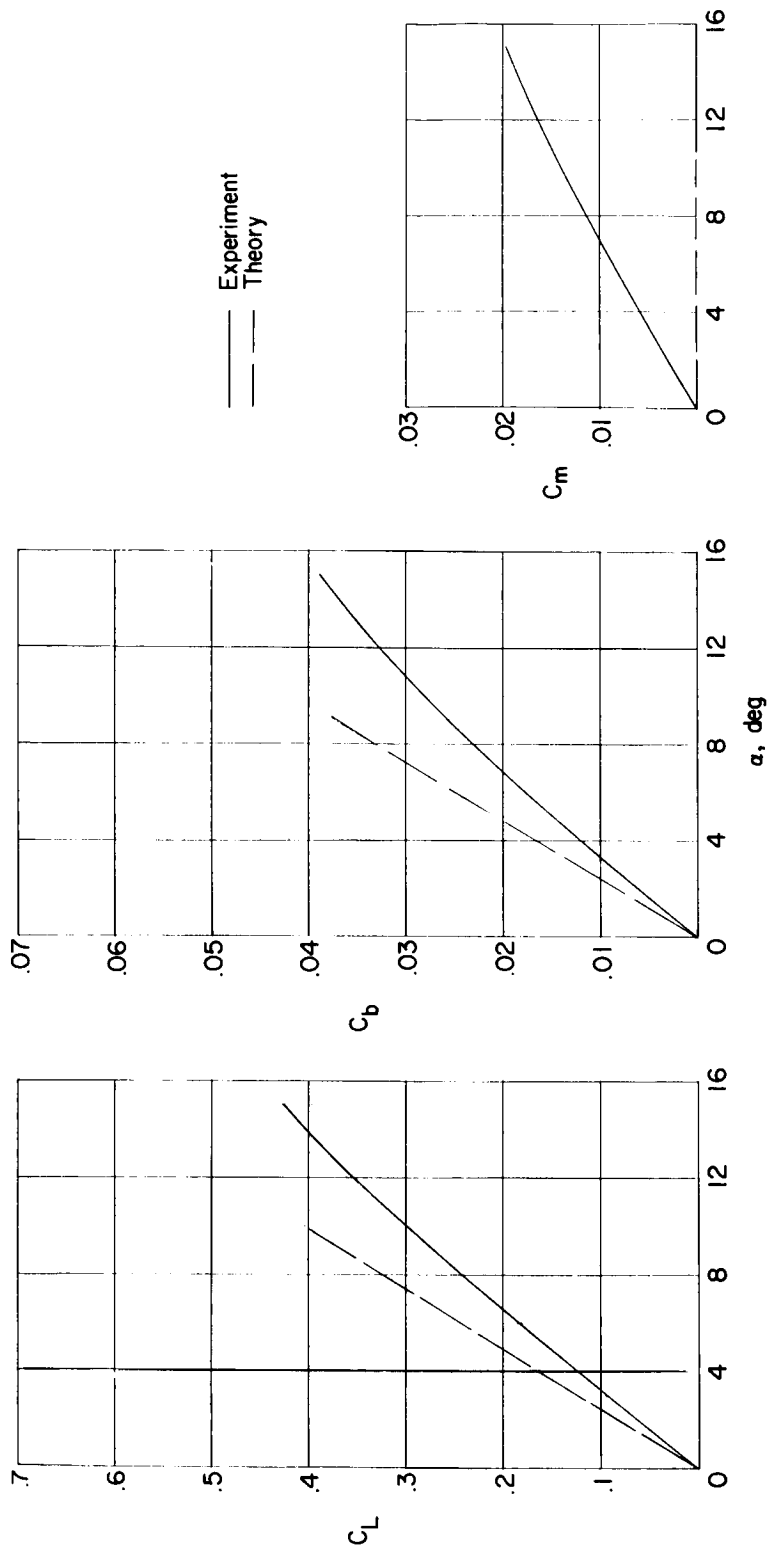


Figure 69.- Variations of wing lift, bending-moment, and pitching-moment coefficients with angle of attack. $M = 2.01$; $\delta = 0^\circ$.

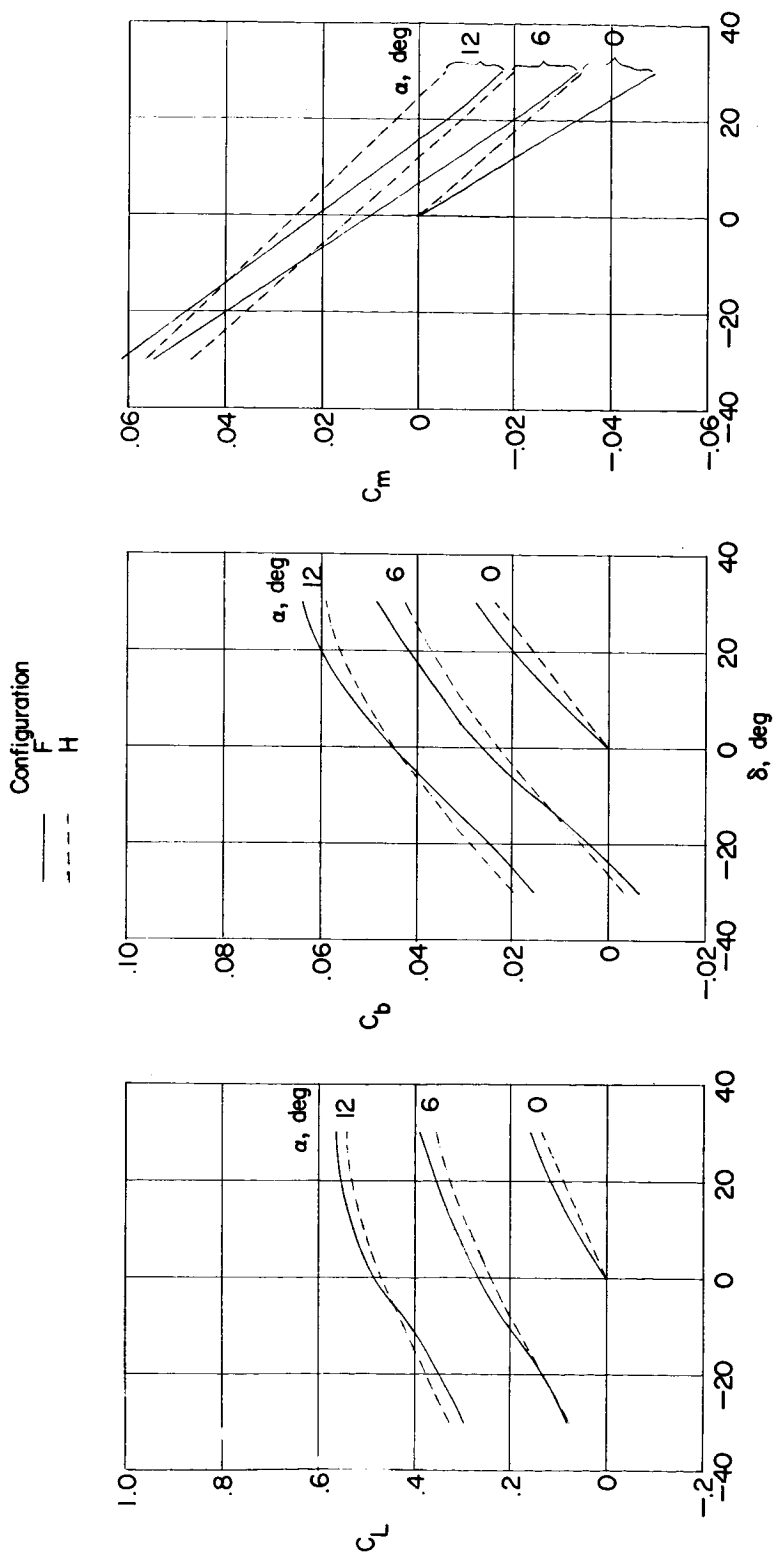


Figure 70.- Effect of offsetting a half-delta tip control with respect to wing on the integrated aerodynamic characteristics. $M = 1.61$.

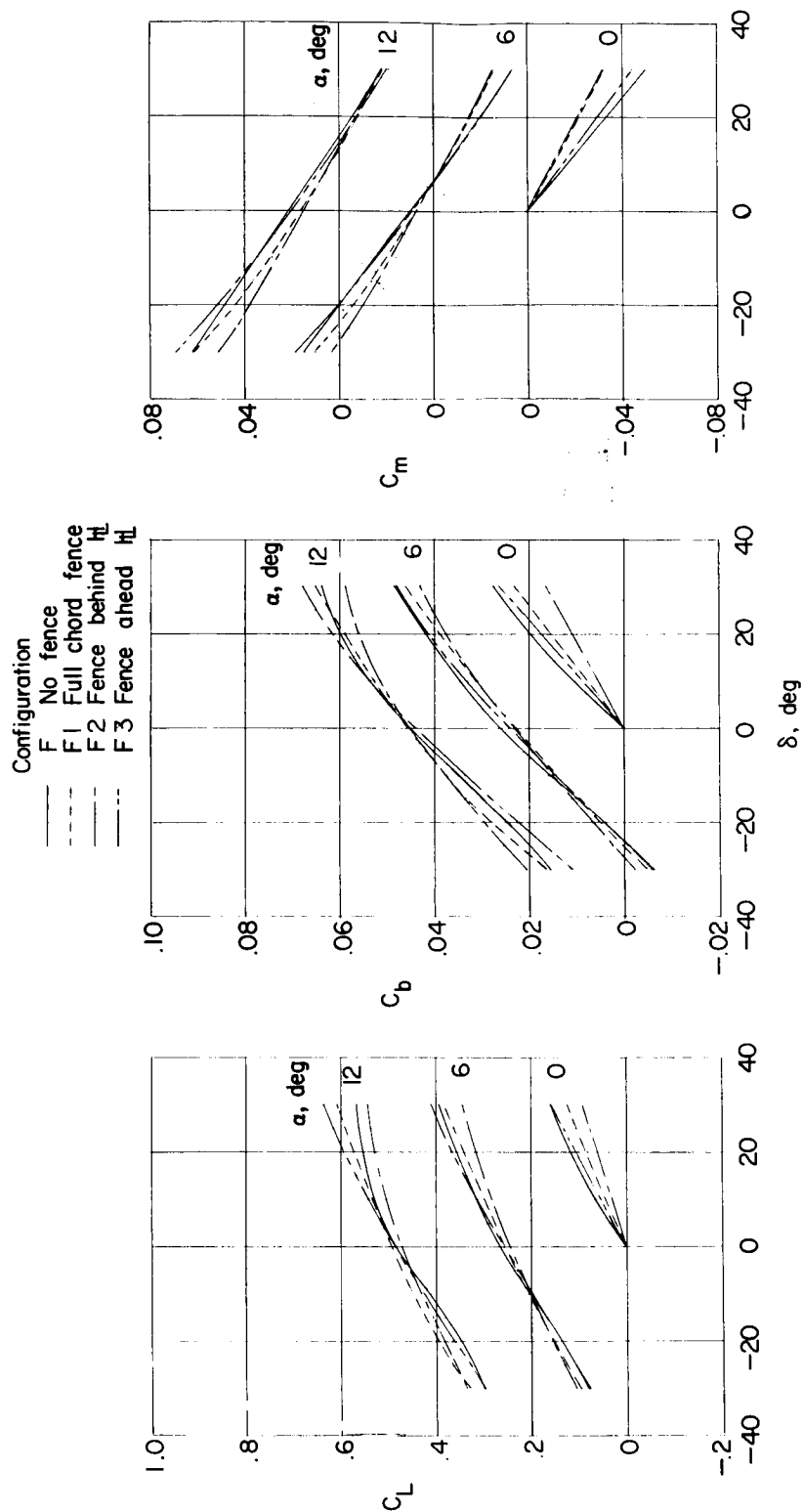


Figure 71.- Effect of partial and full-chord fences on the integrated aerodynamic characteristics of configuration F. $M = 1.61$.

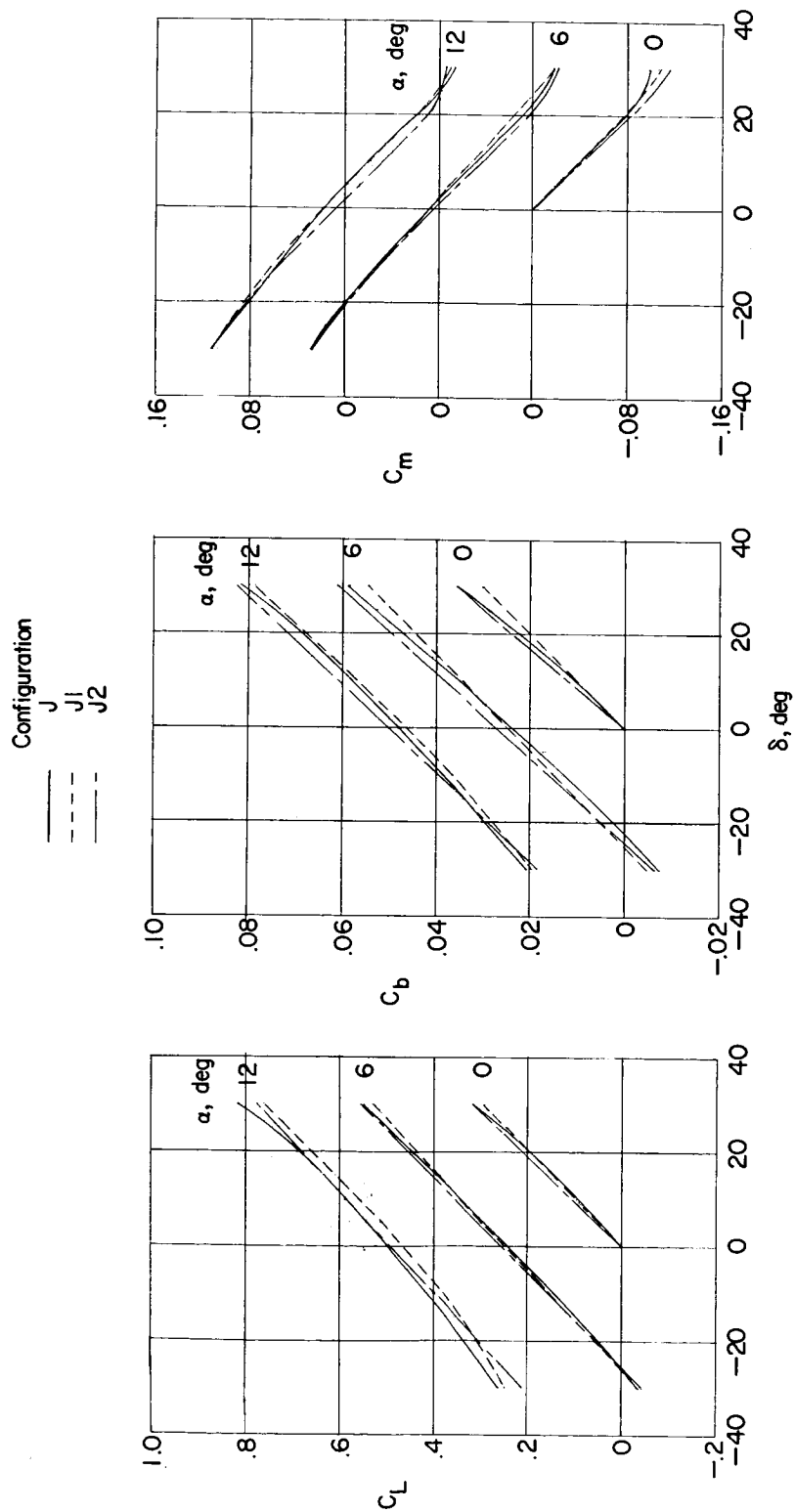
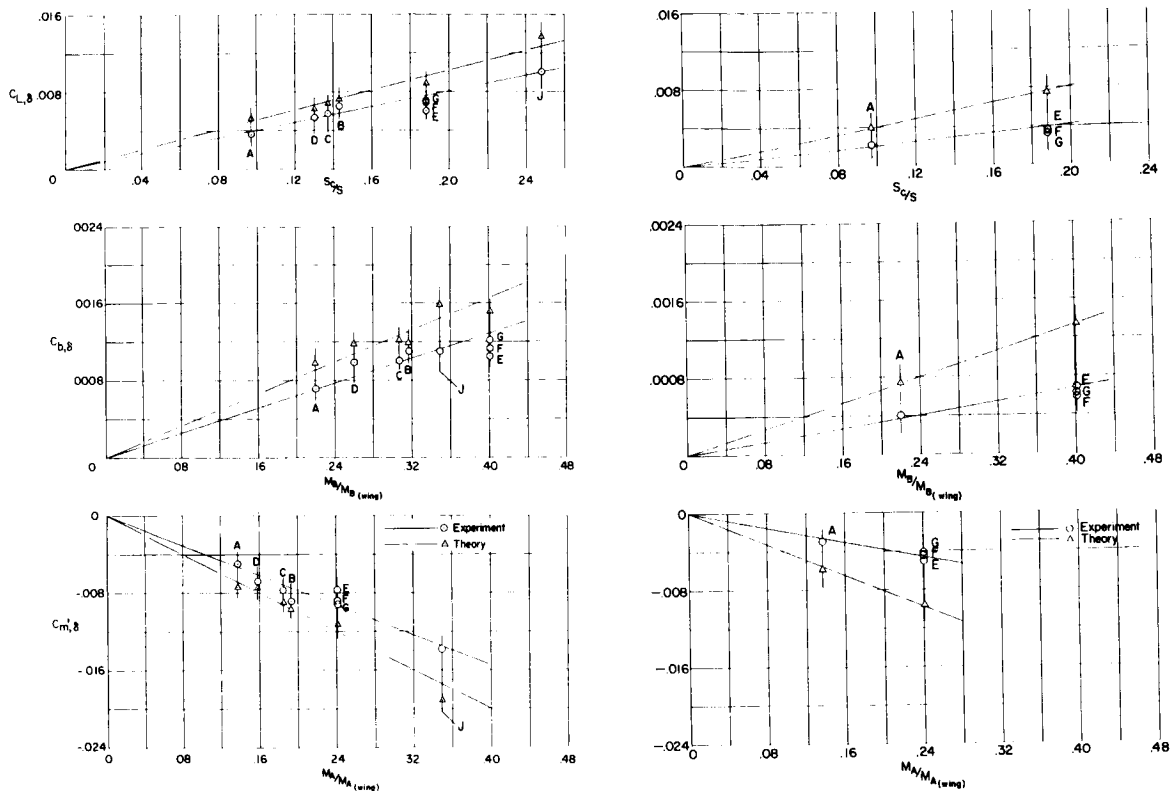


Figure 72.- Effect of trailing-edge thickness on integrated aerodynamic characteristics of the full-span trailing-edge control. $M = 1.61$.

03713 [REDACTED] 30



(a) $M = 1.61$.

(b) $M = 2.01$.

Figure 73.- Correlations of control effectiveness parameter with control areas and control-area moments.